SYNTHESIS, CHARACTERIZATION AND ANION COMPLEXATION OF CATIONIC MAIN GROUP LEWIS ACIDS

A Dissertation

by

YOUNGMIN KIM

Submitted to the Office of Graduate Studies of
Texas A&M University
in partial fulfillment of the requirements for the degree of

DOCTOR OF PHILOSOPHY

August 2010

Major Subject: Chemistry

Synthesis, Characterization and Anion Complexation of

Cationic Main Group Lewis Acids

SYNTHESIS, CHARACTERIZATION AND ANION COMPLEXATION OF CATIONIC MAIN GROUP LEWIS ACIDS

A Dissertation

by

YOUNGMIN KIM

Submitted to the Office of Graduate Studies of
Texas A&M University
in partial fulfillment of the requirements for the degree of

DOCTOR OF PHILOSOPHY

Approved by:

Chair of Committee,	François P. Gabbaï
Committee Members,	Marcetta Y. Darensbourg
	Michael B. Hall
	Perla B. Balbuena
Head of Department,	David H. Russell

August 2010

Major Subject: Chemistry

ABSTRACT

Synthesis, Characterization and Anion Complexation of

Cationic Main Group Lewis Acids. (August 2010)

Youngmin Kim, B.S., Sogang University;

M.S., Sogang University

Chair of Advisory Committee: Dr. François P. Gabbaï

Due to favorable Coulombic effects, cationic main group Lewis acids should be more Lewis acidic than their neutral counterparts. To investigate this idea, this dissertation has been dedicated to the synthesis, characterization and anion binding properties of new cationic Lewis acids for selective anion complexation. The cationic borane $[p\text{-}(Mes_2B)C_6H_4(PPh_3)]^+$ displays an enhanced anion affinity towards fluoride due to a combination of Coulombic and hydrophobic effects, and can be used to detect fluoride at levels below 4 ppm in water. A related phosphonium borane featuring a chromophoric dansyl amide moiety has been synthesized and used for the fluorescence turn on sensing of CN^-. This borane is very sensitive and can be used to measure cyanide concentration in the 20-30 ppb range in water.

The bidentate borane $[o\text{-}(Mes_2B)C_6H_4(PPh_2Me)]^+$ is selective for N_3^- over F^- in water/chloroform biphasic mixtures because of the lipophilic character of the azide anion, as well as its ability to interact with both the boron and phosphorus Lewis acidic sites of the receptor via chelation ($lp_{(N)} \rightarrow \sigma^*_{(P\text{-}C)}$). Sulfonium borane [*o*-

$(Mes_2B)C_6H_4(SMe_2)]^+$ can detect up to 50 ppb of cyanide in water at pH 7 due to favorable Coulombic effects. The sulfonium moiety interacts with the cyanide anion through both bonding and back-bonding interactions, thus enhancing the unusual affinity of [*o*-$(Mes_2B)C_6H_4(SMe_2)]^+$ towards cyanide.

This approach can be extended to Lewis acids containing fluorosilanes such as [1-Ant_2FSi-2-Me_2S-$(C_6H_4)]^+$ whose fluoride affinity exceeds that of neutral fluorosilanes by several orders of magnitude.

ACKNOWLEDGEMENTS

First of all, I would like to thank Prof. François Gabbaï for guiding me through my Ph.D. courses. Synthesis and characterization of new compounds are challenging works in the chemistry field, and Prof. Gabbai has always encouraged and guided me as I have taken on these challenges. I also want to thank my committee members, Dr. Marcetta Y. Darensbourg, Michael B. Hall, Perla B. Balbuena and Timothy R. Hughbanks. I took courses from many of my committee members where I gained valuable knowledge for my chemical research.

Thanks also go to the Gabbai group members (Dr. Min Hyung Lee, Dr, Mieock Kim, Dr. Chammi Palehepitiya Gamage, Dr. Takeshi Matsumoto, Dr. Zureima García Hernandez, Dr. Hyun-Sue Huh, Dr. Duxia Cao, Dr. Thomas Taylor, Dr. Ching-Wen Chiu, Dr. Todd W. Hudnall, Dr. Christopher L. Dorsey, Casey Wade, Haiyan Zhao, Tzu-Pin Lin, Iou-Sheng Ke, and Bibaswan Biswas). I would especially like to thank Casey Wade for his dediction to the group as well as for helping to teach me how to use the instruments in our lab. I also appreciate Jennifer Hess and Jose Delgado for helping me improve my English writing skills.

Finally, I would like to thank my family. My mother and father are always on my side and support me as much as they can. My greatest thanks go to my wife, Jaeyoun Lee, for encouraging me to finish this Ph.D. program in the USA. Without her many sacrifices, I cannot imagine how I would have been able to finish my degree.

TABLE OF CONTENTS

CHAPTER Page

CHAPTER Page

LIST OF FIGURES

Page

Page

Page

Page

Page

LIST OF TABLES

Page

CHAPTER I

INTRODUCTION TO LEWIS ACIDS AS FLUORIDE AND/OR CYANIDE SENSORS

1.1 Introduction

Water fluoridation or addition of fluoride to toothpaste has become a widespread practice because of the beneficial effects of this anion in dental health. However, high doses of this anion are dangerous and can lead to dental or skeletal fluorosis.[1] In order to minimize the potential health risks caused by excessive intake of this anion, the maximum contaminant level for drinking water has been set at 4 ppm (210 μmol) by the Environmental Protection Agency (EPA). The same agency however recommends that a concentration of 2 ppm (referred to a secondary standard) not be exceeded in drinking water. Designing water compatible fluoride anion receptors that are selective in this concentration range is challenging work due to the high hydration enthalpy ($\Delta H^\circ = -504$ kJ/mol) of the fluoride ion.

Cyanide is a toxic anion which binds to and deactivates the cytochrome c oxidase enzyme with sometimes fatal consequences.[2] Because cyanide is widely available in both research and industrial settings, its use for harmful purposes or its release into the environment are sources of concern.[3] The maximum contaminant level of cyanide anions in drinking water is set at 50 ppb by the European Union and 0.2 ppm by the EPA.

This dissertation follows the style of *Journal of American Chemical Society*.

For these reasons, the development of methods that can detect this anion in water is of interest. Designing water compatible cyanide anion receptors that are effective in this concentration range is complicated due to the competitive protonation (p*K*a (HCN) = 9.3) of cyanide ions in water.

1.2. Anion sensors with boron-based Lewis acids

1.2.1. Fluoride complexation by neutral triarylboranes

Because of the vacant p_π-orbital of a boron center, triarylboranes act as anion acceptors. The anion affinity of triarylboranes largely depends on the aryl substituents attached to the boron center. Anion complexation increases the steric repulsion between the aryl groups due to the pyramidal structure formed upon complexation. As a result, increasing the steric bulk of the aryl substituents reduces the anion affinity of triarylboranes. For example, the fluoride ion affinity of Ph_3B is 70 kJ/mol higher that that of Mes_2BPh (Figure 1). [4, 5]

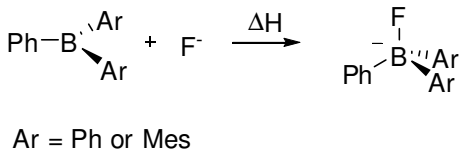

Figure 1. Fluoride complexation by triarylboranes.

Experimentally, Mes_3B and Mes_2PhB bind fluoride anions with an association constant of $K = 3.3 \times 10^5$ M^{-1} and 5.0×10^6 M^{-1}, respectively.[6] Substitution a mesityl group by a phenyl group increases the fluoride affinity by one order of magnitude. Even though a

mesityl group lowers the anion affinity of triarylboranes, Mes_2B fragments have been extensively used in anion sensors because of their water stability and their selectivity for small anions.[7, 8]

The neutral borane **1** featuring three 9-anthryl groups serves as a colorimetric sensor for fluoride.[9] **1** binds fluoride with an association constant K of 2.8×10^5 M^{-1} in THF, which is close to the fluoride binding constant of Mes_3B. Therefore, the steric effects of the 9-anthryl groups are comparable with those of the mesityl groups. Because of the bulk of the anthryl groups, **1** is selective for F^- over other anions such as Cl^-, Br^-, I^-, ClO_4^-, and BF_4^- in THF. Despite the large fluoride binding constant of **1** in THF, addition of water abstracts fluoride from **1**-F suggesting that the neutral borane **1** cannot overcome the high hydration energy of fluoride ($\Delta H^\circ = -504$ kJ/mol).

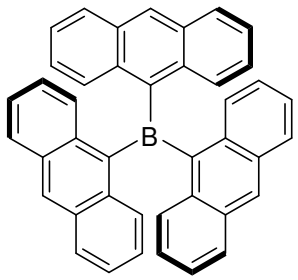

1

Owing to extended π-conjugation, the neutral borane **2** captures fluoride anions in THF/H_2O (9/1, v/v) with a binding constant K of 5.0×10^3 M^{-1} which is larger than the fluoride affinity of **3** (K = 3.3 × 10 M^{-1}).[6] DFT calculations reveal that the boron based LUMO of **2** is delocalized on the *o*-carborane fragment through the π-conjugation. The LUMO energy (−2.10 eV) of **2** was also lower than the LUMO energy (−1.63 eV) of **3**. These provide a rational for the observed difference in fluoride affinity.

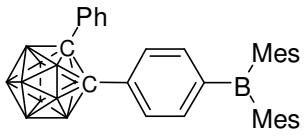

2

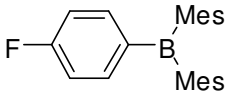

3

Therefore, in order to achieve higher anion affinities, a variety of bidentate Lewis acids which can support anion chelation have been investigated. For example, due to the rigidity and short distance between the C1 and C8 positions of the naphthalene scaffold, functionalizing the substituents on these carbons with Lewis acidic groups is a useful method in generating bidentate Lewis acids. Particularly, the ring opening reaction between the borate [**4**]$^-$ and electrophiles can afford various bidentate Lewis acids featuring the Mes_2B fragment.[10-12] For example, the fluoride affinity of **5** was measured to be $K > 5 \times 10^9$ M^{-1} in THF which is much larger than the fluoride affinity of Mes_2PhB (K = 5.0×10^6 M^{-1}).[12] The single crystal analysis of [**5**-F]$^-$ as a $[S(NMe_2)_3]^+$ salt also demonstrates that the fluoride anion is bound to both boron centers *via* B-F bonds of 1.63 Å and 1.58 Å (Figure 2).

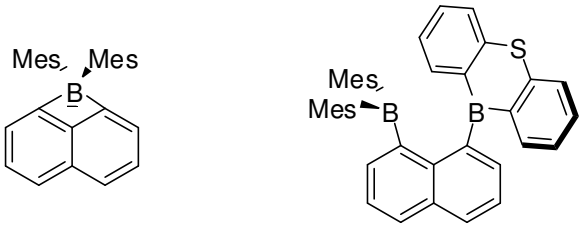

[**4**]$^-$ **5**

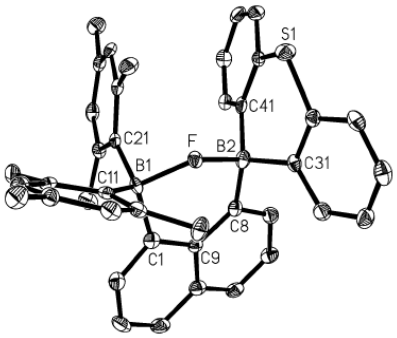

Figure 2. Crystal structure of [**5**-F]$^-$.

The ring opening reaction of the borate [**4**]$^-$ with C_6F_5HgCl affords the B/Hg heteronuclear bidentate Lewis acid **6**.[13] Compound **6** captures fluoride in THF/H_2O (9/1, v/v) with an association constant K of 2.3×10^4 M^{-1}, which is larger than the fluoride affinity ($K = 5.0 \times 10^3$ M^{-1}) of the monodentate borane **2**. The crystal structure of [**6**-F]$^-$ shows that fluoride is bound to both Lewis acidic atoms. The F-Hg distance of 2.589(2) Å is less than the sum of van der Waals radii of the two atoms. The diagnostic ^{199}Hg NMR resonance is coupled with the fluorine nucleus ($^1J_{Hg\text{-}F} = 135.2$ Hz) and is shifted upfield by –69.9 ppm indicating the presence of a Hg-F interaction. The cationic borane [**7**]$^+$ captures fluoride with an association constant K of 6.2×10^4 M^{-1} in THF/H_2O (9/1,

v/v) because of favorable Coulombic effects involving the $[4\text{-}(Me_3N)\text{-}2,6\text{-}Me_2\text{-}C_6H_2]^+$ group.[14]

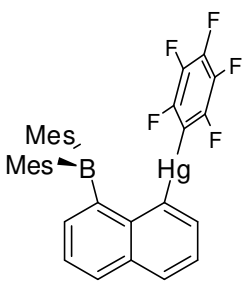

6

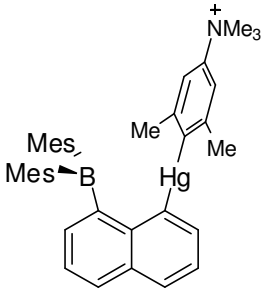

[**7**]$^+$

To generalize the use of adjacent electrophilic groups to enhance the fluoride affinity of triarylboranes, the boron/hydrogen-donor group hybrid **8** was prepared.[15] The fluoride affinity of **8** was measured to be $K \approx 10^8$ M^{-1} in THF, which is larger than the anion affinity ($K = 5 \times 10^6$ M^{-1}) of Mes_2PhB by at least one order of magnitude. This result reflects chelation of the fluoride anion by both the boron center and the amide proton of **8**-F. In the ^{1}H-NMR spectrum, the amide proton appears as a doublet ($^1J_{H\text{-}F}$ = 36 Hz) at 11.43 ppm which confirms the presence of a B-F$^{\cdots}$H-N interaction.

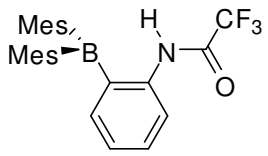

8

1.2.2. Anion complexation by cationic triarylboranes

Another approach to enhance the anion affinity of triarylboranes relies on the use of peripheral cationic groups. The ammonium borane $[\mathbf{9}]^+$ captures fluoride in THF with a binding constant $K > 10^8$ M^{-1} which is also larger than the fluoride affinity of the neutral borane Mes_2BPh by at least one order of magnitude.[16] Structural and computational results reveal that the larger fluoride affinity of $[\mathbf{9}]^+$ is due to both hydrogen bonding and Coulombic effects. Unlike neutral boranes, $[\mathbf{9}]^+$ binds fluoride in water/chloroform biphasic mixtures. The favorable Coulombic effects can overcome the high hydration energy of the fluoride anion.

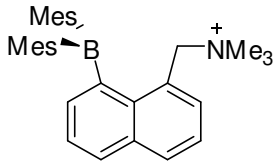

$[\mathbf{9}]^+$

The ammonium ferrocenyl boranes $[\mathbf{10}]^+$ and $[\mathbf{11}]^+$ have also been synthesized.[7] Despite the similar $Fe^{II/III}$ redox potentials of these two derivatives ($E_{1/2}$ = 367 eV for $[\mathbf{10}]^+$ and $E_{1/2}$ = 314 eV for $[\mathbf{11}]^+$), the fluoride affinity of $[\mathbf{10}]^+$ exceeds that of $[\mathbf{11}]^+$ by about 3 orders of magnitude. This difference is assigned to the formation of the B-F···H-C interaction in **10**-F.

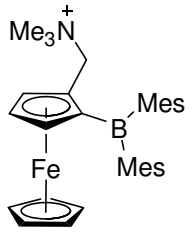

[**10**]$^+$

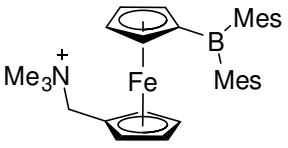

[**11**]$^+$

The anion binding properties of the ammonium borane [**12**]$^+$ and [**13**]$^+$ have also been investigated.[17] Interestingly, while the *o*-isomer [**12**]$^+$ only binds fluoride anions with an association constant K of 910(±50) M^{-1}, the *p*-isomer [**13**]$^+$ only captures cyanide anions with a binding constant K of 3.9(±0.1) × 10^8 M^{-1} in H_2O/DMSO (6/4, v/v) solution at pH 7. This interesting behavior has been attributed to a delicate interplay of steric and electrostatic effects.

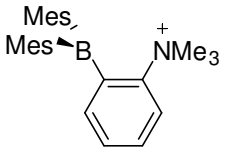

[**12**]$^+$

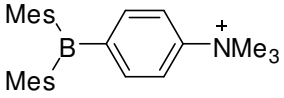

[**13**]$^+$

To further use cationic groups as a means for increasing the anion affinity of boranes, the fluoride binding properties of various phosphonium boranes have been examined.[18] The phosphonium borane [**14**]$^+$ captures fluoride anions in chloroform with an association constant K of 6.5(±0.5) × 10^6 M^{-1} which is larger than the fluoride affinity (K = 2.1(±0.2) × 10^4 M^{-1}) of the neutral diborane **5**. Due to Coulombic effects, [**14**]$^+$ binds fluoride anions in H_2O/MeOH (9/1, v/v) solution with an association constant K of

1000 (±100) M^{-1}. Despite its increased Lewis acidity, this phosphonium borane containing two bulky mesityl groups does not bind other common anions such as Cl^-, Br^-, I^-, NO_3^-, and $H_2PO_4^-$ in this solution.

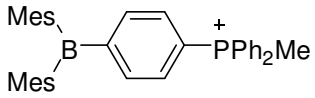

[**14**]$^+$

Inspired by the increased Lewis acidity of the *o*-isomer [**12**]$^+$ compared to the *p*-isomer [**13**]$^+$, the *o*-phosphonium borane [**15**]$^+$was synthesized and investigated.[19] In order to compare the Lewis acidity of the *o*-isomer [**15**]$^+$ with that of the *p*-isomer [**14**]$^+$, an equal molar amount of [**15**]$^+$ and **14**-F were mixed. This competition reaction resulted in complete fluoride transfer from **14**-F to [**15**]$^+$ producing [**14**]$^+$ and **15**-F. The enthalpy change of this reaction is −7.6 Kcal/mol suggesting that the Lewis acidity of the *o*-isomer [**15**]$^+$ is much stronger than that of *p*-isomer [**14**]$^+$. From UV-vis titration data, the fluoride binding constant of *o*-isomer [**15**]$^+$ ($K > 10^6$ M^{-1}) was found to be much larger than that of *p*-isomer [**14**]$^+$ ($K = 400$ M^{-1}) in MeOH. To elucidate the origin of this strong Lewis acidity of [**15**]$^+$, structural and computational analyses of **15**-F were carried out. The fluoride anion interacts with the phosphorus atom *via* a F-P bond of 2.666 Å. This distance is less than the sum of van der Waal radii of the two atoms (*ca.* 3.45 Å) (Figure 3). Another significant feature is the F(1)-P(1)-C(31) angle of 176.36(9)° which indicates that the fluorine atom occupies an axial coordination site directly opposite to a

phenyl ring. The NBO analysis identifies a donor-acceptor interaction (B-F→P) of 5 Kcal/mol involving the fluorine lone-pair as the donor and the phosphorus-carbon σ^*-orbital as the acceptor. The ^{31}P NMR resonance of **15**-F at 28.3 ppm is coupled to the fluorine nucleus ($J_{P\text{-}F}$ = 24.3 Hz) confirming the presence of a P-F interaction.

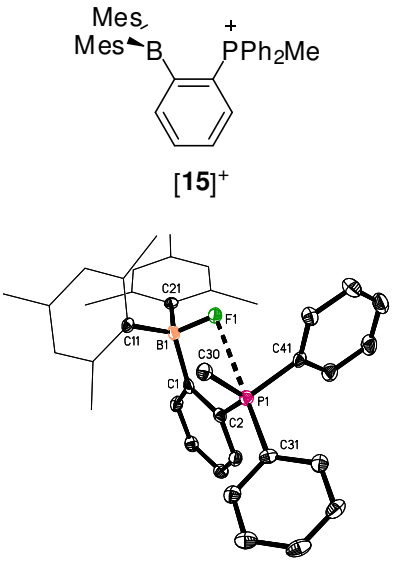

Figure 3. Crystal structure of **15**-F.

In order to study the ability of cationic groups to enhance the Lewis acidity of main group compounds, triarylborane derivatives such as [**16**]$^+$, [**17**]$^{2+}$ and [**18**]$^{3+}$ have been investigated.[20] The cyclovoltammogram showed that substitution of a Mes group by a [4-(Me_3N)-2,6-Me_2-C_6H_2]$^+$ group leads to an increase of the reduction potential by 0.36 V in THF suggesting that [**18**]$^{3+}$ is the most Lewis acidic of the series. However, none of these cationic boranes bind fluoride in water suggesting that the steric repulsion

of three mesityl groups hinders the formation of fluoroborates. Because of this increased Lewis acidity, only [**18**]$^{3+}$ captures cyanide anions in water at pH 7.

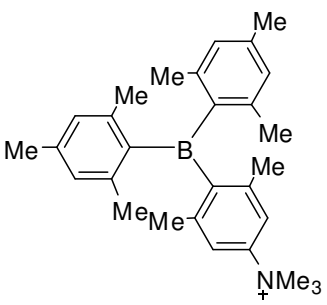

[**16**]$^{+}$

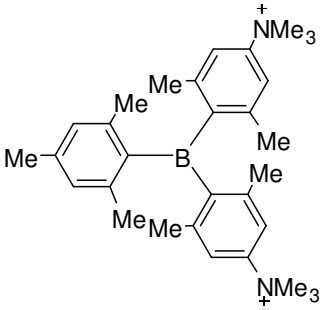

[**17**]$^{2+}$

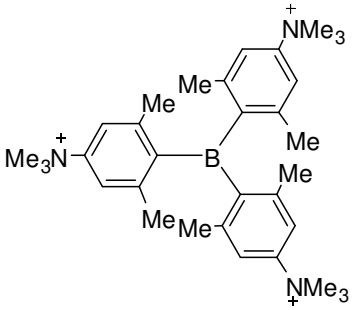

[**18**]$^{3+}$

The anion binding properties of the phosphoniumborin [**19**]$^{+}$ and the diphosphonium azaborines [**20**]$^{2+}$ have also been investigated.[21, 22] Due to favorable Coulombic effects, [**19**]$^{+}$ binds fluoride in water/chloroform mixtures. Interestingly, phoshoniumborin [**19**]$^{+}$ can be used as a solid-phase scavenger for fluoride in water. Dicationic [**20**]$^{2+}$ can be used in aqueous solutions where it displays a moderate affinity for fluoride and cyanide anions ($K(F^-)$ = 1.9(3)×10^2 M^{-1} in H_2O/DMSO (1/3, v/v) solution and $K(CN^-)$ = 5.2(5)×10^4 M^{-1} in water).

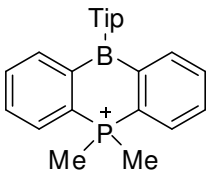

[**19**]$^{+}$

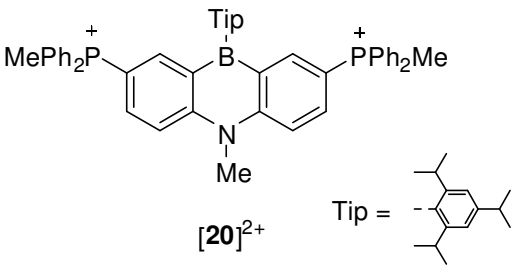

[**20**]$^{2+}$

1.2.3. Cyanide complexation by arylboronic acids

Utilizing the liability of B-O bonds, boronic acids can be applied as anion detectors (Figure 4).[23-25] By displacing the hydroxide molecules with anions, the borate compound can be formed. This changes the properties of the boron center from electron-deficient to electron-rich, which affects the intramolecular charge transfer (ICT) process.

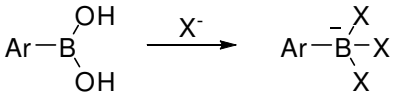

Figure 4. The anion substitution reactions of boronic acids.

In the absence of cyanide, the fluorescence of [**21**]$^+$ was efficiently quenched by ICT involving the aniline moiety as the donor and the ammonium group as the acceptor.[26] However, the conversion of [**21**]$^+$ to the borate in the presence of cyanide reduces the accepting ability of the ammonium center, leading to the revival of fluorescence based on the aniline moiety. The cyanide dissociation constants were measured to be K_D = 4.03 μM^3 for [**21a**]$^+$, 25.50 μM^3 for [**21b**]$^+$, and 4.16 μM^3 for [**21c**]$^+$ in H_2O. Due to the electrostatic effect between ammonium and the borate moieties, the *o*-isomer [**21a**]$^+$ displays the highest cyanide affinity in H_2O.

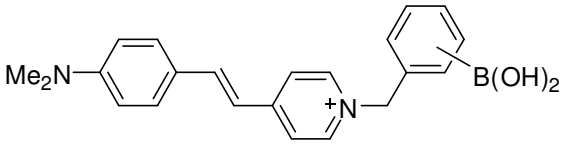

[**21a**]$^+$: *o*-isomer
[**21b**]$^+$: *m*-isomer
[**21c**]$^+$: *p*-isomer

The fluorescence of the boronic acid **22** at 460 nm was also enhanced upon cyanide addition in H_2O/DMSO (1/1, v/v) at pH 7.4.[27] Presumably, the dipole moment change induced by formation of the borate causes a large change in spectral properties. Utilizing the CTAB micellar system, the probe **22** can be used to detect cyanide at 50 μM in aqueous solutions.

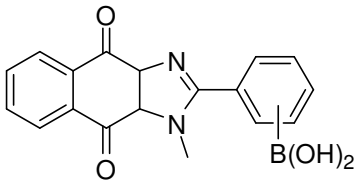

22a: *m*-isomer
22b : *p*-isomer

1.2.4. Fluorescence response induced by anion binding

Triarylboranes such as [**13**]$^+$ emit solvent-dependent fluorescence.[17] This is due to ligand to element charge transfer involving the mesityl fragment as the donor and the vacant p-orbital of boron as the acceptor. Anion binding to the boron center of [**13**]$^+$ quenched the observed fluorescence, indicating that this transfer process was blocked.

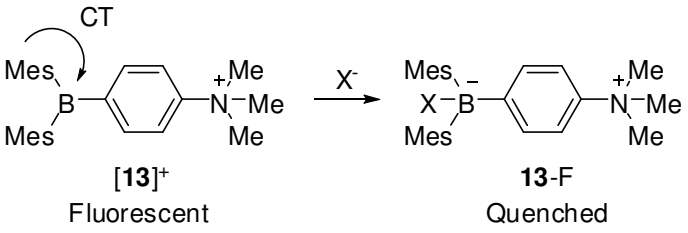

[**13**]$^{+}$
Fluorescent

13-F
Quenched

From an analytical standpoint, this "turn-off" rather than "turn-on" response is not ideal. Realizing this limitation, Wang recently reported a series of bifunctional molecules **23** and **24** containing both a triarylborane and triarylamine moiety.[8, 28, 29] In such systems, the π-π* emission of the excited triarylamine moiety is quenched by an intramolecular charge transfer involving the chromophore potion as the donor and the boron moiety as the acceptor. However, the emission of the triarylamine moiety can be revived upon addition of fluoride to the boron center, so **23** and **24** behave as turn-on fluoride sensors.

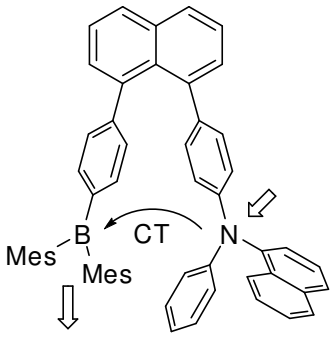

23

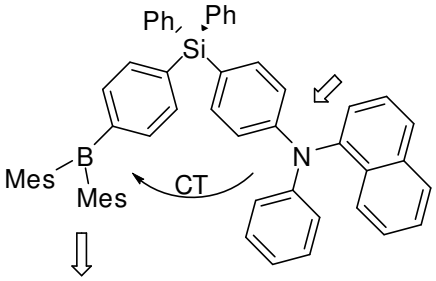

24

Triarylborane **25** displays reverse intra-molecular charge transfer involving borane as the donor and the BODIPY group as the acceptor.[30] Compound **25** features two UV-vis absorption bands at 330 nm (borane moiety) and 501 nm (BODIPY fragment). When compound **25** is excited at 330 nm, it emits fluorescence at 510 nm which corresponds to the BODIPY emission. The charge transfer efficiency of **25** was measured to be 57 % effective relative to the BODIPY emission. Cyanide binding on the boron center of **25** quenches both the UV-vis absorption band and the intense emission band. From UV-vis titration data, the cyanide binding constant of **25** was measured to be $K = 5 \times 10^7\ M^{-1}$ in THF.

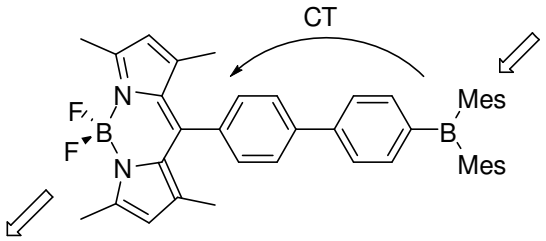

25

1.3. Fluoride sensors with silicon-based Lewis acids

Like boranes, fluorosilanes can also act as anion receptors to form hypervalent silicates.[31-37] For example, the simple reaction of triphenylfluorosilane with KF in the presence of [2,2,2]cryptand affords triphenyldifluorosilicate with K^+/[2,2,2]cryptand salt (Figure 5).[38] The $[Ph_3SiF_2]^-$ complex is arranged as a trigonal bipyramidal in which three phenyl groups occupy the equatorial positions and two fluorine atoms occupy the axial positions.

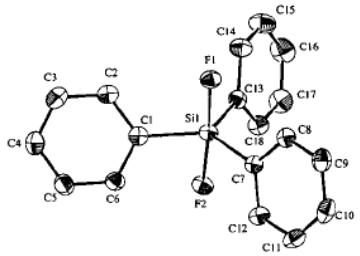

Figure 5. Crystal structure of $[Ph_3SiF_2]^-$.

In a similar manner, the fluoride affinity of fluorosilane **26** containing three 9-anthryl groups was investigated.[39, 40] The addition of fluoride to **26** in THF causes a blue shift in the UV-vis spectrum indicating the formation of [**26**-F]$^-$. This response can be assigned to a decrease in intramolecular anthryl-anthryl π-stacking interactions induced by the change in coordination geometry at the silicon center upon fluoride binding. Based on these spectral changes, the fluoride binding affinity of **26** was calculated to be $K = 2.8(\pm 0.2) \times 10^4$ M^{-1} in THF. Substituting 9-anthryl group with a phenyl group (**27**) causes little change in the fluoride binding affinity. The addition of water to a THF solution of [**26**-F]$^-$ results in fluoride abstraction indicating that the neutral fluorosilane **26** is not sufficiently fluorophilic to overcome the high hydration energy of fluoride.

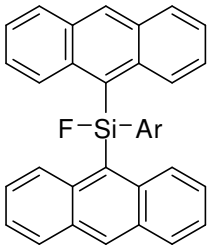

26 : Ar = 9-anthryl
27 : Ar = phenyl

In order to enhance the anion binding affinity of fluorosilanes, bidentate fluorosilane systems have been investigated. The bidentate silane **28** captures fluoride with an association constant $K > 5.9 \times 10^7$ M^{-1} which is larger than the fluoride affinity of Ph_2SiF_2 ($K = 1.5 \times 10^4$ M^{-1}).[41] The crystal structure of [**28**-F]$^-$ shows that F(1) atom is chelated by two silicon atoms (Figure 6).[42] The two silicon centers are nearly trigonal pyramidal with the F(1) atom at the apical positions. The resulting Si-F bonds of 1.898 Å and 2.065 Å indicate a symmetrical chelate structure.

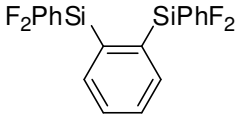

28

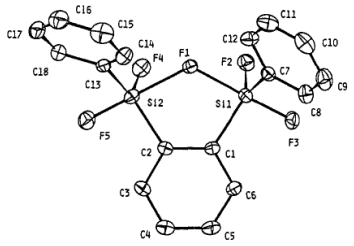

Figure 6. Crystal structure of [**28**-F]$^-$.

Because of these attractive properties, silanes have been incorporated in heteronuclear polydentate Lewis acids.[43, 44] Treatment of **29** containing the 1,8-naphthalene scaffold with tris(dimethylamino)sulfonium difluorotrimethylsilicate (TASF) afforded [**29**-F]$^-$.[43] In the ^{29}Si NMR spectrum, the silicon resonance of [**29**-F]$^-$ (doublet, $J_{Si\text{-}F}$ = 13.2 Hz) was shifted upfield by 6.38 ppm indicating the presence of B-F→Si interaction. The structure of [**29**-F]$^-$ shows that the geometry of the silicon center is a distorted trigonal pyramid with an Si-F distance of 2.714 Å, which is less than the sum of the van der Waals radii of Si and F atoms (*ca.* 3.4 Å). Compound [**29**-F]$^-$ releases the F$^-$ much slower than [**30**-F]$^-$ because of the B-F→Si interaction.

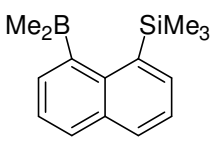

29

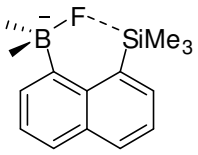

[**29**-F]$^-$

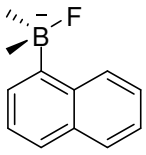

[**30**-F]$^-$

In 2008, Kawachi and Yamamoto reported other neutral B/Si bidentate Lewis acids featuring an *o*-phenylene backbone.[44] When equimolar amounts of **31** and **32** were mixed with [Mes$_2$PhBF]$^-$ in THF, the corresponding [**31**-F]$^-$ (95%) and [**32**-F]$^-$ (78%) were produced, both containing a B-F bond. Like **29**, the fluoride affinities of **31** and **32** were enhanced because the fluoride was chelated by both the boron and the silicon atoms. Both fluoride adducts [**31**-F]$^-$ and [**32**-F]$^-$ have F-Si non-bonded distances of av. 2.4847 Å and av. 2.2568 Å, respectively which are less than the sum of the van der

Waals radii of silicon and fluorine (*ca.* 3.4 Å). DFT calculations reveal that **32** is less fluorophilic than **31** because of the two bulky phenyl groups of **32**.

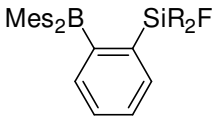

31 : R = Me
32 : R = Ph

1.4. Organic-based cyanide sensors

The trifluoroacetyl group is widely used for covalent carbon-carbon bond formation by nucleophilic addition of cyanide to a carbonyl group.[45] A careful study shows that the intramolecular hydrogen bond of N-H···O in the product (cyanohydrin derivative) drives the C-C bond formation (Figure 7).[46]

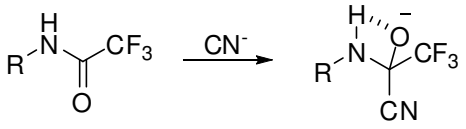

Figure 7. Nucleophilic addition of CN^- to the carbonyl group.

The trifluoroacetyl group of **33** does not react with a large excess of cyanide in CH_3CN/H_2O (95/5, v/v) because the amide proton is engaged in hydrogen bonding with the neighboring C=O unit. On the contrary, the free amide proton of **34** facilitates the formation of [**34**-CN]$^-$ due to the resulting hydrogen bonding interaction. From UV-vis titration data, the cyanide binding constant of **34** was measured to be $K = 7.7 \times 10^4$ M^{-1}.

The detection limit of **34** for cyanide is as low as 0.51 μM in CH_3CN/H_2O (95/5, v/v) solution. Unlike cyanide, the addition of common anions such as F^-, AcO^-, $H_2PO_4^-$, Cl^-, Br^-, I^-, HSO_4^-, NO_3^-, ClO_4^-, SCN^-, and N_3^- does not cause any notable change in the UV-vis spectrum.

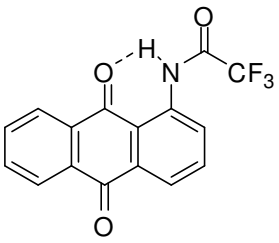

33

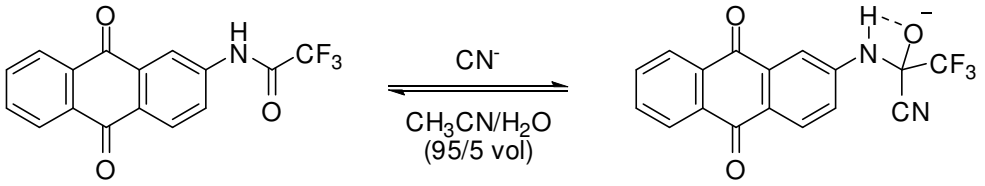

34 [**34**-CN]$^-$

Addition of cyanide to a solution of **35** causes a distinct color change from colorless to orange because of the azo dye fragment.[47] The probe **35** is selective for cyanide with an association constant K of 2.8×10^3 M^{-1} in CH_3CN/H_2O (9/1, v/v) solution. The detection limit of **35** for cyanide anions was below 5μM in the presence of *ca.* 5% of water.

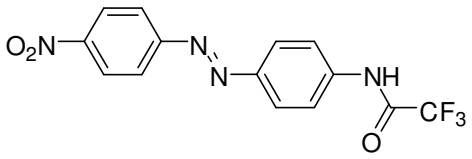

35

As another example, the ensemble of cationic silol [**36**]I and **37** serves as a turn-on cyanide sensor.[48] The nucleophilic attack of cyanide on the carbonyl group of **37** produces [**37**-CN]$^-$. Because of the intermolecular electrostatic and hydrophobic interactions between [**36**]$^+$ and [**37**-CN]$^-$, coaggregation of the two compounds occurs. This aggregation increases the fluorescence of the cationic silol [**36**]$^+$ because silol demostrates aggregation-induced-emission. Experimentally, the fluorescent emission of the ensemble at λ_{max} = 476 nm was enhanced upon cyanide addition with a detection limit of 7.74 μM in H_2O/DMSO (75/1, v/v) solution.

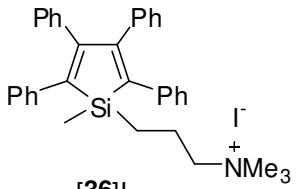

[**36**]I

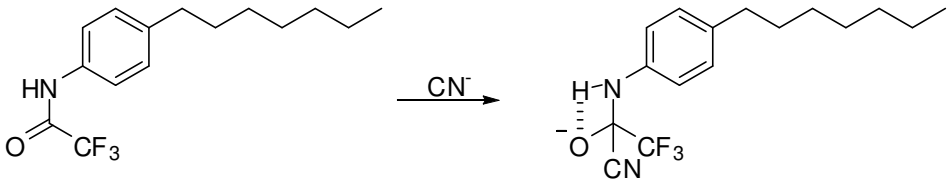

37 **[37**-CN]$^-$

The probe **38** and **39** featuring dipyrrole carboxamide moieties bind cyanide anions in a 1:2 stoichiometry.[49, 50] Due to the strong electron-withdrawing power of the nitro groups, the cyanide binding constant of **39** ($K = 1.1 \times 10^9$ M^{-2}) is larger than that of **38** ($K = 7.9 \times 10^5$ M^{-2}) by three orders of magnitude in CH_3CN/H_2O (9/1, v/v) solution. The addition of cyanide to **39** displays an increase in the absorbance at 465 nm, which can be also observed by the naked eye in 50% water solution.

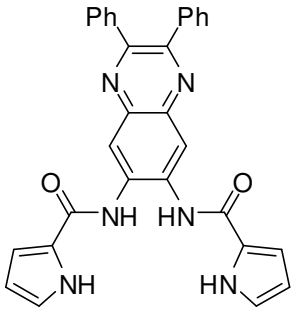

38

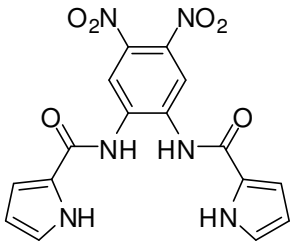

39

Furthermore, due to the non-radiative nπ* excited state, the fluorescence of the chromophores is easily quenched by the lone-pair electrons of the carbonyl groups (Figure 8).[51, 52] However, the C-C bond formation by nucleophilic addition of cyanide to the carbonyl group blocks this quenching process allowing for the π-π* emission of the chromophor to occur.[53-55]

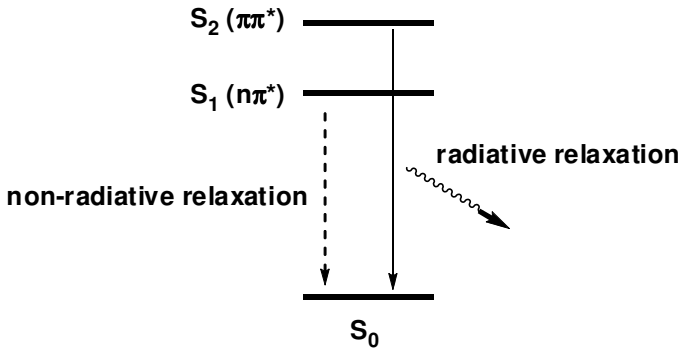

Figure 8. The emission diagram from nπ* and ππ* states.

For example, the addition of cyanide to a solution of [**40**]$^+$ regenerated the fluorescence at λ_{max} = 375 nm, thereby blocking the non-radiative nπ* excited state.[53] Since the aldehyde group is activated by a combination of hydrogen bonding with the amide proton and electrostatic effects, the detection limit of [**40**]$^+$ was lowered to 2.5 μM in water at pH 7.

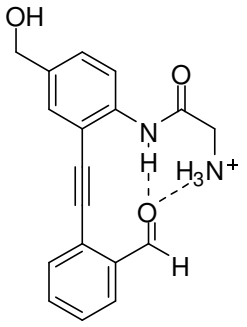

[**40**]$^+$

The aldehyde group of salicylaldehyde is activated and reacts with cyanide to produce cyanohydrin derivatives due to the formation of a six-membered ring driven by

intramolecular hydrogen bonding (Figure 9).[45, 54, 55] Since the cyanohydrin formation results in fluorescence, salicylaldehyde derivatives tethered to a chromophor is expected to act as a turn-on receptor for cyanide.

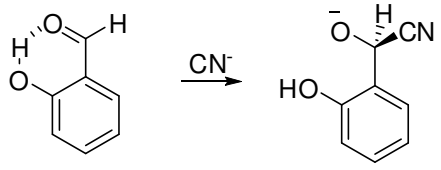

Figure 9. Nucleophilic attack of CN^- on the carbonyl group of salicylaldehyde.

For example, the fluorescence of **41** in CH_3CN/H_2O (9/1, v/v) and **42** in H_2O increased upon addition of cyanide, and was saturated at 50 and 1500 equiv. of cyanide, respectively.[54, 55] In the ^1H NMR spectra of **41** and **42**, the aldehyde proton resonances were shifted upfield by *ca.* 5 ppm upon cyanide addition confirming the formation of the corresponding cyanohydrins. In addition, these compounds were used for cell-imaging to detect cyanide. Both probes allow for highly selective detection of cyanide in aqueous solution.

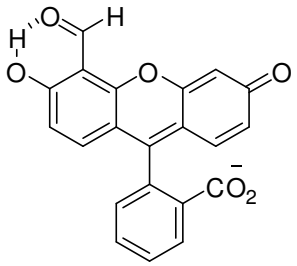

41

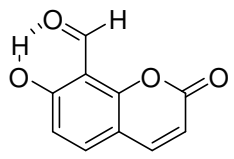

42

The imine group of the salicylaldehyde hydrazone is also activated by hydrogen bonding and reacts with cyanide.[56] The addion of cyanide regenerated fluorescence of **43** at *ca.* λ_{max} = 460 in H_2O/DMSO (1/1, v/v) solution. This is due to the intramolecular hydrogen bond of [**43**-CN]$^-$ which blocks the non-radiative nπ* excitation state (Figure 8).[52] The addition of cyanide to **44** containing an azo dye moiety results in a distinct color change, which can be observed by the naked eye. The detection limit of **43** and **44** for cyanide was measured to be as low as 0.056 μM and 1.5 μM, respectively.

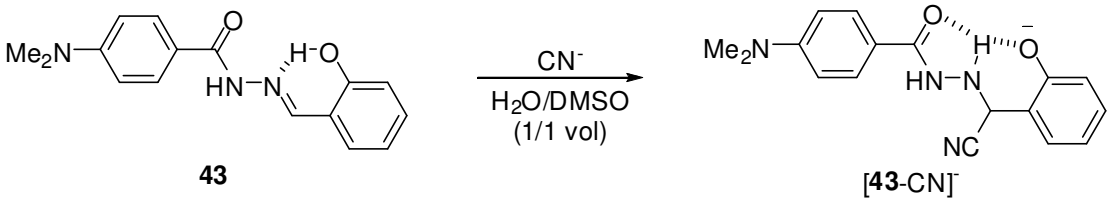

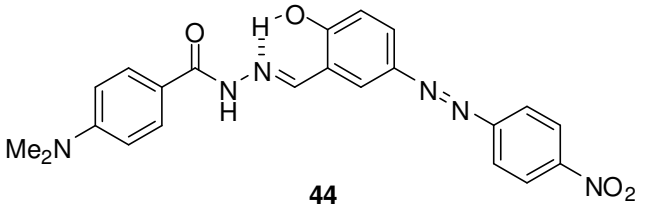

Nucleophilic attack of CN^- on the α,β-unsaturated carbonyl group of **45** has been investigated.[57] This reaction occurs slowly with a rate constant of 1.32×10^{-3} s^{-1} in acetonitrile. This reaction rate was increased upon coordination of a cationic Ir(III) center. The quenched phosphorescence of [**46**]PF_6 at 520 nm was revived upon cyanide addition in H_2O/CH_3CN (1/1, v/v) solution, and was saturated at 10 equiv. of cyanide despite its slow reaction with cyanide. In addition, the pink color of complex [**46**]PF_6 is

quickly quenched upon cyanide addition with a detection limit of 40 μM in a water/chloroform biphasic system.

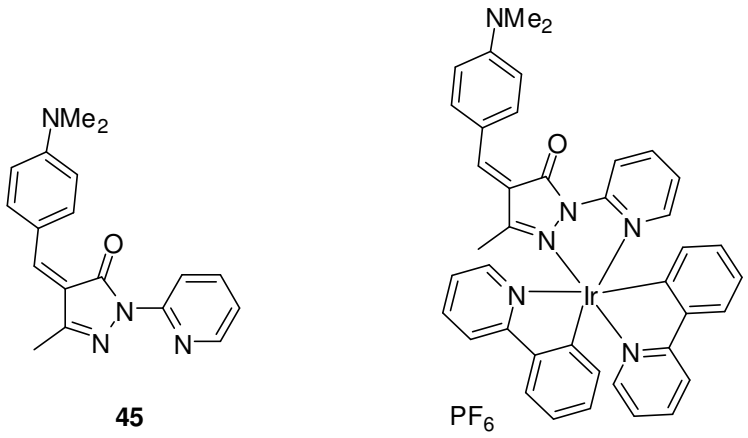

Likewise, the nucleophilic attack of cyanide on the carbonyl carbons of benzil derivatives results in bond cleavage in protic solvents; this is known as the benzil-cyanide reaction (Figure 10).[58-60] Since this reaction breaks the extended π-conjugation of the benzil derivaties, it can be applied to design of chromogenic cyanide sensors.

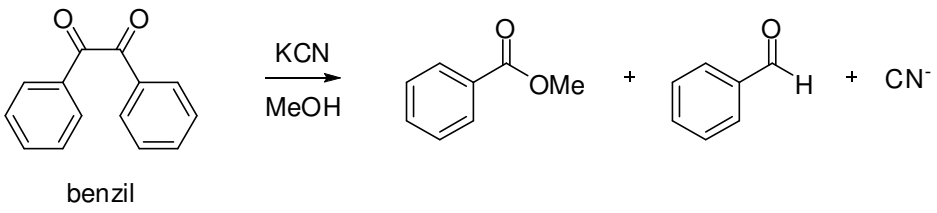

Figure 10. The benzil-cyanide reaction.

Owing to the π-extended substituents on the benzil moiety, **47** features a UV-vis absorption band at λ_{max} = 410 nm in MeOH/H_2O (8/2, v/v).[61] The addition of cyanide to this solution bleaches the yellow color because the π-conjugation of the benzil group is broken. This reaction is facilitated in the presence of OH^-. Compound **47** is selective for cyanide over other common anions in MeOH/H_2O (8/2, v/v). The detection limit of **47** for cyanide is 1.7 μM in MeOH/H_2O (7/3, v/v) in the presence of *ca.* 5 mM of NaOH. Bleaching of the yellow color can be observed by the naked eye.

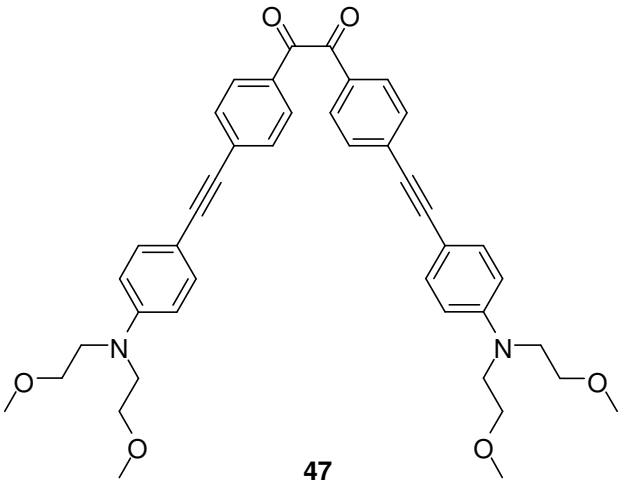

47

Cyanide also activates latent chromophores by the deacylation reaction. The addition of cyanide to **48** in MeOH/H_2O (10/1, v/v) solution changes the color from pale yellow to red-pink.[62] This red-pink colored product was identified as the anionic triazene [**49**]$^-$. The putative deacylation reaction of **48** in the presence of cyanide to produce [**49**]$^-$ was confirmed by ^{1}H-NMR spectroscopy in CD_3CN. **48** is selective for cyanide

over other common anions in MeOH/H_2O (10/1, v/v) solution as well as in water/chloroform biphasic conditions.

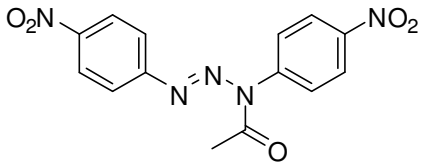

48

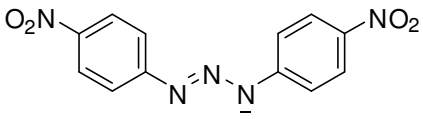

[**49**]$^-$

Like boranes, as mentioned previously, carbocations are intrinsically electron deficient and undergo nucleophilic attack.[45, 63, 64] For example, the acridinium [**50**]$^+$ displays a color change from orange to pale blue in the presence of cyanide in H_2O/DMSO (95/5, v/v) solution due to the nucleophilic addition of cyanide at the C9 position.[65] The corresponding product **50**-CN is readily converted to the acridone **51** in the presence of O_2, which is confirmed by ^{1}H-NMR spectroscopy. [**50**]$^+$ can bind cyanide in the 1–20 μM range in H_2O/DMSO (1/1, v/v) solution despite the filtration process and the higher temperature of 50 °C required for this reaction.

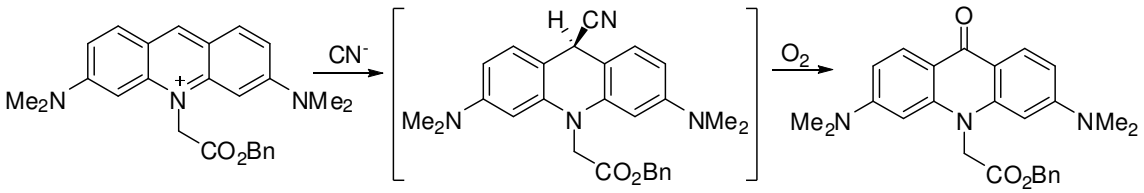

[**50**]$^+$ **50**-CN **51**

Positively charged ions of pyrylium and thiopyrylium can also react with cyanide displaying distinct color changes.[66, 67] Nucleophilic attack of cyanide on the pyrylium group of [**52**]$^+$ produces cyano-enone **52**-CN *via* a ring opening process, accompanied by a color change from yellow to red.[66] **52**-CN was characterized by ^{1}H-NMR spectroscopy and mass analysis. Additionally, a hydrophilic polymer containing [**52**]$^+$ was prepared. The detection limit of this polymer for cyanide was as low as 4 mM in water. Interestingly, acidifying the **52**-CN moiety of the polymer recovered the corresponding [**52**]$^+$ moiety with concomitant color change from red to yellow.

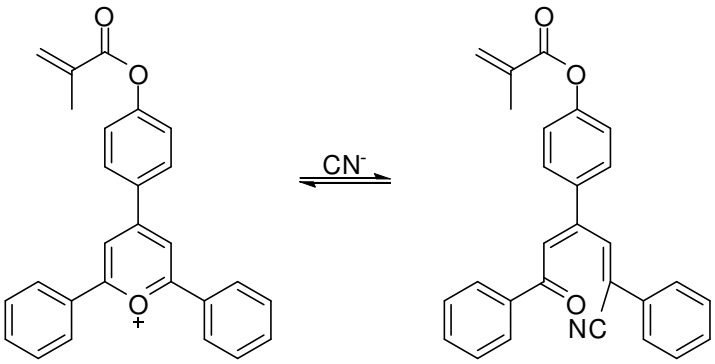

[**52**]$^+$ **52**-CN

In the case of [**53**]$^+$, the nucleophilic addition of cyanide on the thiopyrylium ring bleaches the blue color.[67] This reaction occurs at C2 and C4 of the thiopyrylium ring in a ratio of 25:75, which is confirmed by ^{1}H-NMR spectroscopy. To improve the usefulness of such sensros, [**54**]$^+$ was synthesized and it was incorporated into the micllear system using a surfactant. This system is selective for cyanide over other common anions with a detection limit as low as *ca.* 1 ppm in water.

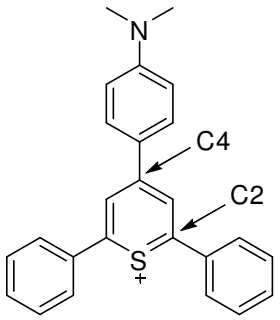

[**53**]$^+$

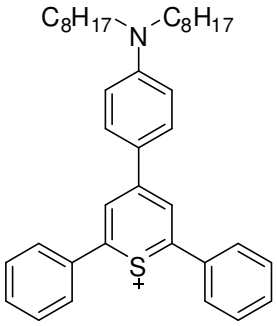

[**54**]$^+$

Electron-deficient indolium groups also undergo nucleophilic attack by cyanide. In solution, benzooxazine **55a** is converted to the intermediate indolium **55b**, which can then be trapped by cyanide addition.[68, 69] The formation of [**55c**]$^-$ causes a color change from yellow to red, which is easily observed by the naked eye. Compound **55a** is selective for CN^- in H_2O/CH_3CN (1/1, v/v) solution at pH 7.6 with a detection limit of 0.1 mM. The detection limit was lowered to 1 μM in H_2O/CH_2Cl_2 biphasic mixtures monitored by UV-vis spectrospcopy.

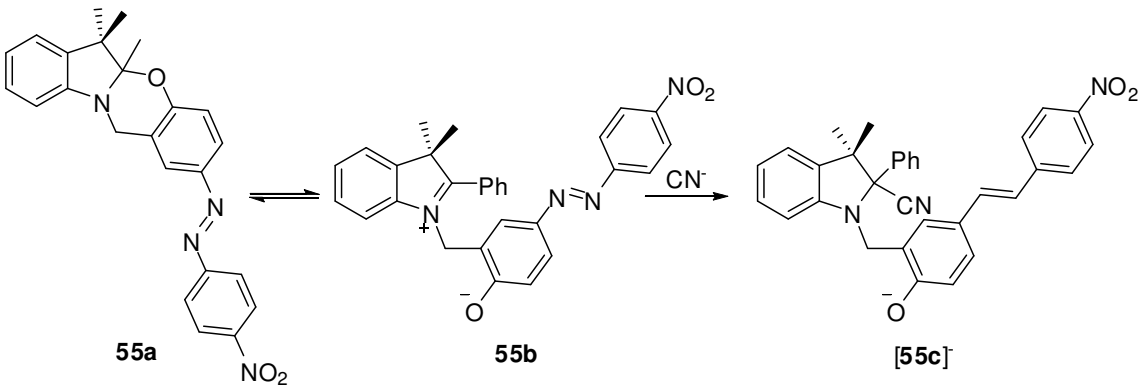

55a **55b** [**55c**]$^-$

Similiarly, upon UV irradiation, spirocyclic **56a** is converted to merocyanine **56b** containing an indolnium group, which is which can be trapped by cyanide addition.[70] The kinetic absorption analysis showed that the formation of [**56c**]$^-$ *via* merocyanine **56b** rather than spirocyclic **56a** was preferred. Interestingly, [**56c**]$^-$ was converted to **56a** upon visible light irradiation demonstrating that the whole process is reversible. Upon UV irradiation, **56a** reacts with cyanide in a 1:1 stoichiometry with an association constant K of 9.8×10^3 M^{-1} in H_2O/MeCN (1/1, v/v) at pH 9.3. Under these conditions, **56a** results in the selective and very sensitive detection of cyanide with a detection limit of 1.7 μM.

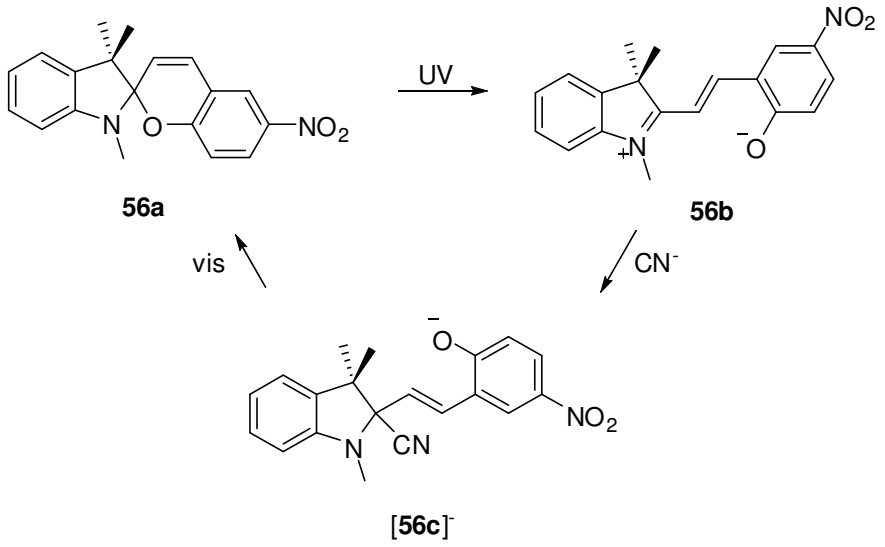

Despite the intense (ε up to 100000) charge transfer band as well as the electron deficient four-membered ring, squadarine dye has not been investigated as a chromogenic anion sensor because of its poor solubility in both organic solvents and

water. By utilizing hydrophilic ether chains, squadarine dye **57** is soluble in acetonitrile as well as H_2O/CH_3CN (8/2, v/v).[71] In acetonitrile, the nucleophilic attack of cyanide on the four-membered ring of **57** bleaches the green color because the charge transfer from the aniline moiety to the electron deficient ring is quenched. The detection limit of **57** for cyanide is as low as 0.1 ppm in H_2O/CH_3CN (8/2, v/v) despite its slow reaction with cyanide.

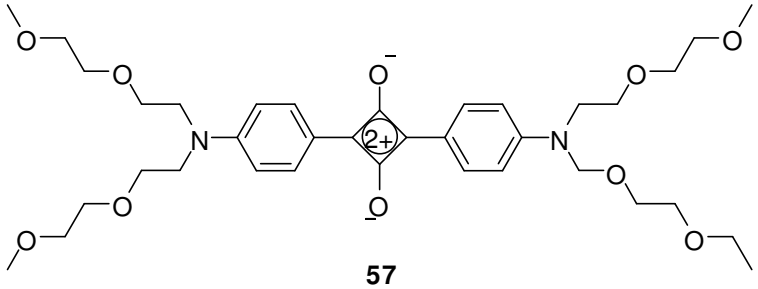

57

Zhang *et al.* utilized the croconine dye **58** as chromogenic sensors for cyanide.[72] The addition of cyanide to **58** induces a decrease in the absorbance in the near-infrared region (823 nm) with a detection limit of 1.5 μM in $EtOH/H_2O$ (7/3, v/v) at pH 9.

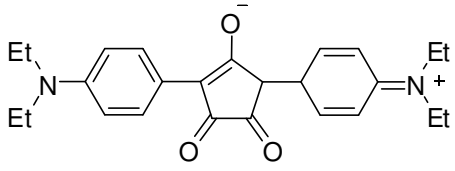

58

Similiarly, boron subphthalocyanine (SubPc) dye also behaves as a chromogenic sensor for cyanide because the nucleophilic addition of cyanide on the macrocyclic ring breaks the 14 π-electron aromatic system.[73, 74] For instance, **59** is pink colored and upon cyanide addition, this color is bleached with an association constant *K* of 1.2(±0.1) × 10^4 M^{-1} in MeCN/H_2O (95/5, v/v). The detection limit of dye **59** for cyanide is as low as 0.1 ppm at pH 9.4 and 10 ppm at pH 7 in H_2O/CH_3CN (1/1, v/v) mixtures.

In order to carry out a dip-and-read test to detect anions in water, the carboxylate functionalized **60** was anchored in a mesoporous TiO_2 film. These systems allow for selective and sensitive detection of cyanide in water despite their slow absorbance decay.

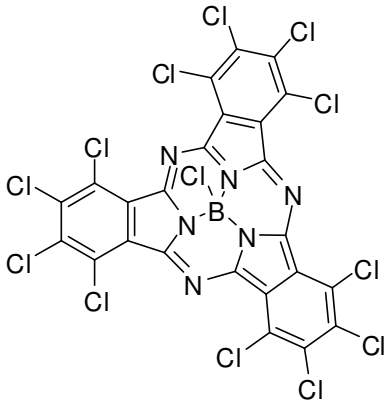

59

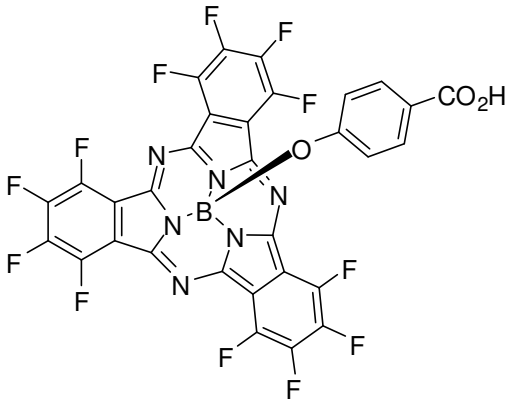

60

Likewise, the organic-based sensor **61** can be used to detect anions in water utilizing mesoporous films.[75] The addition of cyanide to **61** displays an increase in the absorbance at 414 nm in DMSO, which can be observed by the naked eye. This organic dye was incorporated into Al_2O_3 films and used to detect cyanide with a detection limit

of 2.6 ppm in water. Since the Al_2O_3 is positively charged below pH 9, carboxylate-functionalized **61** is stable towards desorption from the film in a practical pH range.

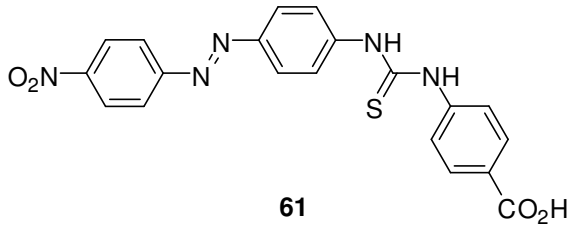

61

1.5. Cyanide sensors based on metal-cyanide complexation

Owing to its high affinity for transition metals, cyanide binds to the metals by displacing weakly-bound ligands on the metal center. For example, addition of cyanide to **62** displaces the Co(III)-bound water with cyanide, accompanied by a color change from orange to pink in water.[76, 77] The cyanide binding constant of **62** equals 0.12(±0.19) $\times 10^6$ M^{-1} at pH 7.5 and 0.55(±0.27) $\times 10^6$ M^{-1} at pH 9.5. Due to the negative charges of the peripheral carboxylate groups, **62** is selective for cyanide over other common anions including thiocyanate, which is the most competitive anion in comparison to cyanide for this system. The detection limit of **62** for cyanide is as low as 10 μM as detected by the naked eye and 1.5 μM as detected by UV-vis spectroscopy. Additionally, complex **62** was used for measuring the rate of enzymatic release of cyanide on the surface of the cassava plant by diffuse reflectance UV-vis spectroscopy.[77]

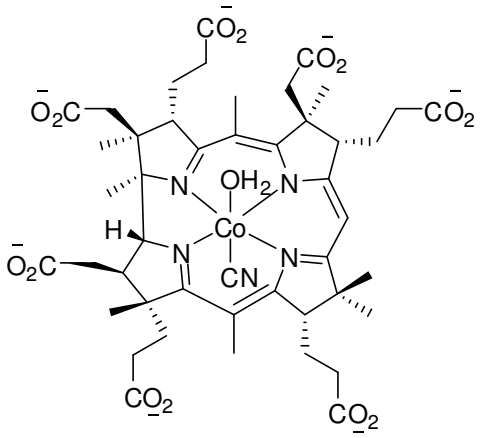

62

In a similar manner, since copper ions display high cyanide affinity with association constants *K* of 1×10^{24} for $[Cu(CN)_2]^-$ and 2×10^{30} for $[Cu(CN)_4]^{3-}$, ligand displacement of copper complexes with cyanide is a promising strategy for detecting cyanide anions.[45, 64, 78] The rhodamine hydrazone **63** forms stable complexs with Cu^{2+} ions in H_2O/CH_3CN (1/1, v/v) solution.[78, 79] The resulting copper complex **64** is magenta colored (λ_{max} = 555 nm) and the addition of cyanide bleaches this color with a detection limit of 0.013 ppm because cyanide displaces the Cu^{2+} ions from complex **64**.

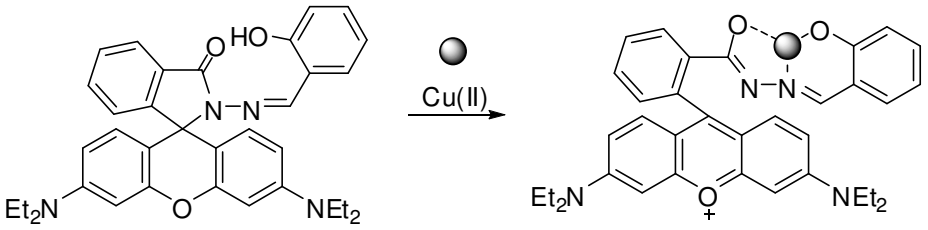

63 **64**

Like the rhodamine hydrazone **63**, zincon can be used to detect cyanide with a detection limit of 0.13 ppm in water in the presence of Cu^{2+} ions.[80] The complex formed by zincon and a Cu^{2+} ion displays a decrease in the absobance at 463 nm and an increase in the absorbance at 600 nm. The addition of cyanide to complex **65** results in an increase in the absorbance at 463 nm, which is observable by the naked eye.

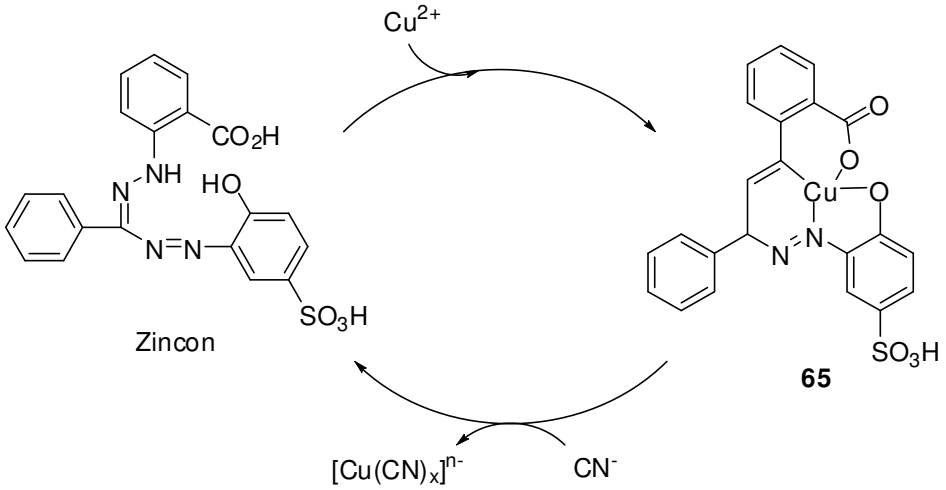

The strong green fluorescence of **66** was quenched in the presence of Cu^{2+} ions in water at pH 7.4.[81] While cyanide induces the revival of fluorescence of complex **67**, other common anions do not cause any change in fluorescence under these conditions. As a practical application, a mixture of **66** and Cu^{2+} ions was used for *in vivo* cell-imaging of cyanide.

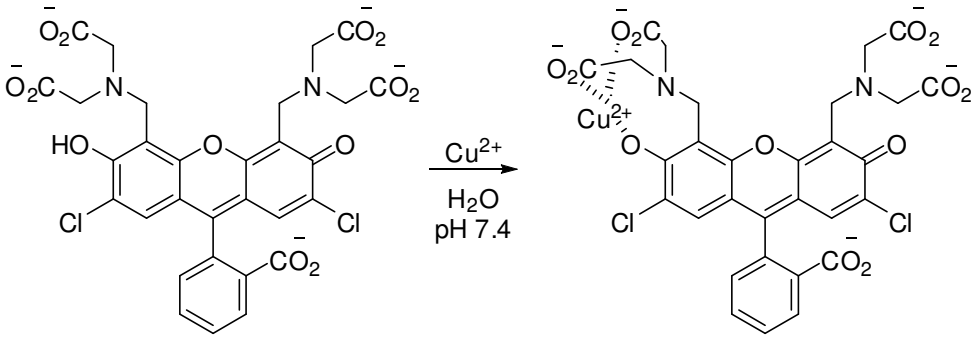

66
Strong fluorescent

67
Less fluorescent

Quantum dots (QDs) are also used in sensor chemistry due to their intense photoluminescence. The emission of the tri-*n*-octylphosphine oxide-coated CdSe QDs was quenched by the [(bipy)$CuCl_2$] complex in chloroform.[82] The incorporation of the [(bipy)$CuCl_2$] complex on the QDs was facilitated by the hydrophobic interactions between bipy and the tri-n-octylphosphine chains. In water/chloroform biphasic mixtures, the addition of cyanide removes Cu^{2+} from [(bipy)$CuCl_2$], recovering the blue-shifted fluorescence of the CdSe QDs.

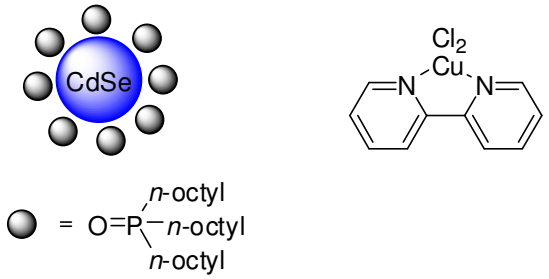

Likewise, the absorption of Cu^{2+} ions on the surface of the CdTe QDs also quenches the fluorescence of the QDs, accompanied by reduction of Cu^{2+} to Cu^{+}.[83] The

addition of cyanide induces the revival of the fluorescence of copper ion-modified QDs with a detection limit of 0.15 μM in water at pH 7.

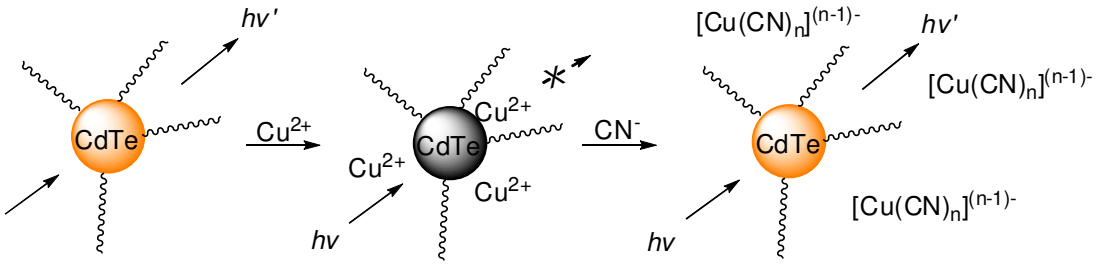

Additionally, the metalloprotein hemoglobin (Hb) can be absorbed on the surface of TiO_2 films stabilizing iron in the Fe^{3+} state which is the necessary oxidation state for capturing cyanide.[84] The cyanide addition to the ferricHb/TiO_2 film exhibited a decrease in the absorbance at 405 nm with a detection limit of 0.2 ppm in water. Other common anions, including potentially competitive thiols did not cause any significant change in the UV spectrum.

CHAPTER II

CATIONIC BORANES FOR THE COMPLEXATION OF FLUORIDE IONS IN WATER BELOW THE 4 PPM MAXIMUM CONTAMINANT LEVEL*

2.1. Introduction

Water fluoridation or addition of fluoride to toothpaste has become a widespread practice because of the beneficial effects of this anion in dental health. High doses of this anion are however dangerous and can lead to dental or skeletal fluorosis.[1] In order to minimize the potential health risks caused by excessive intake of this anion, the maximum contaminant level for drinking water has been set at 4 ppm (210 μmol) by the Environmental Protection Agency (EPA). The same agency however recommends that a concentration of 2 ppm (referred to a secondary standard) not be exceeded in drinking water.[85]

Designing water compatible receptors that are competent in this concentration range is challenging work due to the high hydration enthalpy (ΔH^o = −504 KJ/mol) of the fluoride ion. Original efforts focused on receptors that interact with the anionic guest via hydrogen bonds.[86-97] Unfortunately, such receptors only function in organic solvents and are usually not compatible with water.[98, 99] Faced with these limitations, several groups have considered Lewis acidic receptors which covalently interact with the

---

* Reprinted in part with permission from, "Cationic Boranes for the Complexation of Fluoride Ions in Water below the 4 ppm Maximum Contaminant Level"; Kim, Y.; Gabbaï, F. P.; *J. Am. Chem. Soc.*, **2009**, *131*, 3363-3369, Copyright 2009 by the American Chemical Society.

fluoride anion.[9, 12-14, 28, 29, 44, 100-138] Triarylboranes, for example, complex fluoride anions in organic solvent with binding constants typically in the 10^5-10^6 M^{-1} range (Figure 11).[9, 28, 29, 131-138] Unfortunately, the resulting anionic complexes dissociate in the presence of water, a process driven by the high hydration energy of the small fluoride anion.

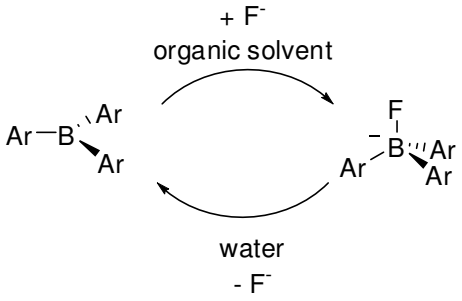

Figure 11. Ar = aryl group.

In order to overcome these limitations, several groups have investigated cationic boron compounds whose anion affinity is increased by Coulombic effects.[107, 114, 129, 139-141] As part of our contribution to this effort, we introduced the cationic boranes [**12**]$^+$, [**14**]$^+$ and showed that these derivatives complex fluoride in aqueous media with binding constant in the 500-900 M^{-1} range.[16-18, 21, 142] Although these results demonstrate that cationic boranes can overcome the hydration enthalpy of fluoride, the binding constants remain too low for measurements of fluoride concentrations near the permissible level. Motivated by this challenge, we are now searching for strategies to enhance the anion affinity of cationic boranes.[19]

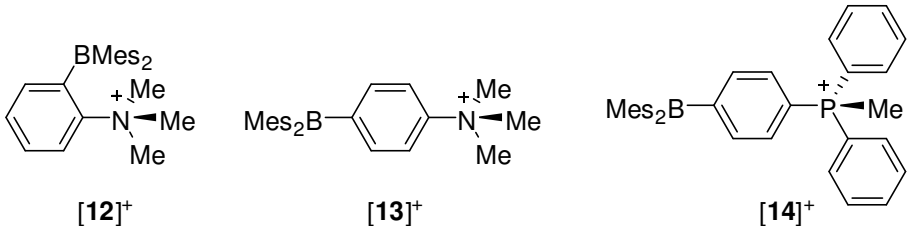

[**12**]$^+$ [**13**]$^+$ [**14**]$^+$

Considering the fact that [**14**]$^+$ captures fluoride in water[18] while the more hydrophilic borane [**13**]$^+$ does not,[17] we postulated that the increased hydrophobicity of [**14**]$^+$ may actually be at the origin of this dichotomy.We further hypothesized that an increase in the hydrophobic character of such cationic boranes may serve to increase their anion affinity. These effects are not unprescedented and have been previously studied. The neutral UO_2 complex **68** binds fluoride in water with an association constant K = 10800 ± 800 M^{-1} in the presence of cetyltrimethylammonium (CTABr).[143] In comparison, the fluoride affinity of **68** in water is much larger than in methanol (K = 360 ± 20 M^{-1}). The paramagnetic relaxation enhancement (PRE) and NOESY NMR studies show that the UO_2 center is protected by the micellar system of CTABr, which enhances the fluoride affinity of **68** in water. Hoping to validate this new paradigm, we have now synthesized a series of phosphonium boranes of varying hydrophobicity and investigated their fluoride ion affinity.

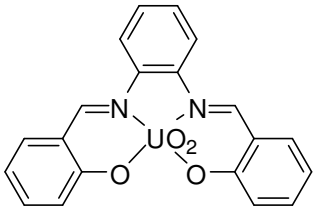

68

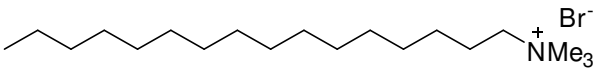

CTABr

2.2. Synthesis and characterization of cationic boranes

Using a similar synthetic strategy to that employed in the case of [**14**]$^+$,[18] we found that the phosphorus atom of the 1-dimesitylboryl-4-diphenylphosphino-benzene **69** could be readily alkylated with ethyliodide in acetonitrile and propyliodide in toluene to afford the corresponding salts [**70**]I and [**71**]I, respectively (Figure 12). The bromide salt [**72**]Br was synthesized by reaction of (4-bromophenyl)dimesitylborane with PPh_3 in refluxing benzonitrile with $NiBr_2$ as a catalyst. The new salts have been characterized by multinuclear NMR. In all cases, the ^{11}B NMR resonance measured in $CDCl_3$ is detected in the 70-80 ppm range which indicates that the boron remains trigonal planar. The presence of a phosphonium center could be easily confirmed by the ^{31}P NMR chemical shift of 26.3, 23.8 and 22.7 ppm for [**70**]$^+$, [**71**]$^+$ and [**72**]$^+$, respectively. Like [**14**]$^+$, these new cationic boranes feature a low energy absorption band detected at 325 for [**70**]$^+$, 322 for [**71**]$^+$ and 325 for [**72**]$^+$ in H_2O/MeOH (9/1, v/v). This low absorption band arises from the boron-centered chromophore[9] and serves to confirm that the boron atom is in a trigonal planar geometry. The crystal structure of [**72**]Br has been determined (Figure 13 and Table 1). As indicated by the sum of the C_{aryl}-B-C_{aryl} angles

($\Sigma_{(C\text{-}B\text{-}C)}$ = 360°), the boron center adopts a trigonal planar coordination geometry and does not interact with the bromide counteranion.

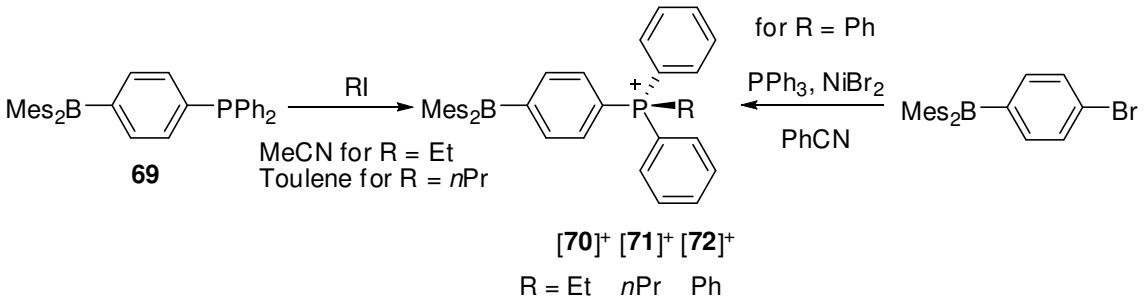

Figure 12. Synthesis of phsophnium boranes.

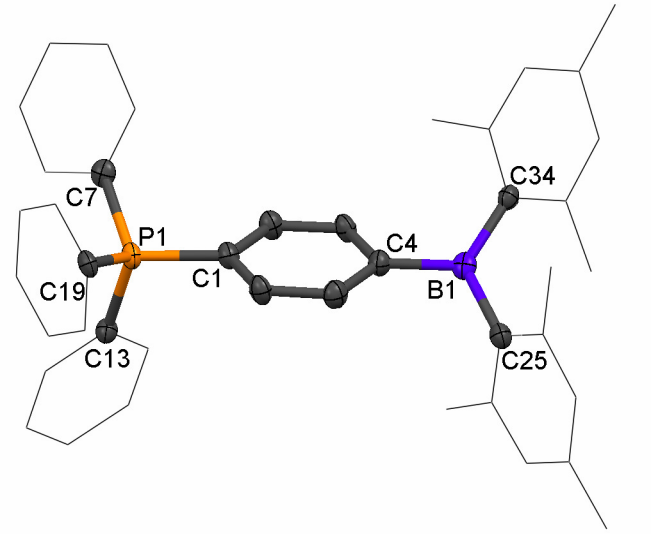

Figure 13. Crystal structure of [**72**]$^+$ with thermal ellipsoids set at 50% probability level. The bromide anion and hydrogen atoms are omitted for clarity. Pertinent metrical parameters can be found in the text.

Table 1. Crystal data, data collections, and structure refinements for [**72**]Br.

Crystal data	[**72**]Br·Et_2O
Formula	$C_{46}H_{51}BBrOP$
M_r	741.56
crystal size (mm^3)	0.37 x 0.25 x 0.09
crystal system	Triclinic
space group	*P-1*
a (Å)	8.1920(16)
b (Å)	10.305(2)
c (Å)	24.315(5)
α (°)	78.84(3)
β (°)	85.45(3)
γ (°)	86.33(3)
V ($Å^3$)	2005.0(7)
Z	2
ρ_{calc} (g cm^{-3})	1.228
μ (mm^{-1})	1.098
F(000)	780
Data collection	
T (K)	110(2)
scan mode	ω
hkl range	-8 → +10, -12 → +12, -30 → +30
measd reflns	11256
unique reflns [R_{int}]	7989 [0.0290]
Reflns used for refinement	7989
Refinement	
refined parameters	451
GooF	1.009
R_1,[a] wR_2[b] all data	0.0830, 0.1354
ρ_{fin} (max/min) (e $Å^{-3}$)	1.156, -0.759

[a] $R_1 = \Sigma||Fo| - |Fc||/\Sigma|Fo|$. [b] $wR_2 = [[\Sigma w(Fo^2 - Fc^2)^2]/[\Sigma w(Fo^2)^2]]^{1/2}$.

2.3. Reaction with hydroxide and pH stability range

In order to better understand the properties of these new boranes and their compatibility with aqueous environments, we have investigated their reaction with hydroxide anions. Interestingly, addition of NaOH to a solution of [**14**]$^+$, [**70**]$^+$, [**71**]$^+$ or [**72**]$^+$ in D_2O/d_4-MeOH (9/1, v/v) results in the formation of the corresponding hydroxide adducts as confirmed by multinuclear NMR. For each of the four cationic boranes, hydroxide binding to the boron center leads to inequivalence of the four hydrogen nuclei of the *p*-phenylene ring. This observation indicates that rotation about the B-C bond connecting the boron atom to the *p*-phenylene moiety is restricted because of steric effects. The ^{11}B NMR signal of these species is detected in the 0-1 ppm range thus confirming the presence of a coordinatively saturated boron center. In order to further establish the formation of these compounds, **14**-OH and **72**-OH have been isolated as solids and analyzed by single crystal X-ray analysis (Figure 14).

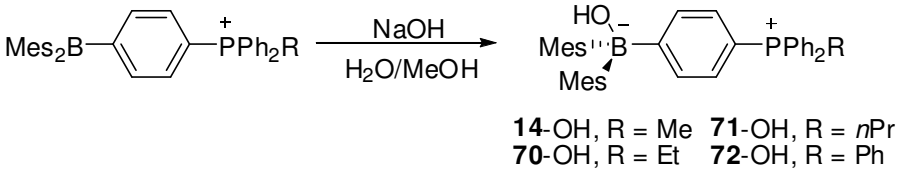

Figure 14. Synthesis of hydroxide adducts of phosphonium boranes.

Examination of the structure shows coordination of the hydroxide anion to the boron center via a B-O bond of 1.519(7) Å for **14**-OH and 1.511(4) Å for **72**-OH (Figures 15 and 16, Table 2). These bond distances are comparable to those observed in other triarylborane hydroxide adducts such as 1-$((C_6F_5)_2BOH)$-2-(Ph_2NH)-C_6H_4 (B-O =

1.521(2) Å).[144] The sum of the C_{aryl}-B-C_{aryl} angles ($\Sigma_{(C\text{-}B\text{-}C)}$ = 336.7° for **14**-OH, 335.8° for **72**-OH) indicates that hydroxide binding induces a substantial pyramidalization of the boron atom which is similar to that observed in **14**-F ($\Sigma_{(C\text{-}B\text{-}C)}$ = 339.4).

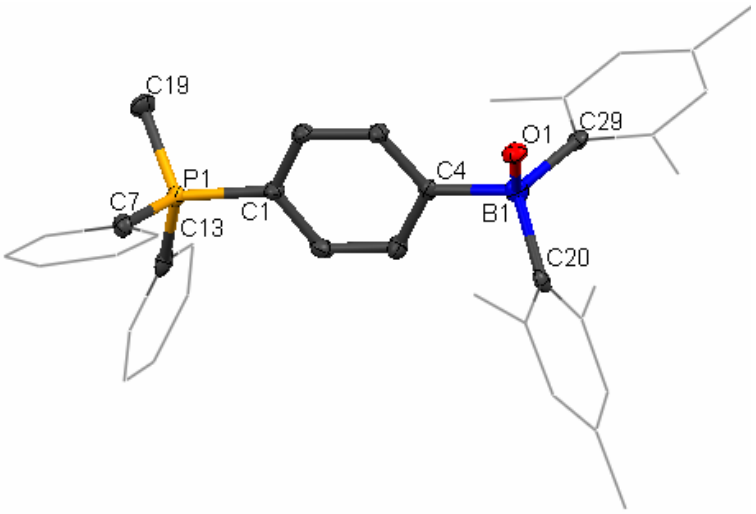

Figure 15. Crystal tructure of **14**-OH with thermal ellipsoids set at 50% probability level. Hydrogen atoms are omitted for clarity. Pertinent metrical parameters can be found in the text.

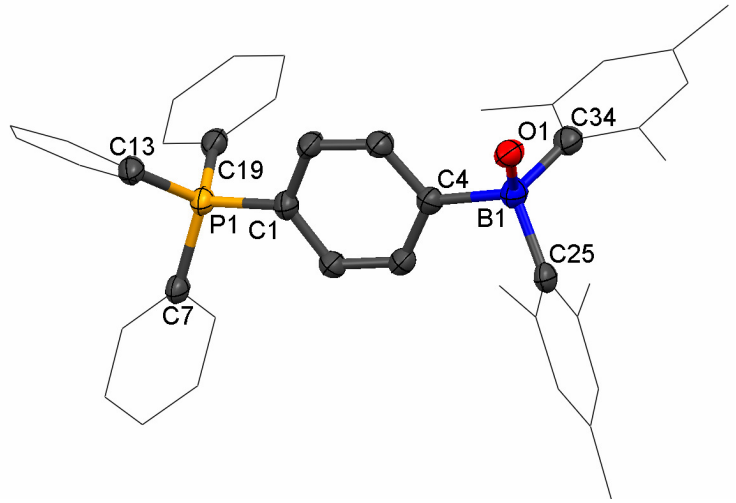

Figure 16. Crystal structure of **72**-OH with thermal ellipsoids set at 50% probability level. Hydrogen atoms are omitted for clarity. Pertinent metrical parameters can be found in the text.

Table 2. Crystal data, data collections, and structure refinement for **14**-OH and **72**-OH.

Crystal data	**14**-OH·$CHCl_3$	**72**-OH·$(H_2O{\cdot}CH_2Cl_2)_{0.5}$
formula	$C_{38}H_{41}BCl_3OP$	$C_{42.5}H_{44}BClO_{1.5}P$
M_r	661.84	656.01
crystal size (mm^3)	0.23 x 0.16 x 0.06	0.35 x 0.12 x 0.06
crystal system	Triclinic	Monoclinic
space group	*P-1*	*C2/c*
a (Å)	12.262(3)	22.702(4)
b (Å)	12.756(3)	14.908(4)
c (Å)	12.976(3)	22.802(5)
α (°)	73.40(3)	90
β (°)	77.77(3)	112.368(4)
γ (°)	62.25(3)	90
V ($Å^3$)	1713.8(6)	7137(3)
Z	2	8
ρ_{calc} (g cm^{-3})	1.283	1.221
μ (mm^{-1})	0.344	0.186
F(000)	696	2784
Data collection		
T (K)	110(2)	110(2)
scan mode	ω	ω
hkl range	-14 → +14, -15 → +7, -15 → +15	-25 → +25, -17 → +17, -26 → +26
measd reflns	8681	30837
unique reflns [R_{int}]	5926 [0.0490]	5606 [0.0680]
reflns used for refinement	5926	5606
Refinement		
refined parameters	397	434
GooF	1.008	1.007
R_1,[a] wR_2[b] all data	0.1303, 0.1739	0.0686, 0.1608
ρ_{fin} (max/min) (e $Å^{-3}$)	0.607, -0.547	0.604, -0.499

[a] $R_1 = \Sigma||Fo| - |Fc||/\Sigma|Fo|$. [b] $wR_2 = [[\Sigma w(Fo^2 - Fc^2)^2]/[\Sigma w(Fo^2)^2]]^{1/2}$.

Having established that these cationic boranes form stable hydroxide adducts, we decided investigate the pH range within which the boron center remain uncoordinated. Since hydroxide binding to the boron center can be expected to interrupt the π-conjugation mediated by the boron vacant p-orbital,[9] we monitored the absorbance of the boron centered chromophore as a function of pH. In all cases, the absorption of the boron centered chromophore is quenched as the pH becomes more basic in agreement with the formation of the hydroxide adducts. Remarkably, acidification of the solution results in a revival of the absorbance indicating that hydroxide binding is reversible. Fitting of the titration data to the equilibrium described in equation 1[145] affords pK_{R+} = 7.3(±0.07) for [**14**]$^+$, 6.92(±0.1) for [**70**]$^+$, 6.59(±0.08) for [**71**]$^+$, 6.08(±0.09) for [**72**]$^+$ (Figures 17, 18, 19 and 20).

$$[R_3B]^+ + H_2O \xrightarrow{K_{R+}} R_3B{-}OH + H^+ \qquad \text{(eq 1)}$$

In turn, these measurements indicate that the Lewis acidity of the boranes increases in the following order: [**14**]$^+$<[**70**]$^+$<[**71**]$^+$<[**72**]$^+$. This data firmly demonstrates that increasing the hydrophobicity of the boranes results in an increase of their Lewis acidity. While the exact thermodynamic origins of this effect have not yet been elucidated, we became eager to verify if a similar trend would be observed in the fluoride ion affinity of these new cationic boranes.

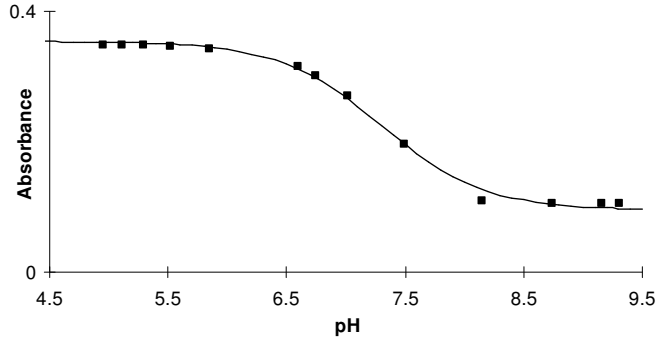

Figure 17. Spectrophotometric titration curve of [**14**]$^+$ in H_2O/MeOH. The absorbance was measured at 320 nm. The experimental data was fitted to eq. 1 using ε([**14**]$^+$) = 9700 M^{-1} cm^{-1}, ε(**14** -OH) = 2600 M^{-1} cm^{-1}, and pK_{R+} = 7.3(±0.07).

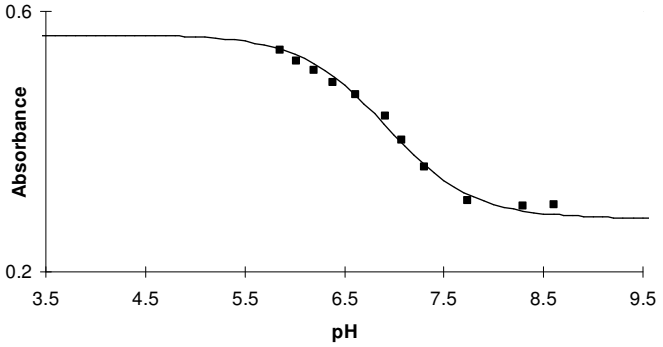

Figure 18. Spectrophotometric titration curve of [**70**]$^+$ in H_2O/MeOH. The absorbance was measured at 322 nm. The experimental data was fitted to eq. 1 using ε([**70**]$^+$) = 9400 M^{-1} cm^{-1}, ε(**70**-OH) = 4700 M^{-1} cm^{-1}, and pK_{R+} = 6.92(±0.1).

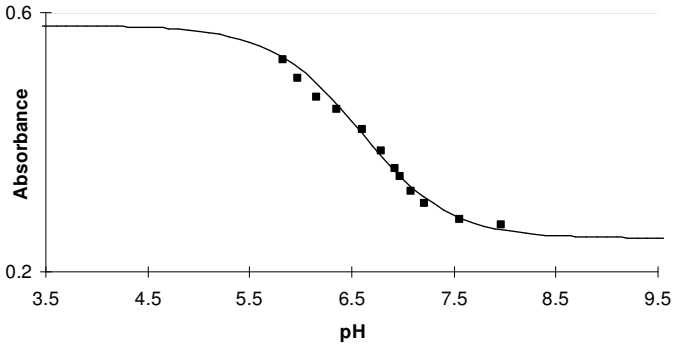

Figure 19. Spectrophotometric titration curve of [**71**]$^+$ in H_2O/MeOH. The absorbance was measured at 322 nm. The experimental data was fitted to eq. 1 using $\varepsilon([\mathbf{71}]^+)$ = 9200 M^{-1} cm^{-1}, ε(**71**-OH) = 4000 M^{-1} cm^{-1}, and pK_{R+} = 6.59(±0.08).

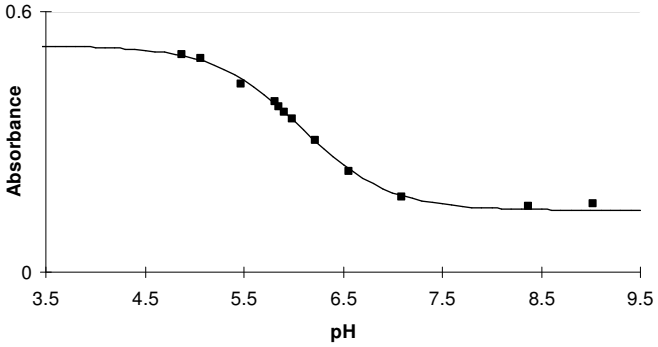

Figure 20. Spectrophotometric titration curve of [**72**]$^+$ in H_2O/MeOH. The absorbance was measured at 325 nm. The experimental data was fitted to eq. 1 using $\varepsilon([\mathbf{72}]^+)$ = 8400 M^{-1} cm^{-1}, ε(**72**-OH) = 2300 M^{-1} cm^{-1}, and pK_{R+} = 6.08(±0.09).

Table 3. Crystal data, data collections, and structure refinements for **72**-F.

Crystal data	**72**-F·$(CH_2Cl_2)_{0.5}$
Formula	$C_{170}H_{168}B_4Cl_4F_4P_4$
M_r	2595.96
crystal size (mm^3)	0.30 x 0.14 x 0.07
crystal system	Triclinic
space group	*P-1*
a (Å)	18.988(4)
b (Å)	19.806(4)
c (Å)	19.918(4)
α (°)	99.42(3)
β (°)	104.07(3)
γ (°)	99.53(3)
V ($Å^3$)	7001(2)
Z	2
ρ_{calc} (g cm^{-3})	1.231
μ (mm^{-1})	0.190
F(000)	2744
Data collection	
T (K)	110(2)
scan mode	ω
hkl range	-21 → +21, -22 → +22, -22 → +22
measd reflns	62266
unique reflns [R_{int}]	21974 [0.0398]
Reflns used for refinement	21974
Refinement	
refined parameters	1675
GooF	1.003
R_1,[a] wR_2[b] all data	0.1001, 0.1669
ρ_{fin} (max/min) (e $Å^{-3}$)	1.125, -0.770

[a] $R_1 = \Sigma||Fo| - |Fc||/\Sigma|Fo|$. [b] $wR_2 = [[\Sigma w(Fo^2 - Fc^2)^2]/[\Sigma w(Fo^2)^2]]^{1/2}$.

2.4. Fluoride ion complexation

We first verified that the new cationic boranes [**70**]$^+$, [**71**]$^+$ and [**72**]$^+$ indeed react with fluoride ions. To this end, these cationic boranes were treated with KF in d_4-MeOH solution to afford the corresponding fluoride complexes **70**-F, **71**-F, and **72**-F (Figure 21). The presence of a boron-bound fluoride anion is confirmed by the detection of ^{11}B NMR resonances in the 4.3-7.5 range and a ^{19}F NMR resonance in the −174 – −171 ppm range. These chemical shifts are close to those measured for **14**-F ($\delta(^{11}B) = 9.8$; $\delta(^{19}F) = -175.5$).[18] The formation of these fluoride adducts was further confirmed by isolation and structural characterization of **72**-F which crystallizes with four molecules in the asymmetric unit (Figure 22 and Table 3). All four molecules have similar structures which approach that of **72**-OH. The av. B(1)-F(1) bond length of 1.46 Å is comparable to those found in other triarylfluoroborate moieties (1.47 Å)[9, 18] and the extent of pyramidalizition of the boron center (av. $\Sigma_{(C\text{-}B\text{-}C)}$ = 338.4°) is almost identical to that observed in **14**-F ($\Sigma_{(C\text{-}B\text{-}C)}$ = 339.4°).

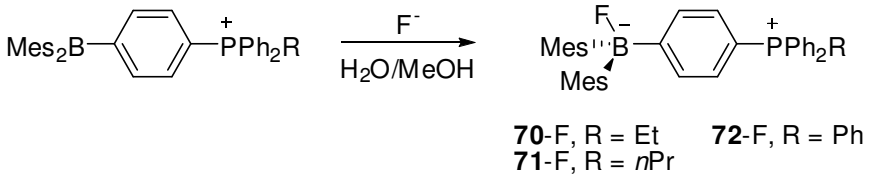

Figure 21. Synthesis of fluoride adducts of phosphonium boranes.

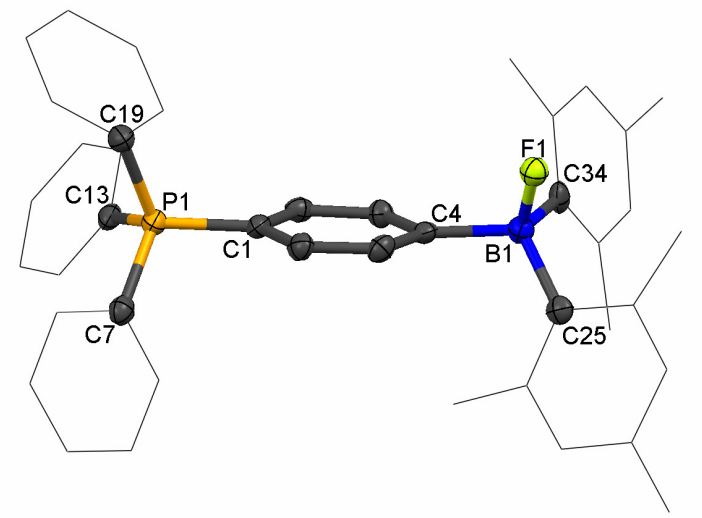

Figure 22. Crystal structure of **72**-F with thermal ellipsoids set at 50% probability level. Hydrogen atoms are omitted for clarity. Pertinent metrical parameters can be found in the text.

Further information on the fluoride affinity of these molecules was gained from titration experiment monitored by UV-vis spectroscopy. In order to maximize the photophysical response of the receptors, these titration were carried out under buffered conditions at slightly acidic pH's (pH = 4.9 for $[\mathbf{14}]^+$, 4.9 for $[\mathbf{70}]^+$, 4.9 for $[\mathbf{71}]^+$ and 4.6 for $[\mathbf{72}]^+$). The resulting titration data were fitted to a 1:1 binding isotherm which afforded K = 840(±50) M^{-1} for $[\mathbf{14}]^+$, 2500(±200) M^{-1} for $[\mathbf{70}]^+$, 4000(±300) M^{-1} for $[\mathbf{71}]^+$ and 10500(±1000) M^{-1} for $[\mathbf{72}]^+$ as fluoride binding constants (Figures 23, 24, 25 and 26). These results show that the fluoride binding constant increases with the hydrophobicity of the borane (Tables 4, 5, 6 and 7). These results are therefore in perfect agreement with the acidity scale established on the basis of the pK_{R+} measurements. These results also show that the replacement of $PMePh_2$ moiety of $[\mathbf{14}]^+$

by a PPh_3 moiety in $[\mathbf{72}]^+$ results in an increase of the fluoride binding constant by more than one order of magnitude.

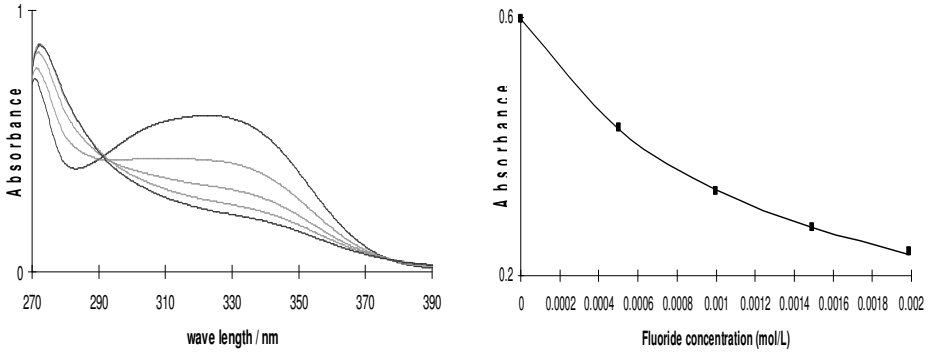

Figure 23. Left: Absorbance change of a solution of $[\mathbf{14}]^+$ after successive additions of fluoride anions; right: The absorbance was measured at 322 nm. Experimental data and calculated 1:1 binding isotherm with K = 840(±50) M^{-1} using ε($[\mathbf{14}]^+$) = 9700 M^{-1} cm^{-1} and ε(**14**-F) = 100 M^{-1} cm^{-1}.

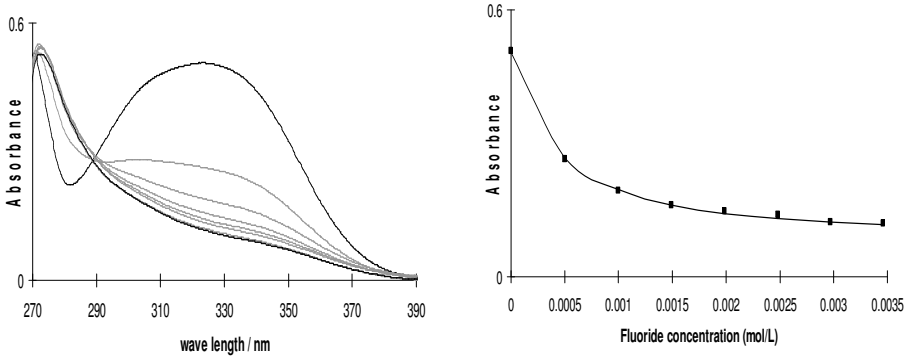

Figure 24. Left: Absorbance change of a solution of $[\mathbf{70}]^+$ after successive additions of fluoride anions; right: The absorbance was measured at 325 nm. Experimental data and calculated 1:1 binding isotherm with K = 2500 (±200) M^{-1} using ε($[\mathbf{70}]^+$) = 9300 M^{-1} cm^{-1} and ε(**70**-F) = 1200 M^{-1} cm^{-1}.

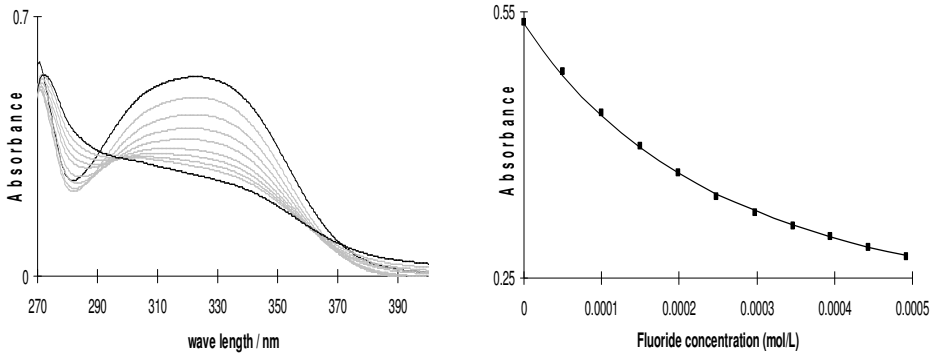

Figure 25. Left: Absorbance change of a solution of [**71**]$^+$ after successive additions of fluoride anions; right: The absorbance was measured at 322 nm. Experimental data and calculated 1:1 binding isotherm with K = 4000 (±300) M^{-1} using ε([**71**]$^+$) = 9100 M^{-1} cm^{-1}, ε(**71**-F) = 2100 M^{-1} cm^{-1}.

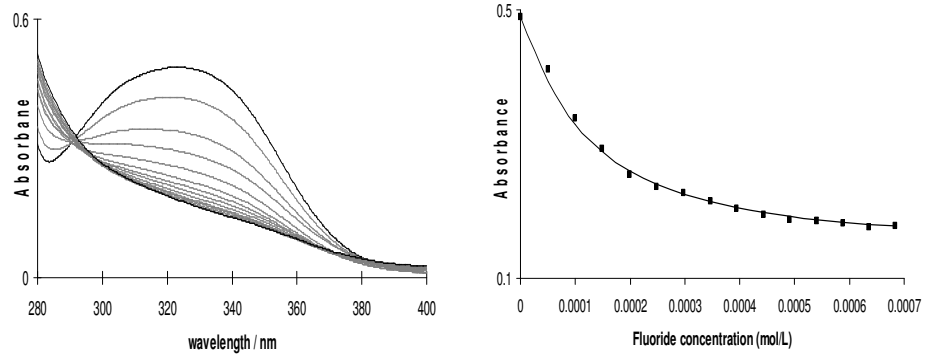

Figure 26. Left: Absorbance change of a solution of [**72**]$^+$ after successive additions of fluoride anions; right: The absorbance was measured at 325 nm. Experimental data and calculated 1:1 binding isotherm with K = 10500 (±1000) M^{-1} using ε([**72**]$^+$) = 8400 M^{-1} cm^{-1}, ε(**72**-F) = 2100 M^{-1} cm^{-1}.

Table 4. Absorbance of a solution of [**14**]$^+$ after successive additions of fluoride anions in H_2O/MeOH (9/1, v/v).

$C_{fluoride}$	Abs_{exp}	Abs_{calc}	$C_{fluoride}$	Abs_{exp}	Abs_{calc}
0.000000	0.598000	0.598167	0.001493	0.275000	0.273814
0.000499	0.429000	0.427980	0.001987	0.238000	0.233104
0.000997	0.331000	0.333392			

Table 5. Absorbance of a solution of [**70**]$^+$ after successive additions of fluoride anions in H_2O/MeOH (9/1, v/v).

$C_{fluoride}$	Abs_{exp}	Abs_{calc}	$C_{fluoride}$	Abs_{exp}	Abs_{calc}
0.000000	0.506000	0.505300	0.001987	0.146000	0.142783
0.000499	0.265000	0.267971	0.002479	0.138000	0.130461
0.000997	0.193000	0.195819	0.002970	0.123000	0.122009
0.001493	0.161000	0.162065	0.003460	0.120000	0.115928

Table 6. Absorbance of a solution of [**71**]$^+$ after successive additions of fluoride anions in H_2O/MeOH (9/1, v/v).

$C_{fluoride}$	Abs_{exp}	Abs_{calc}	$C_{fluoride}$	Abs_{exp}	Abs_{calc}
0.000000	0.538000	0.536900	0.000297	0.323000	0.325772
0.000050	0.482000	0.478168	0.000346	0.309000	0.309774
0.000100	0.436000	0.432662	0.000395	0.297000	0.296271
0.000149	0.399000	0.396851	0.000443	0.284000	0.284757
0.000199	0.369000	0.368208	0.000492	0.274000	0.274853
0.000248	0.341000	0.344942			

Table 7. Absorbance of a solution of [**72**]$^+$ after successive additions of fluoride anions in H_2O/MeOH (9/1, v/v).

$C_{fluoride}$	Abs_{exp}	Abs_{calc}	$C_{fluoride}$	Abs_{exp}	Abs_{calc}
0.000000	0.489000	0.490000	0.000395	0.204000	0.204998
0.000050	0.411000	0.392545	0.000443	0.195000	0.197984
0.000100	0.338000	0.329592	0.000492	0.188000	0.192302
0.000149	0.292000	0.288241	0.000540	0.185000	0.187634
0.000199	0.254000	0.260005	0.000588	0.181000	0.183755
0.000248	0.236000	0.239914	0.000636	0.177000	0.180501
0.000297	0.228000	0.225087	0.000684	0.178000	0.177750
0.000346	0.215000	0.213803	0.000732	0.177000	0.175409

2.5. Complexation of fluoride below the EPA maximum contaminant level in water

Encouraged by these results, we decided to investigate whether $[\mathbf{72}]^+$ could be used for the detection of fluoride in pure water near or below the EPA maximum contaminant level. With this in mind, we first set out to determine the pK_{R+} of $[\mathbf{72}]^+$ in pure water by monitoring the absorbance as a function of pH. Fitting of the resulting data to eq 1. afforded $pK_{R+} = 5.3(\pm 0.08)$ (Figure 27). This value is substantially lower than the pK_{R+} value of 6.1 measured for $[\mathbf{72}]^+$ in H_2O/MeOH (9/1, v/v). This suggest that the acidity of $[\mathbf{72}]^+$ increases as the polarity of the solution increases.

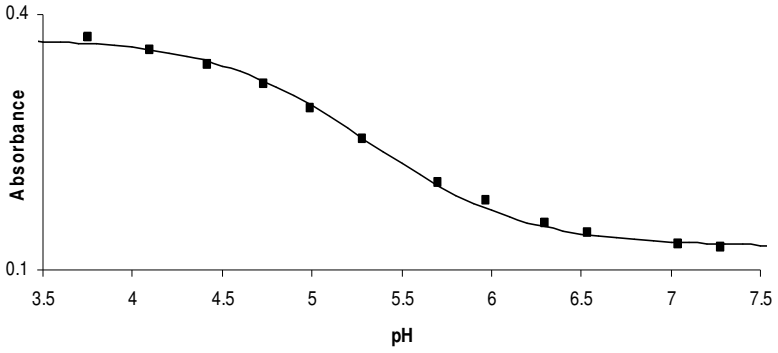

Figure 27. Spectrophotometric titration curve of $[\mathbf{72}]^+$ in H_2O. The absorbance was measured at 322 nm. The experimental data was fitted to eq. 1 using $\varepsilon([\mathbf{72}]^+) = 7300\ M^{-1}\ cm^{-1}$, $\varepsilon(\mathbf{72}\text{-OH}) = 2500\ M^{-1}\ cm^{-1}$, and $pK_{R+} = 5.3(\pm 0.08)$.

Next, we turned our attention to the case of fluoride and measured the binding constant in pure water at pH 4.9. Working at more acidic pH was not an option because of the competitive protonation of the fluoride anion. However, at this pH, hydroxide binding to the boron center of [**72**]$^+$ becomes competitive, a phenomenon that had to be accounted for the fitting the experimental binding isotherm (Figure 28). The resulting fluoride binding constant in pure water is equal to 30000(±5000) M^{-1}again indicating that [**72**]$^+$ is more Lewis acidic in pure water (Figure 29, Table 8). This observation further supports that maximizing hydrophobic effects by increasing the water content of the medium leads to an increase of the acidity of the receptor. To finish these studies, we decided to focus on the response that the receptor [**72**]$^+$ would give in pure water in the presence of fluoride ions near the secondary standard (2 ppm) set by the EPA. To this end, we measured the extent of absorbance quenching experienced by [**72**]$^+$ (3.67×10^{-5} M) in the presence fluoride ions (100 μM or 1.9 ppm) in water. At pH 4.9, a easily detectable 63% quenching of the absorbance is observed thereby demonstrating that [**72**]$^+$ is competent for fluoride sensing at the permissible level in pure water (Figure 29). This test can also be carried out at pH 6 where hydroxide binding to [**72**]$^+$ occurs (Figure 30). Despite this competitive process, an absorbance quenching of 50% is observed once again pointing to the performance of [**72**]$^+$ as a fluoride binder in pure water.

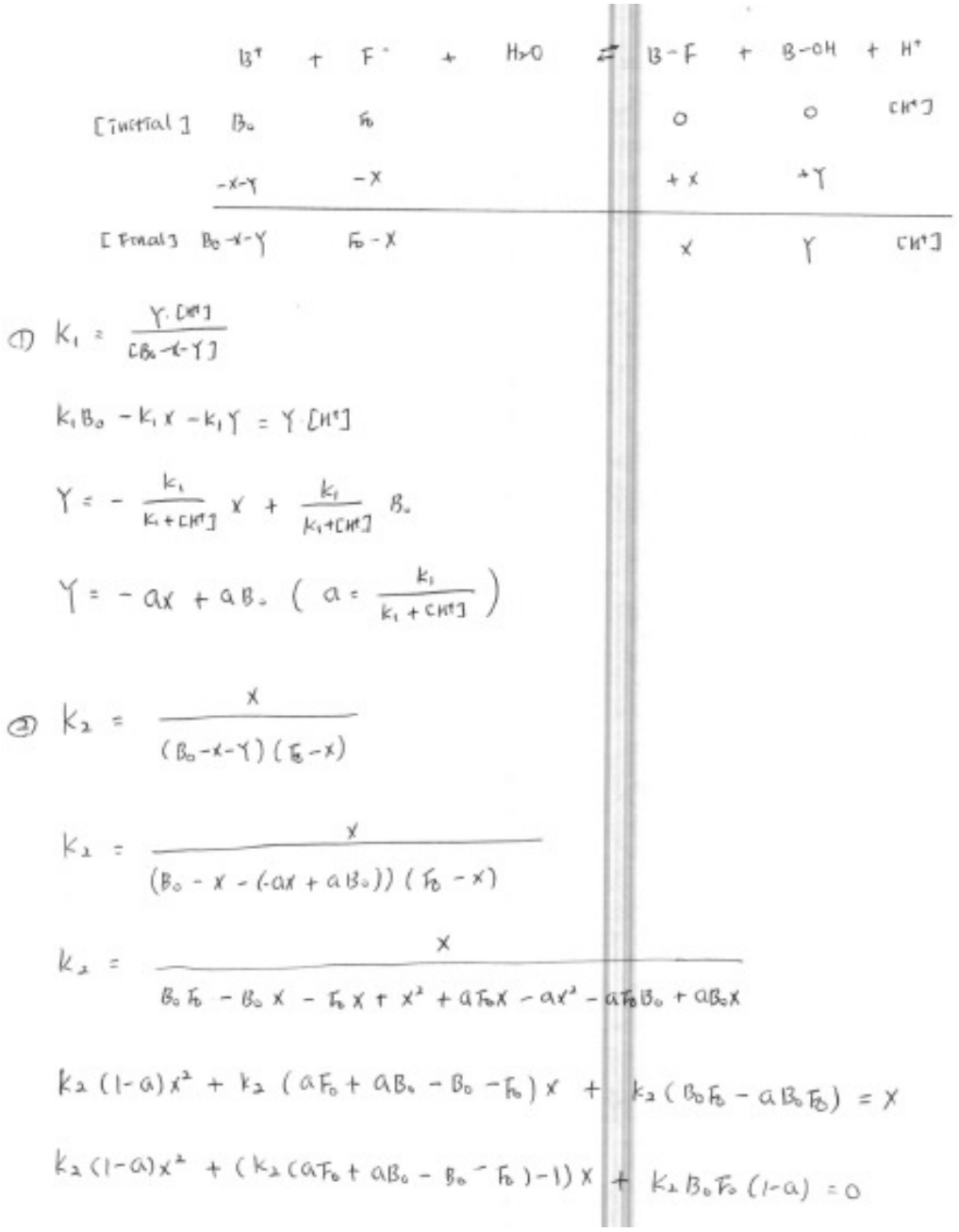

Figure 28. Derivation of the equation used to fit the fluoride titration data when hydroxide binding to the borane is competitive.

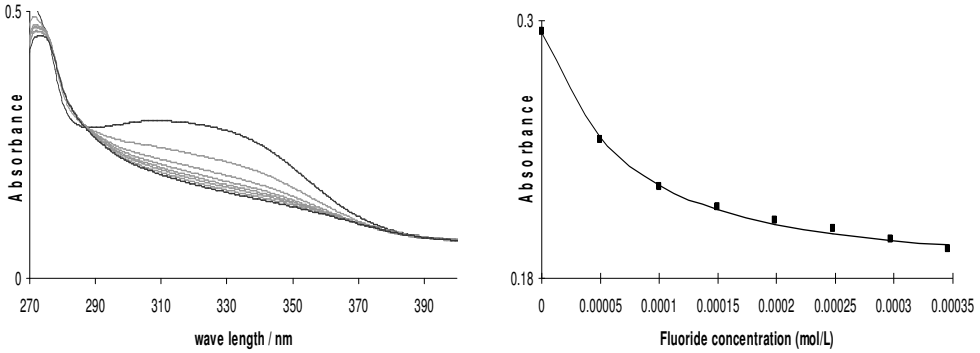

Figure 29. Left: Absorbance change of a solution of [**72**]$^+$ after successive additions of fluoride anions in H_2O (10mM pyridine buffer, pH 4.9); right: The absorbance was measured at 310 nm. Experimental data and calculated 1:1 binding isotherm with K = 30000 (±5000) M^{-1} using ε([**72**]$^+$) = 7300 M^{-1} cm^{-1}, ε(**72**-F) = 4900 M^{-1} cm^{-1} and ε(**72**-OH) = 2500 M^{-1} cm^{-1}. The second experimental point of the titration corresponds to a solution containing 100 μM or 1.9 ppm of fluoride ions; a 63% absorbance quenching is observed at this point.

Table 8. Absorbance of a solution of [**72**]$^+$ after successive additions of fluoride anions in water.

$C_{fluoride}$	Abs_{exp}	Abs_{calc}	$C_{fluoride}$	Abs_{exp}	Abs_{calc}
0.000000	0.295000	0.294433	0.000199	0.207000	0.206590
0.000050	0.245000	0.245297	0.000248	0.203000	0.202885
0.000100	0.223000	0.223247	0.000297	0.198000	0.200404
0.000149	0.213000	0.212555	0.000346	0.194000	0.198654

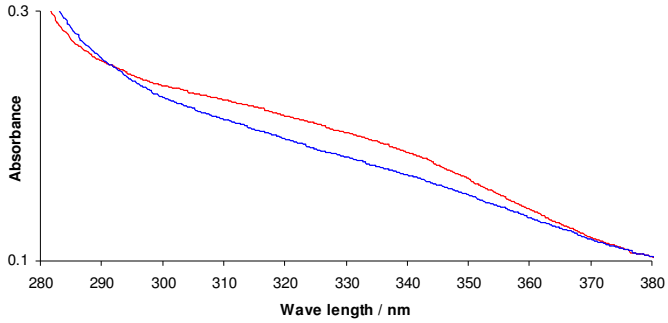

Figure 30. Absorbance change of a solution of [**72**]$^+$ after addition of 1.9 ppm fluoride in pure water (3 mL, 2.97 x 10^{-5}; MES buffer 10mM, pH 6); before (red line) and after (blue line). The absorbance was decreased by 50%.

2.6. Conclusion

The results presented in this paper show that the 1-dimesitylboryl-4-phosphonio-benzenes [**14**]$^+$, [**70**]$^+$, [**71**]$^+$, and [**72**]$^+$ are water stable and reversibly form the corresponding hydroxide complexes under basic conditions. More importantly, we also show that the Lewis acidity of these cationic boranes depends on the nature of the phosphorus substituents and readily increases with the hydrophobic character of the phosphonium unit. This trend can be observed both in the pK_{R+} value of the different cationic boranes as well as in their fluoride binding constants. While the exact origin of this effect is still under study, we propose that the decreased solvation of the most hydrophobic cationic boranes facilitates the covalent ion pairing process that occurs upon reaction with fluoride. In the series of compound studied, the resulting Lewis acidity increase is substantial and exceed one order of magnitude on going from [**14**]$^+$ to [**72**]$^+$. In turn, [**72**]$^+$ is sufficiently fluorophilic to bind fluoride ions below the EPA contaminant level. These results indicate that phosphonium boranes related to [**72**]$^+$

could be used as molecular recognition units in chemosensors for drinking water analysis.

2.7. Experimental Section

General Considerations. [**14**]I and (4-bromophenyl)dimesitylborane was prepared by following the known method. Iodoethane, 1-iodidopropane, dimesitylboron fluoride, potassium fluoride, nickel(II) bromide, triphenyl and potassium bromide were purchased from Aldrich, methyl iodide from Across. Solvents were dried by passing through an alumina column (toluene, acetonitrile), using activated 4 Å molecular sieves (benzonitrile) or reflux under N_2 over Na/K (Et_2O and THF). UV-vis spectra were recorded on an Ocean Optics USB4000 spectrometer with a Ocean Optics ISS light source. Elemental analyses were performed by Atlantic Microlab (Norcross, GA). pH Measurements were carried out with a Radiometer PHM290 pH meter equipped with a VWR SympHony electrode. NMR spectra were recorded on Varian Inova 300 FT NMR (299.96 MHz for ^{1}H, 121.43 MHz for ^{31}P) and Varian Unity Inova 400 FT NMR (399.59 MHz for ^{1}H, 375.99 MHz for ^{19}F, 128.19 MHz for ^{11}B, 161.75 MHz for ^{31}P, 100.45 MHz for ^{13}C) spectrometers at ambient temperature. Chemical shifts δ are given in ppm, and are referenced against external $BF_3{\cdot}Et_2O$ (^{11}B), $CFCl_3$ (^{19}F), and 85% H_3PO_4 (^{31}P).

Crystallography. The crystallographic measurements were performed using a Bruker APEX-II CCD area detector diffractometer (Mo KR radiation, λ) 0.71069 Å) for **72**-F and **72**-OH and a Siemens SMART-CCD area detector diffractometer (Mo-Kα

radiation, λ = 0.71069 Å) for **14**-OH and [**72**]Br. In each case, a specimen of suitable size and quality was selected and mounted onto a nylon loop. The structure was solved by direct methods, which successfully located most of the non-hydrogen atoms. Subsequent refinement on F^2 using the SHELXTL/PC package (version 5.1) allowed location of the remaining non-hydrogen atoms.

Synthesis of [70]I. Iodoethane (0.1 mL, 1.25mmol) was added to a solution of 1-dimesitylboryl-4-diphenylphosphinobenzene (50 mg, 0.098 mmol) in MeCN (4 mL) at room temperature. The mixture was refluxed overnight and cooled to room temperature (rt). The solvent was removed in vacuo to yield a residue which was washed with Et_2O (5 mL) and isolated as a pale yellow solid by filtration. Additional washing with Et_2O (5 mL) afforded [**70**]I as a yellow solid (50 mg, 76% yield). ^{1}H-NMR (400 MHz, $CDCl_3$): δ 1.39 (d, t, 3H, $^3J_{H\text{-}P}$=20Hz, $^3J_{H\text{-}H}$=7.6Hz), 1.96 (s, 12H), 2.29 (s, 6H), 3.81 (d, q, 2H, $^2J_{H\text{-}P}$=12.6Hz, $^3J_{H\text{-}H}$=7.2Hz), 6.82 (s, 4H), 7.67-7.74(m, 8H), 7.78-7.83 (m, 6H). ^{13}C-NMR (100 MHz, $CDCl_3$): δ 6.93 (d, *J*=5.5 Hz), 17.72 (d, *J*=50.9 Hz), 21.22, 23.52, 117.76 (d, *J*=85.4 Hz), 120.23 (d, *J*=83.6 Hz) 128.54, 130.50 (d, *J*=12.5 Hz), 132.83 (d, *J*=9.5 Hz), 133.69 (d, *J*=9.5 Hz), 135.09 (d, *J*=2.7 Hz), 136.43 (d, *J*=12.2 Hz), 139.83, 140.49, 140.83, 153.37. ^{11}B-NMR (128 MHz, $CDCl_3$): δ +75.0. ^{31}P-NMR (161 MHz, $CDCl_3$): δ +26.26. Anal. Calcd for $C_{38}H_{43}BIOP$ ([**70**]I+H_2O): C, 66.68; H, 6.33. Found: C, 66.76; H, 6.19.

Synthesis of [71]I. 1-Iodopropane (0.1 mL, 1.03mmol) was added to a solution of 1-dimesitylboryl-4-diphenylphosphinobenzene (50 mg, 0.098 mmol) in Toluene (4 mL) at room temperature. The mixture was refluxed overnight and cooled to rt. The solvent was removed in vacuo to yield a residue which was washed with Et_2O (5 mL) and isolated as a pale yellow solid by filtration. Additional washing with Et_2O (5 mL) afforded [**71**]I as a yellow solid (50 mg, 75% yield). ^{1}H-NMR (400 MHz, $CDCl_3$): δ 1.25 (t, 3H, $^3J_{H-H}$=7.6 Hz), 1.70 (m, 2H), 1.96 (s, 12H), 2.29 (s, 6H), 3.73 (d, t, 2H, $^2J_{H-P}$=12.4 Hz, $^3J_{H-H}$=8 Hz), 6.81 (s, 4H), 7.68-7.84 (m, 14H). ^{13}C-NMR (100 MHz, $CDCl_3$): δ 15.37 (d, *J*=17.1 Hz), 16.60 (d, *J*=4.2 Hz), 21.21, 23.51, 24.77 (d, *J*=49.3 Hz), 117.95 (d, *J*=85.4 Hz), 120.53 (d, *J*=83.5 Hz), 128.52, 130.48 (d, *J*=12.5 Hz), 132.80 (d, *J*=9.5 Hz), 133.67 (d, *J*=9.9 Hz), 135.05 (d, *J*=3 Hz), 136.40 (d, *J*=12.1 Hz), 139.89, 140.68, 140.82, 153.28. ^{11}B-NMR (128 MHz, $CDCl_3$): δ +78.0. ^{31}P-NMR (161 MHz, $CDCl_3$): δ +23.85. Anal. Calcd $C_{39}H_{45}BIOP$ ([**71**]I+H_2O): C,67.06; H, 6.49. Found: C, 67.05; H, 6.35.

Synthesis of [72]Br. A mixture of $NiBr_2$ (0.335 g, 1.53 mmol), PPh_3 (0.67 g, 2.55 mmol) and (4-bromophenyl)dimesitylborane (0.67 g, 1.65 mmol) in benzonitrile (30 mL) was heated at 200 °C for 3 h. After cooling to rt, the solvent was removed in *vacuo*. The residue was extracted using CH_2Cl_2 (20 mL) and water (10 mL) containing KBr (10 weight %). The organic layer was separated, dried over $MgSO_4$, filtered and concentrated in *vacuo* to a final volume of about 3 mL. This concentrate was further purified by flash chromatography over silica gel using first ethyl acetate (50 mL) and

then methanol (50 mL). The methanol fraction was then dried under in *vacuo* to afford [**72**]Br as a pale yellow solid. Further purification was achieved by recrystallization induced by diffusion of Et_2O into a concentrated solution of CH_3CN (0.55 g, 50 % yield). ^{1}H-NMR (300 MHz, $CDCl_3$): δ 1.98 (s, 12H), 2.29 (s, 6H), 6.83 (s, 4H), 7.53-7.68 (m, 8H), 7.75-7.85 (m, 8H), 7.90-7.95 (m, 3H). ^{13}C-NMR (100 MHz, $CDCl_3$): δ 21.13, 23.45, 116.96 (d, *J*=88.8 Hz), 119.73 (d, *J*=86.9 Hz), 128.50, 130.79 (d, *J*=11.4 Hz), 130.86 (d, *J*=12.6 Hz), 133.43 (d, *J*=9.9 Hz), 134.22 (d, *J*=10.3 Hz), 135.89, 136.34 (d, *J*=12.6 Hz), 139.99, 140.60, 153.97 (bs). ^{11}B-NMR (128 MHz, $CDCl_3$): δ +75.0. ^{31}P-NMR (121 MHz, $CDCl_3$): δ +22.71 (s). Anal. Calcd for $C_{42}H_{44}BBrO_{1.5}P$ ([**72**]Br+1.5H_2O): C, 72.64; H, 6.39. Found: C, 72.58; H, 6.31.

Synthesis of 14-OH. [**1**]I (50 mg, 0.077 mmol) was dissolved in H_2O/MeOH (9/1, v/v, 3 mL) and treated with an aqueous solution of NaOH (2 mL, 2.5 M). After stirring for 30 min, CH_2Cl_2 (10 mL) was added to the reaction mixture. The organic layer was separated, dried over $MgSO_4$, filtered and concentrated in *vacuo*. The residue was washed with Et_2O (5 mL) to afford **14**-OH as a white solid (30 mg, 72 % yield). ^{1}H-NMR (400 MHz, $CDCl_3$): δ 2.00 (s, 12H), 2.19 (s, 6H), 2.54 (d, 3H, $^2J_{H\text{-}P}$=12.8 Hz), 6.62 (s, 4H), 6.81 (bs, 1H), 6.93 (bs, 1H), 7.48-7.53 (m, 4H), 7.65 (m, 5H), 7.77-7.79 (m, 2H), 8.61 (bs, 1H). ^{13}C-NMR (100 MHz, $CDCl_3$): δ 10.15 (d, *J*=59.2 Hz), 20.72, 25.63, 108.15 (d, *J*=91.9Hz), 120.78 (d, *J*=88.5Hz), 128.74, 129.73, 130.37 (d, *J*=12.6 Hz), 131.51, 133.10 (d, *J*=10.2 Hz), 134.98 (d, *J*=3Hz), 136.45, 141.12, 156.95. ^{11}B-NMR

(128 MHz, $CDCl_3$): δ +0.29. ^{31}P-NMR (121 MHz, $CDCl_3$): δ +18.63. Anal. Calcd for $C_{37.33}H_{40.33}BClOP$ (**14**-OH+0.33$CHCl_3$): C, 77.01; H, 6.98. Found: C, 77.08; H, 7.11.

Synthesis of 72-OH. [**72**]Br (50 mg, 0.075 mmol) was dissolved in H_2O (3 mL) and treated an aqueous solution of NaOH (2 mL, 2.5 M). After stirring for 30 min, CH_2Cl_2 (10 mL) was added to the reaction mixture. The organic layer was separated, dried over $MgSO_4$, filtered and concentrated in *vacuo*. The residue was washed with Et_2O (5 mL) to afford **72**-OH as a white solid (35 mg, 77 % yield). ^{1}H-NMR (400 MHz, $CDCl_3$): δ 2.03 (s, 12H), 2.20 (s, 6H), 6.63 (s, 4H), 6.99 (bs, 1H), 7.56-7.67 (m, 14H), 7.80-7.83 (m, 3H), 8.62 (bs, 1H). ^{13}C-NMR (100 MHz, $CDCl_3$): δ 20.82, 25.56, 105.60 (d, *J*=91.1 Hz), 119.74 (d, *J*=88.8 Hz), 128.43, 130.05 (d, *J*=12.5 Hz), 131.06, 131.86, 134.24 (d, *J*=9.9 Hz), 134.78 (d, *J*=2.7 Hz), 136.84 (d, *J*=12.6Hz), 141.47, 156.58. ^{11}B-NMR (128 MHz, $CDCl_3$): δ +0.16. ^{31}P-NMR (121 MHz, $CDCl_3$): δ +22.44. Anal. Calcd for $C_{42.5}H_{44}BCl_1O1.5P$ (**72**-OH+0.5CH_2Cl_2+0.5H_2O): C, 77.81; H, 6.76. Found: C, 75.97, H, 6.70.

Syntheses of 70-OH and 71-OH. These two compounds, which have not been isolated, were prepared as follows and characterized in situ. A D_2O solution of NaOH (0.9 mL, 2.5 M) was mixed with a d_4-MeOH solution of the cationic borane salt ([**70**]I or [**71**]I) (0.1 mL, 0.2 M) in an NMR tube. The corresponding hydroxide adduct (**70**-OH or **71**-OH), which precipitated immediately upon mixing, was extracted with $CDCl_3$. The $CDCl_3$ layer, which separated at the bottom of the NMR tube, was analyzed by

multinuclear NMR spectroscopy. NMR data for **70**-OH: ^{1}H-NMR (400 MHz, $CDCl_3$): δ 1.37 (d, t, 3H, $^{3}J_{H\text{-}P}$ = 19.2 Hz, $^{3}J_{H\text{-}H}$ = 7.6 Hz), 1.95 (s, 12H), 2.18 (s, 6H), 2.90 (m, 2H), 6.61 (s, 4H), 7.00 (bs, 1H), 7.52-7.67 (m, 10H), 7.77-8.00 (m, 2H), 8.47 (bs, 1H). ^{11}B-NMR (128 MHz, $CDCl_3$): δ +0.36. ^{31}P-NMR (161 MHz, $CDCl_3$): δ +23.64. NMR data for **71**-OH: ^{1}H-NMR (400 MHz, $CDCl_3$): δ 1.14 (t, 3H, $^{3}J_{H\text{-}H}$ = 7.2Hz), 1.74 (m, 2H), 1.96 (s, 12H), 2.18 (s, 6H), 2.81 (m, 2H), 6.61 (s, 4H), 7.00 (bs, 1H), 7.51-7.66 (m, 10H), 7.76-7.79 (m, 2H), 8.47 (bs, 1H). ^{11}B-NMR (128 MHz, $CDCl_3$): δ +0.25. ^{31}P-NMR (161 MHz, $CDCl_3$): δ +21.41.

Synthesis of 72-F. [**72**]Br (200 mg, 0.3 mmol) was dissolved in MeOH (5 mL) and treated with excess of KF which resulted in the formation of a white solid. After 30 min, the solid was isolated by filtration, washed with MeOH, and dried in *vacuo* to afford **72**-F as a white solid (100 mg, 55% yield). ^{1}H-NMR (300 MHz, $CDCl_3$): δ 2.01 (s, 12H), 2.19 (s, 6H), 6.62 (s, 4H), 7.06 (bs, 1H), 7.54-7.70 (m, 14H), 7.78-7.85 (m, 3H), 8.41 (br, 1H). ^{13}C-NMR (100 MHz, $CDCl_3$): δ 20.87, 25.03, 106.61 (d, *J*=91.9 Hz), 119.50 (d, *J*=89.2 Hz), 128.25, 130.16, 131.39, 132.24, 134.25, 134.89, 136.16, 141.69, 153.08. ^{11}B-NMR (128 MHz, $CDCl_3$): δ +5.22. ^{31}P-NMR (121 MHz, $CDCl_3$): δ +22.58. ^{19}F-NMR (376 MHz, $CDCl_3$): δ −173.83. Anal. Calcd for $C_{42.17}H_{41.33}BCl_{0.33}FP$ (**72**-F+0.17CH_2Cl_2): C, 81.61; H, 6.71. Found: C, 81.57; H, 6.65.

Syntheses of 70-F and 71-F. These two compounds, which have not been isolated, were prepared by mixing a d_4-MeOH solution of the cationic borane salt ([**70**]I

or [**71**]I) (15 mg) with excess of KF in an NMR tube. The resulting clear solution was analyzed by multinuclear NMR spectroscopy. NMR data for **70**-F: ^{1}H-NMR (400 MHz, CD_3OD): δ 1.37 (d, t, 3H, $^{3}J_{H\text{-}P}$=19.6 Hz, $^{3}J_{H\text{-}H}$=7.2 Hz), 1.90 (s, 12H), 2.16 (s, 6H), 3.30 (m, 2H), 6.54 (s, 4H), 7.30 (bs, 1H), 7.43 (bs, 2H), 7.74-7.81 (m, 8H), 7.85-7.89 (m, 2H), 8.15 (bs, 1H). ^{11}B-NMR (128 MHz, CD_3OD): δ +4.35. ^{31}P-NMR (121 MHz, CD_3OD): δ +25.31. ^{19}F-NMR (376 MHz, CD_3OD): δ −171.31. NMR data for **71**-F: ^{1}H-NMR (400 MHz, CD_3OD): δ 1.17 (t, 3H, *J*=7.2 Hz), 1.73 (m, 2H), 1.90 (s, 12H), 2.16 (s, 6H), 3.27 (m, 2H), 6.54 (s, 4H), 7.30 (bs, 1H), 7.42 (bs, 2H), 7.72-7.80 (m, 8H), 7.84-7.89 (m, 2H), 8.15 (bs, 1H). ^{11}B-NMR (128 MHz, CD_3OD): δ +7.47. ^{31}P-NMR (121 MHz, CD_3OD): δ +22.98. ^{19}F-NMR (376 MHz, CD_3OD): δ −171.62.

Acid-base Titration of $[14]^+$, $[70]^+$, $[71]^+$ and $[72]^+$ in H_2O/MeOH (9/1, v/v). A solution of [**14**]I (3.0 mL, 3.65×10^{-5} M; MES buffer 9mM), [**70**]I (3.0 mL, 6.0×10^{-5} M; MES buffer 9mM) [**71**]I (3.0 mL, 6.3×10^{-5} M; MES buffer 9mM) [**72**]Br (3.0 mL, 6.2×10^{-5} M; MES buffer 9mM) was titrated by incremental addition of a solution of NaOH in water. The resulting data was fitted to the equilibrium shown in eq 1 which yielded the relevant K_R^+. The solutions were buffered in order to obtain a better control of the pH near the equivalence point.

Acid-base of $[72]^+$ in Pure Water. A solution of [**72**]Br (3.0 mL, 5.1×10^{-5} M; pyridine buffer, 10mM) was titrated by incremental addition of a solution of NaOH in water. The resulting data was fitted to the equilibrium shown in eq 1 which yielded the

relevant K_{R+}. The solution was buffered in order to obtain a better control of the pH near the equivalence point.

Titration of $[14]^+$, $[70]^+$, $[71]^+$ and $[72]^+$ with Fluoride in H_2O/MeOH (9/1, v/v). A solution of [**14**]I (3.0 mL, 6.17×10^{-5} M; pyridine buffer 9mM, pH 4.9), [**70**]I (3.0 mL, 5.43×10^{-5} M; pyridine buffer 9mM, pH 4.9) [**71**]I (3.0 mL, 5.9×10^{-5} M; pyridine buffer 9mM, pH 4.9) [**72**]Br (3.0 mL, 5.83×10^{-5} M; pyridine buffer 9mM, pH 4.6) was titrated by incremental addition of a solution of KF in water (0.3 M for $[\mathbf{14}]^+$, $[\mathbf{70}]^+$ and 0.03 M for $[\mathbf{71}]^+$ and $[\mathbf{72}]^+$).

Titration of $[72]^+$with fluoride in pure water. A solution of [**72**]Br (3.0 mL, 3.67×10^{-5} M; pyridine buffer, 10mM, pH 4.9) was titrated by incremental addition of a solution of KF (0.03 M in water).

Calculation of % decrease when 2ppm amount of fluoride was added (pH 6).

After adding 16 eq of KF into the solution, the absorbance was close to 0.18 at 320nm;

The initial absorbance = 0.216

The final absorbance = 0.18

When 1.9 ppm amount of fluoride is added to the solution, the absorbance was 0.198

% decrease = (0.216-0.198) / (0.216-0.18)

= 50 %

CHAPTER III

FLUORESCENT TURN-ON SENSING OF CYANIDE IONS IN WATER BY PHOSPHONIUM BORANES

3.1. Introduction

Cyanide is a highly toxic anion which has become a key component of many industrial processes. It is also produced naturally by a number of higher order plants which use it as a protection against predators. Release of this anion into the environment as well as an increase in the farming and consumption of cyanogenic plants such as cassava have served to spark a renewed interest in methods that can be used to sense the presence of this anion in aqueous media.

One of the current strategies adopted for the design of cyanide sensors is based on the use of electrophilic organic derivatives which interact with the cyanide anion via formation of a new covalent bond.[46, 49, 50, 61, 65, 68, 69] Examples of such compounds include benzil derivatives, dipyrrole carboxamides, oxazines,' acridinium salts, trifluoroacetamides and aldehydes.[54] Although advantageous properties have been discovered, only a limited number of receptors function in water.[54, 66, 68, 71, 73] Some of these receptors necessitate basic pH and high cyanide concentrations. Moreover, the reversibility of their reaction with cyanide is not always well documented. Because of these limitations, strategies that rely on the use of Lewis acidic derivatives have been considered. Such derivatives include zinc-porphyrins,[146, 147] iron-hemes,[84] and transition metal complexes[148] that interact with the cyanide anion via formation of a strong

coordination bond. This approach, which is typically characterized by elevated binding constants, has been successfully applied to the detection of ppm level of cyanides. Some of these receptors have also been shown to be compatible with biological matrices, making the detection of cyanide possible directly in plants.[76, 77]

As demonstrated in by a series of recent contributions, three coordinate boranes possessing an accessible boron center can also be used as sensors for cyanide anions.[7, 17, 20, 22, 30, 118, 149-151] While neutral boranes can only be used in mostly organic environments,[30, 149] we have demonstrated that the incorporation of peripheral cationic groups in such compounds could be used to enhance their cyanide ion affinity.[17, 20, 150] Examples of such compounds include [**13**]$^+$ which captures cyanide in water at neutral pH.[17] Although the cyanide affinity displayed by some of these boranes is very high, their practical use remains limited by the nature of the photophysical response observed during the recognition event. Indeed, cyanide coordination leads to population of the boron empty p-orbital thus quenching the absorbance and fluorescence of the triarylboron chromophore. The turn-off rather than turn-on response observed in these complexes is not ideal from an analytical point of view and constitute one of the major limitations affecting the practical use of cationic boranes as cyanide sensors.

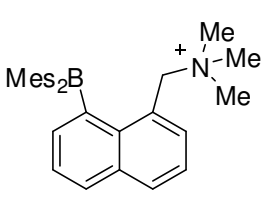

[**9**]$^+$

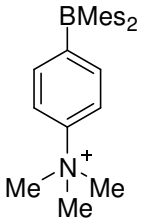

[**13**]$^+$

It has been shown by Wang,[8, 28, 29, 152] and later by Fang,[135] that bifunctional amino-boranes containing both a triarylamine and a triarylborane unit exhibit a CT transition involving the amine as a donor and the borane as the acceptor. These researchers have also shown that anion coordination to the boron center leads to a quenching of this process, accompanied by a turn-on of the fluorescence of the triarylamine. These anion sensors are neutral and have only been shown to operate in organic solvents. In an effort to develop water compatible turn-on anion sensors, we have decided to emulate the elegant approach pioneered by Wang and see if it could be translated to the case of cationic boranes. With this approach in mind, we have now decided to investigate the synthesis of cationic borane/fluorophore conjugates, their cyanide affinity, and their photophysical responses.

3.2. Electron-accepting properties of phosphonium boranes

It occurred to us that phosphonium boranes derived from the neutral phosphinoborane **69** via alkylation of the phosphorus atom may constitute an ideal cyanide-sensing platform that could be easily conjugated with a pendant fluorophore (Figure 31). Prior to engaging into the synthesis of the said conjugates, we decided to survey the electron acceptor characteristic of the prototypical phosphonium borane [**14**]I whose synthesis has been previously reported. The cyclic voltammogram of [**14**]$^+$ in THF displays a single reversible reduction wave at $E_{1/2}^{Red}$ = –1.81 V vs Fc/Fc$^+$ (Figure 32). The reduction potential of [**14**]$^+$ is distinctively more positive than that of neutral boranes,[153-162] such as Mes_3B which is reduced at –2.73 V (vs Fc/Fc$^+$).[160] This reduction

potential difference may be assigned to the cationic character of [**14**]$^+$ which increases its electrophilicty.[150]

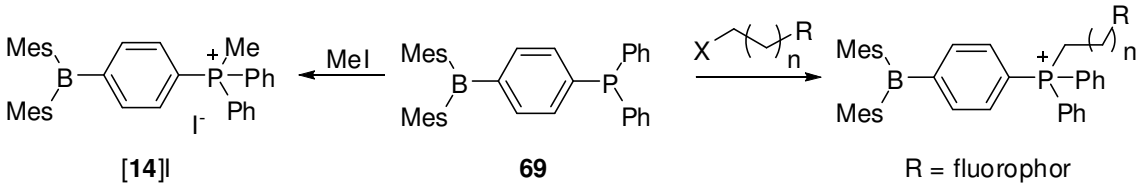

Figure 31. Synthesis of phosphonium borane/fluorophore conjugates.

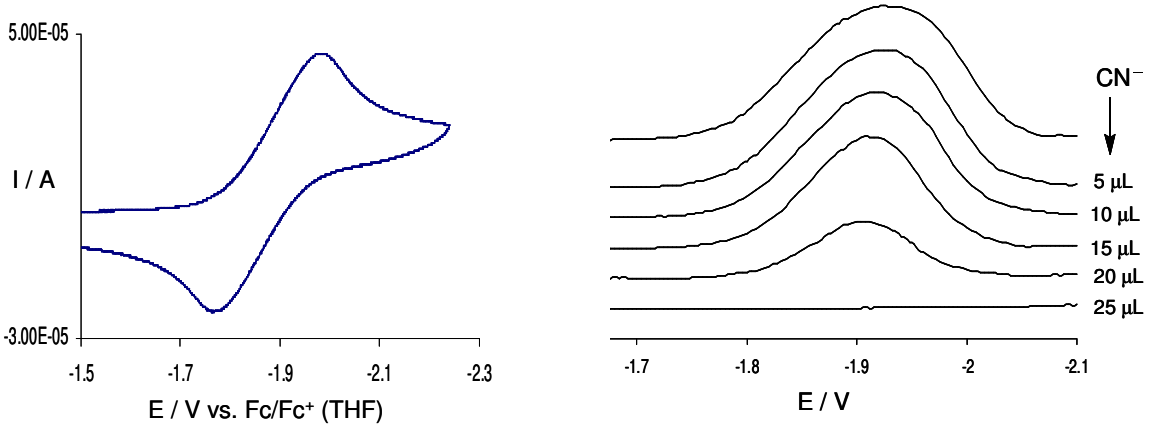

Figure 32. Left: Cyclic voltammograms of [**14**]$^+$ in THF with a glassy-carbon working electrode (0.1M*n*Bu_4NPF_6). Scan rates: v = 200 mV s^{-1} for [**14**]$^+$. Right: changes in the differential pulsed voltammogram of [**14**]I (0.0016 M) observed upon the addition of Et_4NCN (0.11 M in CH_3CN) to a THF solution.

It also indicates that cationic boranes such as [**14**]$^+$ should possess enhanced electron accepting properties in charge transfer processes. By arbitrarily setting the HOMO energy of ferrocene to –4.8 eV,[163] these measurements place the LUMO level of

cationic boranes such as [**14**]$^+$ in THF solution at near –3.0 eV. In turn, fluorophores whose HOMO and excited state lie respectively below and above –3.0 eV should be efficiently quenched by cationic boranes such as [**14**]$^+$. On the basis of these considerations we decided to focus on the anthracenyl and dansyl chromophores whose HOMO and excited state energy fit the energetic requirement (Figure 33).

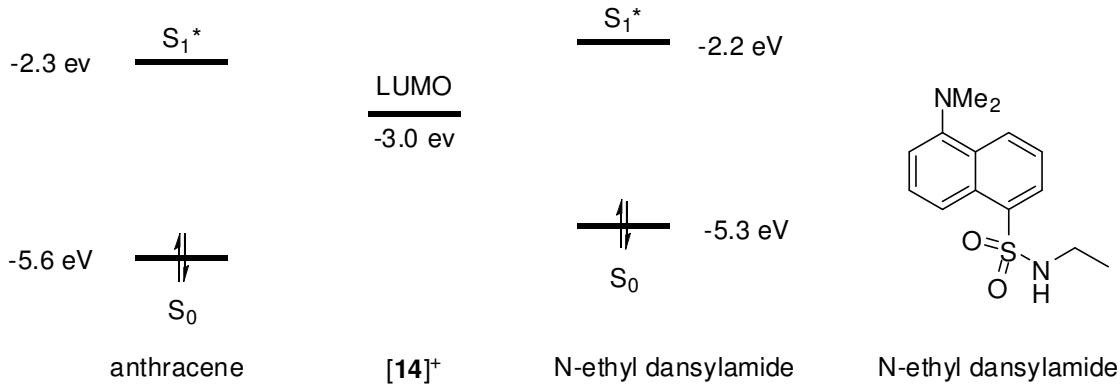

Figure 33. HOMO of anthracenyl[164] and N-ethyl dansylamide[165] energy values were obtained from first oxidation potential values (E_{ox}) measured in acetonitrile against ferrocene and calculated by taking the HOMO energy value of ferrocene to be –4.8 eV with respect to zero energy level. The first exited state energy was calculated from the intercept of the normalized plot of the absorption and fluorescence spectra.

3.3. Cyanide ion complexation of [**14**]$^+$

Having confirmed the potential of phosphonium boranes to act as acceptors in charge transfer processes, we decided to investigate the reactivity of [**14**]I toward cyanide. To this end, [**14**]I was allowed to react with NaCN in MeOH which resulted in the precipitation of **14**-CN in 70% yield. This zwitterion has been fully characterized. Some of its salient spectroscopic features include: 1) a ^{11}B NMR resonance at $\delta =$ −13.28 ppm indicating the presence of a four-coordinate boron center; 2) an intense IR

band at 2165.5 cm^{-1} confirming the presence of the boron-bound cyano group. Examination of the structures shows coordination of the cyanide anion to the boron center via a B-C bond of 1.617(5) Å which are comparable to those typically found in triarylcyanoborate anions such as $[Ph_3BCN]^-$ (1.65 Å) (Figure 34, Table 9). The sum of the C_{aryl}-B-C_{aryl} angles (Σ(C-B-C)=339.9°) indicates that cyanide binding induces a substantial pyramidalization of the boron atom that is similar to that observed in **14**-F (Σ (C-B-C)=339.4°). This reaction can also be followed electrochemically by monitoring the progressive quenching of the reduction wave of the $[\mathbf{14}]^+$ induced by incremental addition of cyanide. This quenching, which reflects the binding of the cyanide anion to the borane, also indicates that the electron accepting properties of phosphonium boranes are neutralized by coordination of an anion to the boron center.

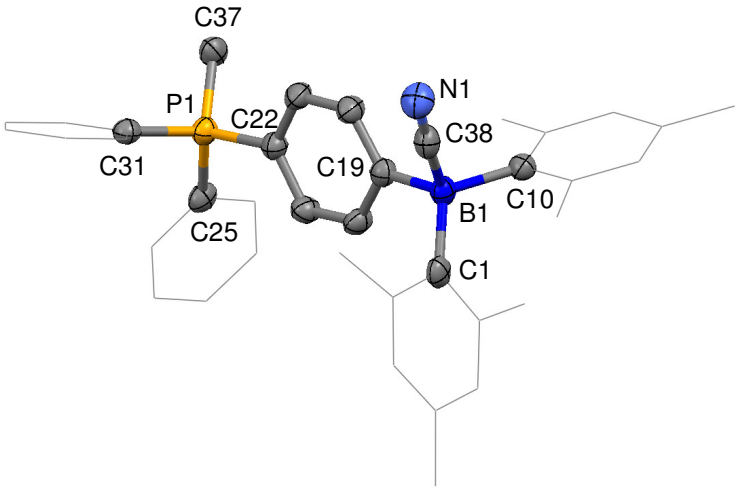

Figure 34. Crystal structure of **14**-CN with thermal ellipsoids set at 50% probability level. Hydrogen atoms are omitted for clarity. Pertinent metrical parameters can be found in the text.

Table 9. Crystal data, data collections, and structure refinement for **14**-CN.

Crystal data	**14**-CN·(H_2O)·(CH_3OH)
Formula	$C_{39}H_{45}BNO_2P$
M_r	601.54
crystal size (mm^3)	0.40 x 0.11 x 0.08
crystal system	Monoclinic
space group	*C*2/*c*
a (Å)	23.119(3)
b (Å)	12.2595(16)
c (Å)	24.171(3)
α (°)	90
β (°)	105.593(2)
γ (°)	90
V ($Å^3$)	6598.8(15)
Z	8
ρ_{calc} (g cm^{-3})	1.211
μ (mm^{-1})	0.119
F(000)	2576
Data collection	
T (K)	140(2)
scan mode	ω
hkl range	-30 → +30, -16 → +16, -32 → +32
measd reflns	37715
unique reflns [R_{int}]	8073 [0.0926]
reflns used for refinement	8073
Refinement	
refined parameters	397
GooF	1.006
R_1,[a] wR_2[b] all data	0.1539, 0.1937
ρ_{fin} (max/min) (e $Å^{-3}$)	0.722, -0.768

[a] $R_1 = \Sigma||Fo| - |Fc||/\Sigma|Fo|$. [b] $wR_2 = [[\Sigma w(Fo^2 - Fc^2)^2]/[\Sigma w(Fo^2)^2]]^{1/2}$.

3.4. Synthesis and properties of the borane/fluorophore conjugates

To test this idea, **69** was treated with 9-bromomethyl anthracene in refluxing toluene to afford [**73**]Br in 82% yield. A similar reaction involving **69** and N-(3-bromopropyl)-5-(dimehtylamino)-1-naphthalenesulfonamide in acetonitrile afforded [**74**]I in 40% yield (Figure 35).

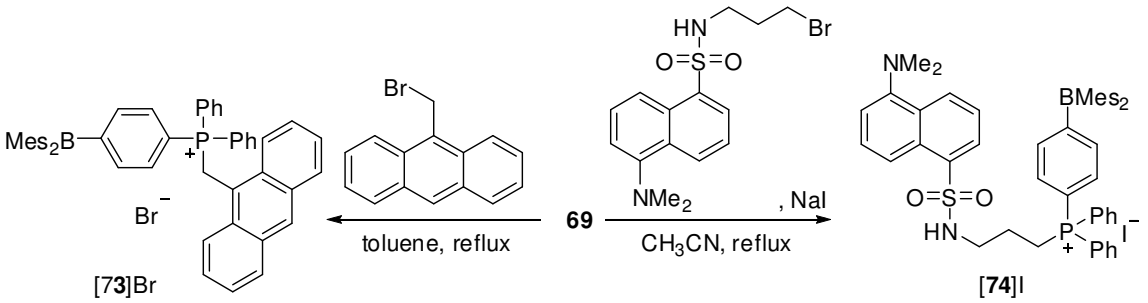

Figure 35. Synthesis of [**73**]Br and [**74**]I.

These phosphonium salts have been fully characterized. In all cases, for long periods of time, the ^{11}B NMR resonance measured in $CDCl_3$ is not detected. The presence of a phosphonium center gives rise to a characteristic ^{31}P NMR resonance detected at 26.3 and 23.8 for [**73**]Br and [**74**]I, respectively. The absorbance spectra of these new phopshonium boranes are shown in Figure 36. The low energy part of the absorption spectrum of [**73**]Br in MeOH is dominated by anthracenyl-based absorptions which can be identified based on the characteristic vibronic progression. The broad absorption band centered at λ_{max} = 340 nm is close to that observed for simple phosphonium

boranes such as [**14**]$^+$ and can be assigned to the triarylboron chromophore. In the case of [**74**]I, a single broad absorption band bearing contributions from both the triarylboron and dansyl chromophores is observed at λ_{max} = 335 nm in MeOH.

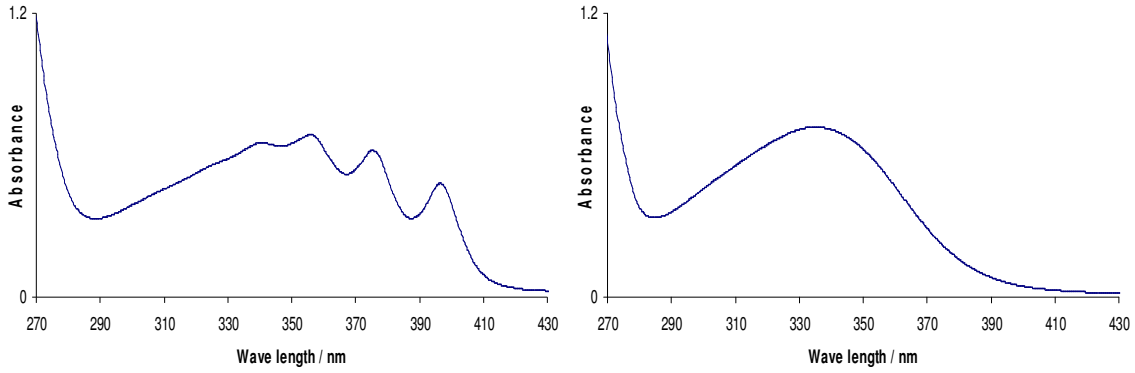

Figure 36. UV-vis absorption spectrum of [**73**]$^+$ (left) and [**74**]$^+$ (right) in methanol solution.

These two compounds are weakly fluorescent with emission bands centered at λ_{fluo} = 470 nm for [**73**]$^+$ ($\Phi = 0.7\%$) and λ_{fluo} = 475 nm for [**74**]$^+$ ($\Phi = 1.7\%$) in chloroform. Bearing in mind that the fluorescence quantum yields of the anthracene and dansyl chromophores are typically much higher, the weak fluorescence of [**73**]$^+$ and [**74**]$^+$ may be the result of an intramolecular charge transfer process involving the excited chromophore as the donor and the phosphonium borane as the acceptor. To further test this hypothesis, we decided to monitor the fluorescence intensity of these compounds upon cyanide coordination. As demonstrated electrochemically in the case of [**14**]$^+$ (Figure 32), cyanide binding to [**73**]$^+$ and [**74**]$^+$ should result in a neutralization of the

electron accepting properties the phosphonium borane moiety thereby inhibiting electron transfer. In line with these expectations, addition of cyanide to [**73**]$^+$ and [**74**]$^+$ in methanol results in a major increase of the fluorescence intensity of the conjugates assigned to the formation of **73**-CN and **74**-CN, respectively. This increase can be quantified by a comparison of the quantum yields of the phosphonium borane conjugates (ϕ = 0.007 and 0.017 for [**73**]$^+$ and [**74**]$^+$) and that of their cyanide adducts (ϕ = 0.140 and 0.490 for **73**-CN and **74**-CN, respectively). To confirm their formation, **73**-CN and **74**-CN have been isolated and characterized. Both derivatives precipitate spontaneously upon addition of KCN to a methanol solution of the corresponding phosphonium boranes whose spectroscopic features ($\delta(^{11}B)$ = −13.53 ppm for **73**-CN and −12.45 ppm for **74**-CN; $\nu(CN^-)$ = 2163.2 cm^{-1} for **73**-CN and 2166.8 cm^{-1} for **74**-CN). The crystal structures of **74-**CN has also been determined (Figure 37 and Table 10). This compound crystallizes in the *P*-1 space group. Examination of the crystal structure confirms the presence a pendant dansyl chromophore as well as of a zwitterionic phosphonium/cyanoborate moiety. The structure of the latter is close to that observed in **14**-CN as indicated by the sum of the C_{aryl}-B-C_{aryl} angles ($\sum$(C-B-C) = 338.53°) and the B(2)-C(53) bond of 1.616 Å.

Table 10. Crystal data, data collections, and structure refinement for **74**-CN.

Crystal data	**74**-CN
Formula	$C_{52}H_{55}BN_3O_2PS$
M_r	827.83
crystal size (mm^3)	0.40 x 0.32 x 0.28
crystal system	Triclinic
space group	*P*-1
a (Å)	15.5546(11)
b (Å)	16.4483(10)
c (Å)	21.8088(14)
α (°)	72.301(4)
β (°)	73.109(4)
γ (°)	66.247(4)
V ($Å^3$)	4774.1(5)
Z	4
ρ_{calc} (g cm^{-3})	1.152
μ (mm^{-1})	0.143
F(000)	1760
Data collection	
T (K)	110(2)
scan mode	ω
hkl range	-17 → +17, -18 → +18, -24 → +24
measd reflns	86481
unique reflns [R_{int}]	14858 [0.1137]
reflns used for refinement	14858
Refinement	
refined parameters	1081
GooF	1.004
R_1,[a] wR_2[b] all data	0.1866, 0.1614
ρ_{fin} (max/min) (e $Å^{-3}$)	0.329, -0.244

[a] $R_1 = \Sigma||Fo| - |Fc||/\Sigma|Fo|$. [b] $wR_2 = [[\Sigma w(Fo^2 - Fc^2)^2]/[\Sigma w(Fo^2)^2]]^{1/2}$.

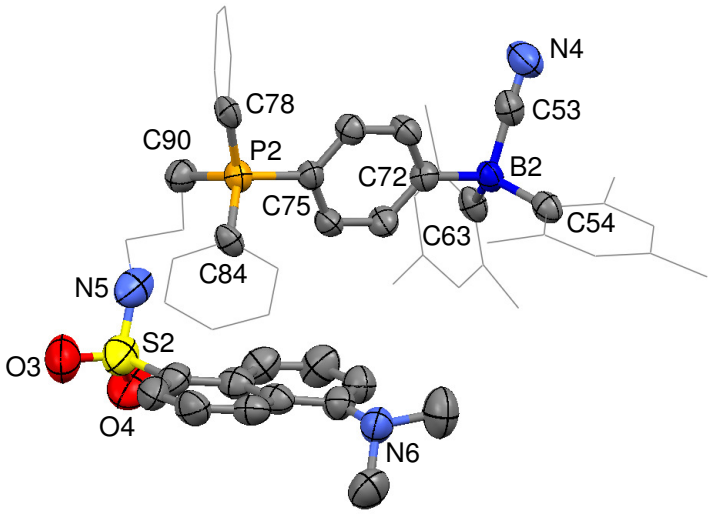

Figure 37. Crystal structure of **74**-CN with thermal ellipsoids set at 50% probability level. Hydrogen atoms are omitted for clarity. Pertinent metrical parameters can be found in the text.

3.5. Cyanide ion complexation of [**73**]$^+$ and [**74**]$^+$

Having observed that both [**73**]$^+$ and [**74**]$^+$ can be readily converted into their corresponding cyanide adduct, we decided to determine their cyanide binding constants in a protic solvent such as MeOH. To this end, UV-vis titrations experiments were carried out by addition of increasing amounts of cyanide to solution of the cationic boranes. Binding of the cyanide to the boron center of [**73**]$^+$ and [**74**]$^+$ resulted in a quenching of the absorption band of the triarylboron chromophore resulting a net decrease of the absorbance in the 300 – 370 nm range. The resulting data was fitted to a 1:1 binding isotherm affording binding constants of 1 (±0.1) × 10^6 M^{-1} for [**73**]$^+$ and K = 3 (±0.5) × 10^6 $M^{-1}$for [**74**]$^+$ (Figures 38 and 39, Tables 11 and 12) . A complete

quenching of the band was not observed because both the anthryl and dansyl chromophore also absorb in the 300 – 400 nm range.

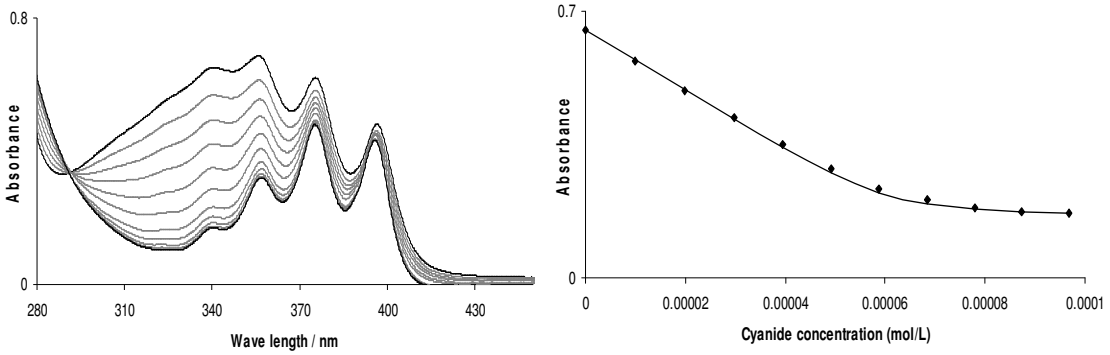

Figure 38. Left: Absorbance change of a solution of [**73**]Br after successive additions of cyanide anions; right: The absorbance was measured at 340 nm. Experimental data and calculated 1:1 binding isotherm with $K = 1(\pm 0.2) \times 10^6$ M^{-1} using $\varepsilon([\mathbf{73}]^+) = 10500$ M^{-1} cm^{-1} and $\varepsilon(\mathbf{73}\text{-CN}) = 2600$ M^{-1} cm^{-1}.

Table 11. Absorbance of a solution of [**73**]Br after successive additions of cyanide anions in MeOH.

$C_{cyanide}$	Abs_{exp}	Abs_{calc}	$C_{cyanide}$	Abs_{exp}	Abs_{calc}
0.0000E+00	0.651	0.651	5.8824E-05	0.233	0.224
9.9668E-06	0.569	0.572	6.8404E-05	0.205	0.193
1.9868E-05	0.493	0.493	7.7922E-05	0.185	0.179
2.9703E-05	0.422	0.417	8.7379E-05	0.175	0.172
3.9474E-05	0.350	0.343	9.6774E-05	0.170	0.168
4.9180E-05	0.286	0.276			

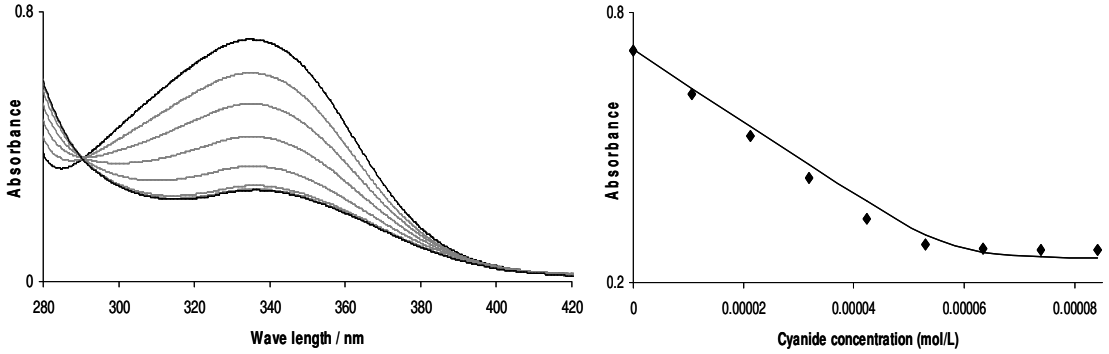

Figure 39. Left: Absorbance change of a solution of [**74**]I after successive additions of cyanide anions; right: The absorbance was measured at 335 nm. Experimental data and calculated 1:1 binding isotherm with $K = 3(\pm1) \times 10^6$ M^{-1} using $\varepsilon([\mathbf{74}]^+) = 12300$ M^{-1} cm^{-1} and $\varepsilon(\mathbf{74}\text{-CN}) = 4300$ M^{-1} cm^{-1}.

Table 12. Absorbance of a solution of [**74**]I after successive additions of cyanide anions in MeOH.

$C_{cyanide}$	Abs_{exp}	Abs_{calc}	$C_{cyanide}$	Abs_{exp}	Abs_{calc}
0.00E+00	0.717	0.718	5.29E-05	0.284	0.307
1.06E-05	0.619	0.632	6.34E-05	0.275	0.267
2.13E-05	0.527	0.547	7.38E-05	0.273	0.257
3.18E-05	0.432	0.462	8.42E-05	0.271	0.253
4.24E-05	0.342	0.380			

Encouraged by these elevated binding constants, we decided to test if these cationic boranes could be used in water. While [**73**]$^+$ was found to irreversibly decompose in H_2O/MeOH (6/4, v/v), the fluorescence spectrum of a solution of [**74**]$^+$ at pH 7 in H_2O/MeOH (6/4, v/v) remained unchanged for 1 hour. Further information into the stability of [**74**]$^+$ was obtained by monitoring its UV-vis spectrum as a function of pH. At pH 5.6, the characteristic absorption band of [**74**]$^+$ at 333 nm is readily observed

indicating that the boron center remains triganol planar (Figure 40). At pH 6.8, an initial decrease of the band is observed signaling the onset of hydroxide binding. This phenomenon is quickly followed by formation of a precipitate assigned to the hydroxide adduct. Such adducts are not unprecedented and have been previously obtained with other phosphonium boranes such as [**72**]$^+$. In agreement with the formation and precipitation of the hydroxide adduct, we found that re-acidification of the solution leads to a 98% revival of the absorption band of [**74**]$^+$ at 333 nm. These observations indicate that the pK_{R+} of [**74**]$^+$ cannot be accurately determined because of the precipitation of **74**–OH, and is in the range 7 – 8.

$$[R_3B]^+ + H_2O \xrightarrow{K_{R+}} R_3B{-}OH + H^+ \qquad \text{(eq 1)}$$

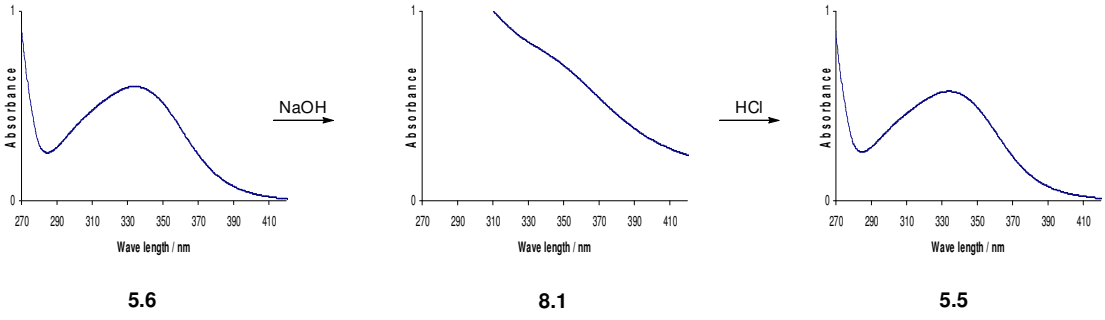

Figure 40. Reversibility of the conversion of [**74**]$^+$ into **74**-OH in H_2O/MeOH 6/4 vol. (3 mL; 5.14×10^{-5} M; MES buffer).

Similar complications were encountered when attempting to determine the cyanide binding constant of [**74**]$^+$ in aqueous solutions. Indeed, a UV-vis titration carried out by addition of cyanide to a 51 μM solution of [**74**]$^+$ resulted in the precipitation of the cyanide adduct after addition of only 0.1 equivalents of cyanide. Precipitation was not observed when a 5.1 μM solution was employed. Under these conditions, however, the cyanide binding reaction proved to be slow such that an accurate determination of the binding constant could not be determined. Despite these limitations, micromolar solutions of [**74**]$^+$ give a reproducible and highly sensitive response to very low concentrations of cyanide. For example, [**74**]$^+$ gives a readily detectable response to cyanide concentrations as low as 26 ppb (Figure 41), which is below the drinking water maximum allowable concentrations recommended by the European Union (50 ppb) or EPA (200 ppb).

At these concentrations, [**74**]$^+$ gives a response which can be easily observed by the naked eye as shown in Figure 41. In addition to being highly sensitive for cyanide, [**74**]$^+$ is also very selective. It shows no response to the presence of other anions such as F^-, Cl^-, Br^-, I^-, NO_3^-, $H_2PO_4^-$, SO_4^{2-}, and $CH_3CO_2^-$. For example, the addition of 10 equivalents of these anion to a 4.28 μM solution of [**74**]$^+$ causes a negligible change in fluorescence spectrum. However, more than a 9-fold fluorescence enhancement was observed upon cyanide addition (Figure 42).

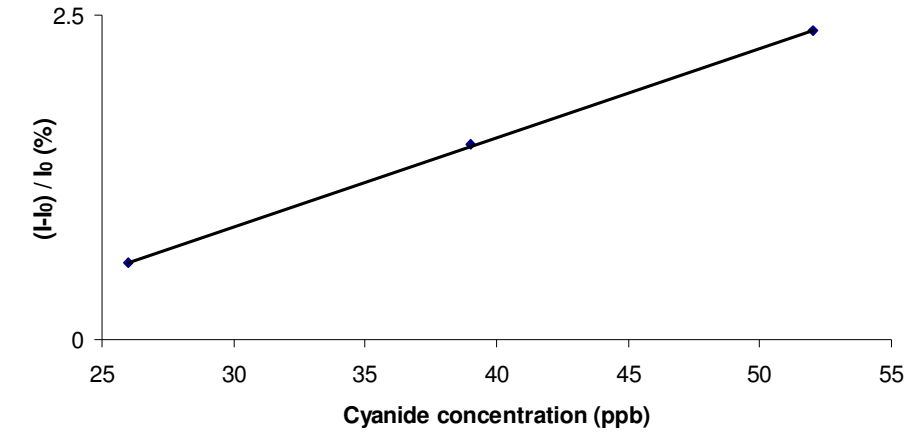

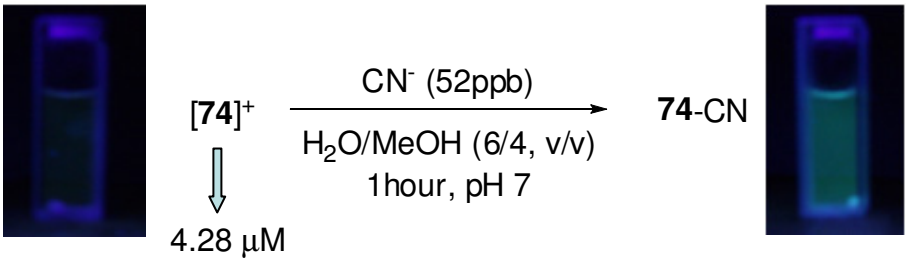

Figure 41. Top: Plots of $(I-I_0)/I_0$ in H_2O/MeOH (6/4, v/v) at pH 7 (I and I_0 refer the fluorescent intensity of $[\mathbf{74}]^+$ at 500 nm in the presence and absence of cyanide). Each data point was obtained after 1h once cyanide was added. Bottom: Visible fluorescence changes (under a hand-held UV-lamp) accompanying the formation of **74**-CN.

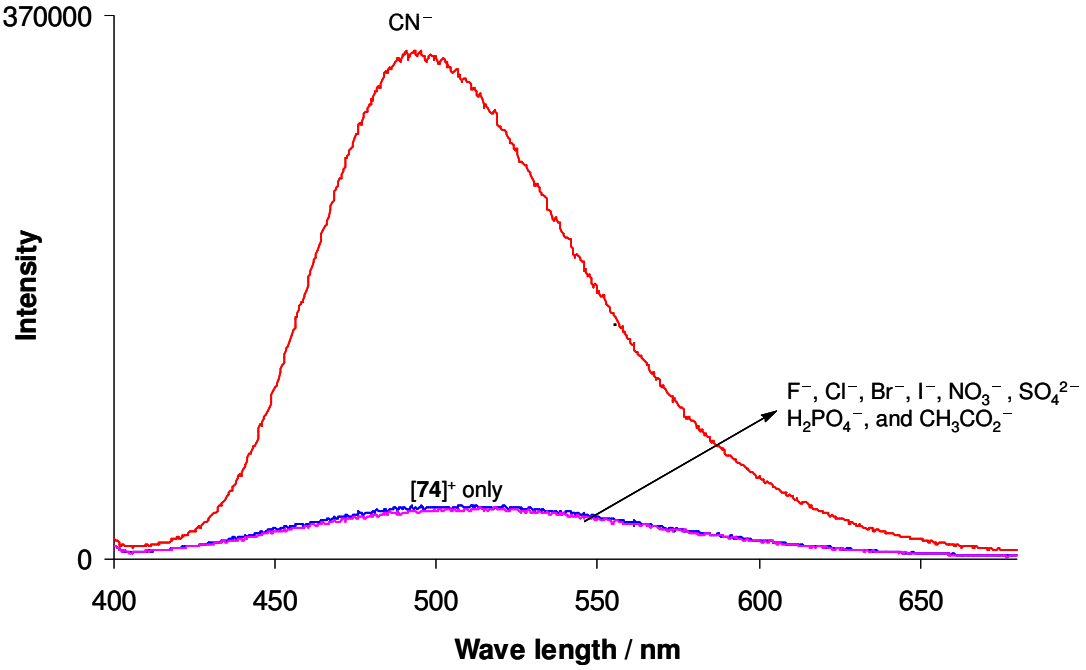

Figure 42. Changes in the fluorescence spectrum of a solution of [**74**]$^+$ (3 mL, 4.28 μM) in H_2O/MeOH (6/4, v/v) after addition of 10 equiv. of F^-, Cl^-, Br^-, I^-, NO_3^-, $H_2PO_4^-$, SO_4^{2-}, and $CH_3CO_2^-$ (pink) followed by the addition of 10 equiv. of CN^- (red).

3.6. Conclusion

In conclusion, we have demonstrated that cyanide binding to the boron center of phosphonium boranes [**73**]$^+$ and [**74**]$^+$ results in a turn-on response of the fluorescence of the anthracenyl and dansyl chromophores, respectively. This increase can be explained by assuming: 1) that the chromophore of [**73**]$^+$ and [**74**]$^+$ is quenched via intramolecular charge transfer from the excited chromophore to the electron deficient boron center; 2) that addition of cyanide to the boron center annuls its electron accepting properties leading to a revival of the fluorescence of the chromophore. While [**73**]$^+$ decomposes in water, [**74**]$^+$ allows for sensitive and selective detection of cyanide with a detection limit

of 26 ppb in H_2O/MeOH (6/4, v/v). The high affinity of this borane arises from favourable Coulombic effects which serve to stabilize the cyanoborate complex against dissociation.

3.7. Experimental Section

General Considerations. [**14**]I was prepared by following the known method. Dimesitylboron fluoride and potassium cyanide were purchased from Aldrich, dansyl chloride from TCI. Solvents were dried by passing through an alumina column (toluene, acetonitrile), reflux under N_2 over Na/K (Et_2O and THF). UV-vis spectra were recorded on an Ocean Optics USB4000 spectrometer with a Ocean Optics ISS light source. Elemental analyses were performed by Atlantic Microlab (Norcross, GA). NMR spectra were recorded on Varian Inova 300 FT NMR (299.96 MHz for ^{1}H, 121.43 MHz for ^{31}P) and Varian Unity Inova 400 FT NMR (399.59 MHz for ^{1}H, 375.99 MHz for ^{19}F, 128.19 MHz for ^{11}B, 161.75 MHz for ^{31}P, 100.45 MHz for ^{13}C) spectrometers at ambient temperature unless otherwise stated. Chemical shifts δ are given in ppm, and are referenced against external $BF_3{\cdot}Et_2O$ (^{11}B), and 85% H_3PO_4 (^{31}P).

Crystallography. The crystallographic measurements of **74**-CN were performed using a Bruker APEX-II CCD area detector diffractometer, with a graphite-monochromated Mo-K_α radiation (λ= 0.71069 Å). A specimen of suitable size and quality was selected and mounted onto a nylon loop. The structure was solved by direct methods, which successfully located most of the non-hydrogen atoms. Subsequent

refinement on F^2 using the SHELXTL/PC package (version 5.1) allowed location of the remaining non-hydrogen atoms.

The crystallographic measurements of **14**-CN were performed using a Siemens SMART-CCD area detector diffractometer, with a graphite-monochromated Mo-K_α radiation (λ= 0.71069 Å). A specimen of suitable size and quality were selected and mounted onto glass fiber with apiezon grease. The structure was solved by direct methods, which successfully located most of the non-hydrogen atoms. Subsequent refinement on F^2 using the SHELXTL/PC package (version 5.1) allowed location of the remaining non-hydrogen atoms.

Synthesis of [73]Br. 9-(bromomethyl)anthracene (110 mg, 0.4 mmol) was added to a solution of **69** (200 mg, 0.39 mmol) in toluene (7 mL) at room temperature. The mixture was refluxed overnight and cooled to rt. The solvent was removed in *vacuo* to yield a powder which was recrystallized from dichloromethane and *n*-pentane. The solid was isolated by filtration, washed with *n*-pentane and dried in *vacuo* to afford [**73**]Br as a yellowish solid (250 mg, 82% yield). ^{1}H-NMR (300 MHz, $CDCl_3$) δ 1.87 (s, 12H), 2.28 (s, 6H), 6.32 (d, 2H, $J_{H\text{-}P}$=14.4Hz), 6.79 (s, 4H), 7.08 (t, 2H, *J*=7.6 Hz), 7.21-7.24 (m, 2H), 7.39-7.48 (m, 8H), 7.52-7.58 (m, 4H), 7.64 (t, 2H, *J*=7.2 Hz), 7.82-7.90 (m, 4H), 8.33 (d, 1H, *J*=3.3 Hz). ^{13}C-NMR (100MHz, $CDCl_3$) δ 21.38 (Mes-*C*H_3), 23.69 (Mes-*C*H_3), 26.04 (d, $J_{C\text{-}P}$=45.6 Hz), 118.01 (d, $J_{C\text{-}P}$=83.5 Hz), 119.03 (d, $J_{C\text{-}P}$=10.6 Hz), 120.40 (d, $J_{C\text{-}P}$=82.0 Hz), 124.34 (d, $J_{C\text{-}P}$=3.0 Hz), 125.18, 126.71, 128.62, 129.03, 129.98(d, $J_{C\text{-}P}$=12.9 Hz), 131.16, 131.28(d, $J_{C\text{-}P}$=6.1 Hz), 133.81 (d, $J_{C\text{-}P}$=9.1 Hz), 134.54

(d, $J_{C\text{-}P}$=9.1 Hz), 134.92 (d, $J_{C\text{-}P}$=3.0 Hz), 135.73(d, $J_{C\text{-}P}$=12.2 Hz), 139.98, 140.79, 140.99, 152.89. ^{11}B-NMR (128 MHz, $CDCl_3$) δ no observance. ^{31}P-NMR (121 MHz, $CDCl_3$) δ +19.69. Anal. Calcd for $C_{51}H_{47}BBrP$-0.3H_2O([**73**]Br-0.3H_2O): C, 77.87; H, 6.10. Found: C, 77.29; H, 5.95.

Synthesis of [74]I. A mixture of N-(3-bromopropyl)-5-(dimehtylamino)-1-naphthalenesulfonamide (0.55 g, 1.48 mmol), sodium iodide (0.54 g, 3.6 mmol) and **69** (0.61 g, 1.2 mmol) in acetonitrile (10 mL) was refluxed overnight. After cooling to rt, the solvent was removed in *vacuo*. The residue was extracted using CH_2Cl_2 (20 mL) and concentrated in *vacuo* to a final volume of about 5 mL. This concentrate was purified by flash chromatography over silica gel using first ethyl acetate (20 mL) and then methanol (20 mL). After methanol was removed in *vacuo*, the residue was extracted using CH_2Cl_2 (20 mL) and water (10 mL). The organic layer was separated, dried over $MgSO_4$, filtered and concentrated in *vacuo* to afford **[74]**I a yellow solid. Further purification was achieved by washing the solid with Et_2O (0.45 mg, 40% yield). ^{1}H-NMR (300 MHz, $CDCl_3$) δ 1.90 (bs, 2H), 1.97 (s, 12H), 2.30 (s, 6H), 2.84 (s, 6H), 3.31 (m, 2H), 3.82 (m, 2H), 6.83 (s, 4H), 7.15 (d, 1H, *J*=7.5 Hz), 7.43 (t, 1H, *J*=8.0 Hz), 7.59-7.63 (m, 2H), 7.64-7.83 (m, 13H), 8.14 (d, 1H, *J*=6.6 Hz), 8.44 (m, 2H). ^{13}C-NMR (100 MHz, $CDCl_3$) δ 20.68 (d, $J_{C\text{-}P}$=52.4 Hz), 21.39, 23.70, 23.88, 42.12 (d, $J_{C\text{-}P}$=17.5 Hz), 45.53 (N-CH_3), 115.52, 117.90 (d, $J_{C\text{-}P}$=85.8 Hz), 119.68, 120.45 (d, $J_{C\text{-}P}$=84.3 Hz), 123.10, 128.71, 128.77, 128.96, 129.56, 129.94, 130.24, 130.72 (d, $J_{C\text{-}P}$=12.1 Hz), 132.77 (d, $J_{C\text{-}P}$=9.1 Hz), 133.67 (d, $J_{C\text{-}P}$=9.9 Hz), 135.18, 135.32, 136.62 (d, $J_{C\text{-}P}$=12.1 Hz), 140.10, 140.87,

140.99, 151.71, 153.63. ^{11}B-NMR (128 MHz, $CDCl_3$) δ no observation. ^{31}P-NMR (121 MHz, $CDCl_3$) δ +25.12. IR (film on KBr plate): ν = 2166.8 cm^{-1} (CN^-). MS (ESI) *m/z* calcd $C_{51}H_{55}BN_2O_2PS$ (M-I) : 801.38, found 801.3569. Anal. Calcd for $C_{51.45}H_{55.9}BCl_{0.9}IN_2O_2PS$ ([**74**]I-0.45CH_2Cl_2): C, 63.91; H, 5.83. Found: C, 63.88; H, 5.80 (^{1}H-NMR shows dichloromethane residue).

Synthesis of 14-CN. [**14**]I (20 mg, 0.03 mmol) was dissolved in MeOH (1 mL) and treated with a solution of NaCN (4.5 mg, 0.09 mmol) in MeOH (2 mL). The mixture was partially evaporated at room temperature to induce crystallization for 1 d. Colorless crystals of **14**-CN formed was filtered and washed with MeOH. Drying in *vacuo* gave **14**-CN in a 70% yield. ^{1}H-NMR (300 MHz, $CDCl_3$) δ 1.94 (s, 12H), 2.13 (s, 6H), 2.35 (d, 3H, $J_{H\text{-}P}$=13.2 Hz), 6.59 (s, 4H), 6.84 (bs, 1H), 7.40-7.47 (m, 6H), 7.57-7.63 (m, 4H), 7.71-7.77(m, 2H), 8.67 (bs, 1H). ^{13}C-NMR (100MHz, $CDCl_3$) δ 9.32 (d, $J_{C\text{-}P}$=58.9 Hz, P-*C*H_3), 20.77, 25.53, 109.03 (d, $J_{C\text{-}P}$=109.0 Hz), 120.54 (d, $J_{C\text{-}P}$=88.0 Hz), 128.57, 128.81, 129.79, 130.17 (d, $J_{C\text{-}P}$=12.6 Hz), 132.72 (d, $J_{C\text{-}P}$=12.6 Hz), 134.74 (d, $J_{C\text{-}P}$=2.7 Hz), 137.33, 138.59, 142.03. ^{11}B-NMR (128 MHz, $CDCl_3$) δ −13.28. ^{31}P-NMR (121 MHz, $CDCl_3$) δ +19.61. Anal. Calcd for $C_{38}H_{39}BNP$-CH_3OH (**14**-CN-CH_3OH): C, 80.27; H, 7.43. Found: C, 79.98; H, 7.35. IR (film on KBr plate): ν = 2165.5 cm^{-1} (CN^-).

Synthesis of 73-CN. [**73**]Br (50 mg, 0.064 mmol) was dissolved in MeOH (5 mL) and treated with a solution of KCN (33mg, 0.51 mmol) in MeOH (2 mL) which resulted in the formation of a solid. After 30 min, the solid was collected by filtration, washed

with MeOH, and dried in *vacuo* to afford **73**-CN as a pale yellow solid (25 mg, 54% yield). ^{1}H-NMR (300 MHz, $CDCl_3$) δ 1.98 (s, 12H), 2.19 (s, 6H), 5.30 (2H, d, $J_{H\text{-}P}$=13.5 Hz), 6.65 (s, 4H), 7.08-7.21 (m, 7H), 7.34-7.39 (m, 7H), 7.45 (bs, 1H), 7.56-7.62 (m, 4H), 7.98 (2H, d, *J*=8.1 Hz), 8.51 (bs, 1H), 8.66 (bs, 1H). ^{13}C-NMR (100 MHz, 1,2-dichloroethane-d^4) δ 20.73 (Mes-*C*H_3), 25.67 (Mes-*C*H_3), 26.31 (d, $J_{C\text{-}P}$=50.1Hz), 108.99 (d, $J_{C\text{-}P}$=86.6 Hz), 118.07 (d, $J_{C\text{-}P}$=84.3 Hz), 118.66 (d, $J_{C\text{-}P}$=10.3 Hz), 123.15, 125.52, 127.29, 129.09, 129.74, 129.95 (d, $J_{C\text{-}P}$=12.1 Hz), 131.14 (d, $J_{C\text{-}P}$=5.7 Hz), 131.42, 131.45, 312.74, 134.24 (d, $J_{C\text{-}P}$=9.5 Hz), 135.08 (d, $J_{C\text{-}P}$=3.0 Hz), 137.61, 141.85. ^{11}B-NMR (128 MHz, $CDCl_3$) δ −13.53. ^{31}P-NMR (121 MHz, $CDCl_3$) δ +17.59. IR (film on KBr plate): ν = 2163.2 cm^{-1} (CN^-).

Synthesis of 74-CN. [**74**]I (50 mg, 0.054 mmol) was dissolved in MeOH (5 mL) and treated with a solution of KCN (33mg, 0.51 mmol) in MeOH (2 mL) which resulted in the formation of a solid. After 30 min, the solid was isolated by filtration washed with MeOH, and dried in *vacuo* to afford **74**-CN as a pale yellow solid (23 mg, 51% yield). ^{1}H-NMR (400 MHz, $CDCl_3$) δ 1.56 (bs, 2H), 1.82 (s, 12H), 2.04 (s, 6H), 2.69 (m, 2H), 2.77 (m, 2H), 2.83 (s, 6H), 6.48 (s, 4H), 6.72 (m, 1H), 7.11 (d, 1H, *J*=7.2 Hz), 7.39-7.60 (m, 13H), 7.71-7.74 (m, 2H), 8.08 (d, 1H, *J*=7.6 Hz), 8.31 (d, 1H, *J*=8.4 Hz), 8.45 (d, 1H, *J*=8.4 Hz), 8.50 (bs, 1H). ^{13}C-NMR (100 MHz, $CDCl_3$) δ 19.40 (d, $J_{C\text{-}P}$=54.7 Hz), 20.81, 23.92, 25.67, 42.10 (d, $J_{C\text{-}P}$=16.7 Hz), 45.51, 109.89 (d, $J_{C\text{-}P}$=88.9 Hz), 115.53, 118.64, 119.07 (d, $J_{C\text{-}P}$=85.5 Hz), 119.30, 123.07, 128.72 (d, $J_{C\text{-}P}$=12.9 Hz), 128.92, 129.57, 129.92, 130.20, 130.30 (d, $J_{C\text{-}P}$=12.2 Hz), 131.12, 132.85, 133.54 (d, $J_{C\text{-}P}$=9.8

Hz), 134.77, 135.31, 137.89 (m), 141.86, 145.98, 149.14, 151.76, 170.82. ^{11}B-NMR (128 MHz, $CDCl_3$) δ −12.45. ^{31}P-NMR (161 MHz, $CDCl_3$) δ 23.90. Anal. Calcd for $C_{53.2}H_{59.8}BN_3O_{3.2}PS$ (**74**-CN-1.2CH_3OH): C, 73.76; H, 6.96. Found: C, 73.28; H, 6.76 (^{1}H-NMR shows methanol residue). IR (film on KBr plate): ν = 2166.8 cm^{-1} (CN^-).

UV-vis Titration Experiments. A solution of [**73**]Br (3.0 mL, 6.20×10^{-5} M), [**74**]I (3.0 mL, 5.83×10^{-5} M) was titrated by incremental addition of a solution of KCN in methanol.

Anion selectivity test. To a solution of $[\mathbf{74}]^+$ in H_2O/MeOH 6/4 vol. (3 mL, 4.28×10^{-6} M; pH 7; 6 mM HEPES buffer) was added 10 equiv. of X^- (X = F, Cl, Br, I, NO_3, H_2PO_4, CH_3CO_2) and SO_4^{2-}. After 10 min, to a solution of $[\mathbf{74}]^+$ containing all anions was added 10 equiv. of CN^-.

Fluorescence titration. Compound [**74**]I in H_2O/MeOH 6/4 vol. (3.0 mL, 5.10×10^{-6} M, pH 7, 6 mM MES buffer) was titrated by incremental addition of KCN in water (0.00015 M). Each data point was recorded after 1h once cyanide was added.

Electrochemistry. Changes in the differential pulsed voltammogram of $[\mathbf{14}]^+$ (0.0016 M) observed upon the addition of Et_4NCN (0.11 M in CH_3CN) to a THF solution.

CHAPTER IV

AZIDE ION RECOGNITION IN WATER/$CHCl_3$ USING A CHELATING PHOSPHONIUM BORANE AS A RECEPTOR*

4.1.Introduction

Like cyanide, azide (N_3^-) is a toxic anion which binds to and deactivates cytochrome oxidase enzymes. This anion is also found in explosives such as NaN_3 or $Pb(N_3)_2$ used in airbags and detonators, respectively. Because of its toxicity, as well as its use in explosive devices, the development of simple methods for the molecular recognition of N_3^- are of interest.[166, 167] Earlier contributions have shown that this anion can be selectively captured by organic[168] or bimetallic[169-171] hosts to form complexes in which each extremities of the N_3^- anion forms hydrogen or coordination bonds with the binding sites of the host. More recently, the chelation of this anion by group 13 bidentate Lewis acids has been reported[172, 173] leading us to question whether water compatible polyfunctional boranes could be used for the molecular recognition of this anion in aqueous environments.

As part of our interest in the chemistry of cationic boranes,[14, 16, 18-22, 107, 114, 129, 139-142, 150, 174] we have recently reported the synthesis of [**15**]$^+$ (as a I^- salt) and investigated its affinity for halide anions.[19] In the context of these studies, we found

---

* Reprinted in part with permission from, "Azide ion recognition in water–$CHCl_3$ using a chelating phosphonium borane as a receptor"; Kim, Y.; Todd, W. H.; Bouhadir, G.; Bourissou D; Gabbaï, F. P.; *Chem. Commun.*, **2009**, 3729-3731, Copyright 2009 by the Royal Society of Chemistry.

that $[\mathbf{15}]^+$ complexes F^- in MeOH to form the zwitterionic fluoroborate **15**-F in which the F^- anion is asymmetrically chelated by the B/P^+ bidentate Lewis acid. In parallel, we have also shown that PhN_3 reacts with *ortho*-$(Mes_2B)C_6H_4(P(i\text{-}Pr)_2)$ to afford the phosphazide **75** thus suggesting that the boron and phosphorus atom of such compounds are well positioned to interact with the terminal nitrogen atom of an organic azide.[175] In this paper, we now show that $[\mathbf{15}]^+$ can be used for the complexation of N_3^-. We also report that this complexation is selective in biphasic organic solvent/water mixtures.

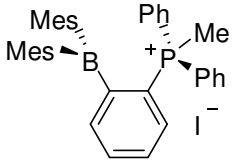

[**15**]I

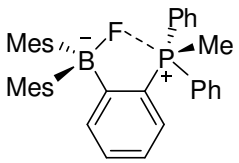

15-F

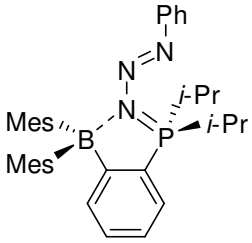

75

4.2. Hydroxide anion complexation

In the initial phase of this work, we decided to carefully investigate the behavior of $[\mathbf{15}]^+$ in aqueous solution. Having previously noted that $[\mathbf{15}]^+$ is not stable at neutral pH,[19] its behavior at acidic pH was investigated by UV-vis spectrocopy. At pH 2.3, the characteristic absorption band of $[\mathbf{15}]^+$ at 330 nm can be readily observed indicating that the boron center retains sp^2 hybridization.[9] Upon elevation of the pH to 3.5, the intensity of this band decreases before precipitation of a new product occurs. Acidification of the solution leads to the rapid disappearance

of this new product and triggers a resurection of the original absorption spectrum of $[\mathbf{15}]^+$ (Figure 43).

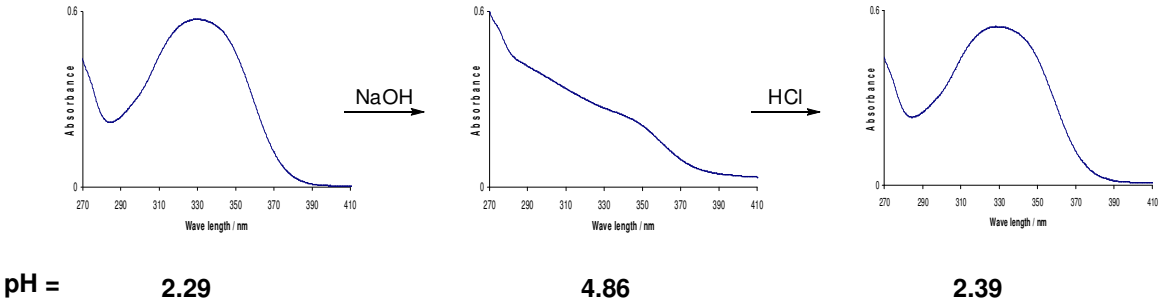

Figure 43. Reversibility of the conversion of $[\mathbf{15}]^+$ into **15**-OH in H_2O/MeOH 9/1 vol. (3 mL; 6.7×10^{-5} M; 9 mM phosphate buffer).

These observations suggest that the new product is the hydroxide adduct *ortho*-$(Mes_2(HO)B)C_6H_4(PMePh_2)$ (**15**-OH). Its formation at such a low pH suggests that the pK_{R+} of $[\mathbf{15}]^+$ (eq. 1) which cannot be accurately determined because of the precipitation of **15**-OH, is in the 3-4 range. This value is much lower than that measured for [*para*-$(Mes_2B)C_6H_4(PMePh_2)]^+$ (pK_{R+} = 7.3)[174] thus confirming that $[\mathbf{15}]^+$ is a stronger Lewis acid which cannot be used in neutral water.

$$[R_3B]^+ + H_2O \xrightarrow{K_{R+}} R_3B{-}OH + H^+ \qquad \text{(eq 1)}$$

In an effort to overcome this limitation while still being able to use $[\mathbf{15}]^+$ for the capture of aqueous anions, we decided to consider the use of a biphasic solvent mixture. To this end, we investigated the behavior of $[\mathbf{15}]^+$ (0.0125 M) in $D_2O/CDCl_3$ (1/3, v/v) by monitoring the ^{31}P and/or ^1H NMR spectrum of the organic phase. After 2.5 hours, analysis of the organic phase indicated the presence of $[\mathbf{15}]^+$ as the major species (91%, $\delta(^{31}P)$ 23.9 ppm) and **15**-OH as a minor species (9%, $\delta(^{31}P)$ 20.8 ppm) (Figure 44). In agreement with this view, acidification of the aqueous phase (by addition of HBr, 0.07 M) leads to complete disapperance of **15**-OH leaving $[\mathbf{15}]^+$ as the only remaining species. The ^{11}B NMR resonance of **15**-OH at 0.2 ppm is close to the value of 0.3 ppm observed for *para*-$(Mes_2(HO)B)C_6H_4(PMePh_2)$.[174] Formation of **15**-OH is quantitative when 1.2 eq of NaOH is added to the aqueous phase.

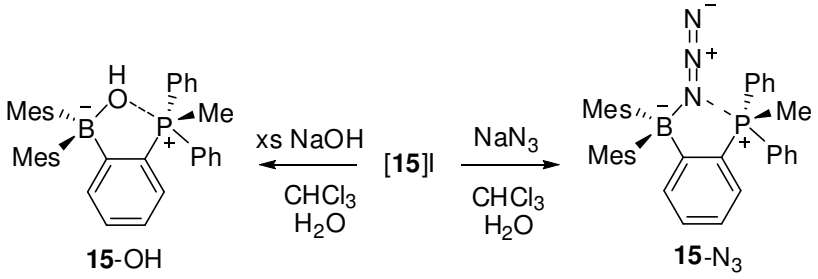

Figure 44. Synthesis of **15**-OH and **15**-N_3.

4.3. Azide ion complexation

Encouraged by these observations, we set out to investigate the ability of $[\mathbf{15}]^+$ to capture anions in $D_2O/CDCl_3$. When 2 eq. of the sodium salts of Cl^-, Br^-, I^-,

NO_3^-, $H_2PO_4^-$ were used, no new species (except for **15**-OH) could be detected in the organic phase indicating the lack of affinity of [**15**]$^+$ for these anions. In the case of F^- (2 eq.), analysis of the organic phase after 20 minutes indicated the formation of **15**-F $\delta(^{31}P)$ 28.3 ppm, $J_{P\text{-}F}$ =24.0 Hz) in 7% yield (as well as **15**-OH in 10% yield). The low yield observed for **15**-F suggests that its formation is disfavored by the efficient solvation of F^- in the aqueous phase. By contrast, a rapid reaction was observed with N_3^- leading to the formation of **15**-N_3 in 66% yield (as well as **15**-OH in 8% yield) after 20 min as indicated by the detection of a new ^{31}P NMR resonance at 25.5 ppm (Figure 44). The rapid formation of **15**-N_3 not only corroborates the lipophilic behavior of N_3^-,[176] but also suggests a strong interaction of the anion with the Lewis acidic borane. In order to shed light on this point, **15**-N_3 was isolated by reaction of [**15**]I with NaN_3 in methanol and fully characterized. The diagnostic antisymmetric stretching vibration of the azide group[177] was observed at 2109 cm^{-1} in the IR spectrum. Examination of the ^{13}C-NMR spectrum indicates that the phosphorus bound phenyl groups are either equivalent or in rapid exchange. To clarify this point, the crystal sturcture of **15**-N_3 was determined (Figure 45, Table 13).

The DFT optimized structure of **15**-N_3 is in excellent agreement with that experimentally determined (Figure 46, Table 14). In particular, the P(1)-N(1) separation of 2.799 Å is almost identical to that observed in the crystal (2.790(2) Å). A Natural Bond Orbital analysis performed at the optimized geometry indicates that the P(1)-N(1) bond is best described as donor-acceptor interaction involving a nitrogen lone-pair as a

donor and the phosphorus-carbon σ^*-orbital as the acceptor (Figures 47). Moreover, zeroing the Kohn-Sham matrix elements corresponding to the $lp_{(N)} \rightarrow \sigma^*_{(P\text{-}C)}$ interaction leads to an increase of the total energy of the molecule by a deletion energy of 5.8 kcal/mol. This deletion energy, which provides a measure of the strength of the $lp_{(N)} \rightarrow \sigma^*_{(P\text{-}C)}$ interaction, is comparable to that of a strong hydrogen-bond,[183] and very similar to that computed for the $lp_{(F)} \rightarrow \sigma^*_{(P\text{-}C)}$ interaction present in **15**-F (5.0 kcal/mol).[19] It is important to point out that **15**-N_3 is further stabilized by favourable electrostatic effects.

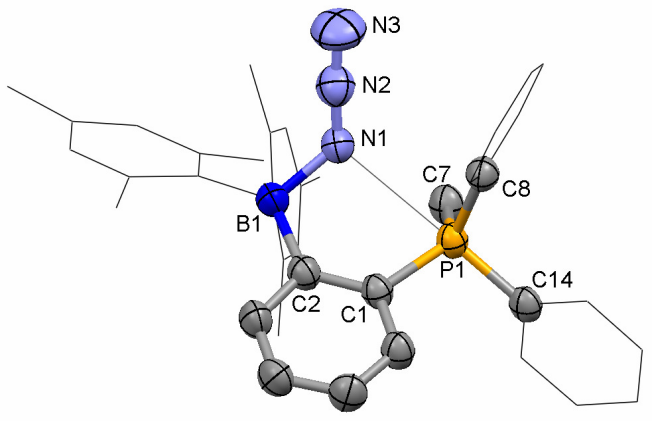

Figure 45. Crystal structure of **15**-N_3 with thermal ellipsoids set at 50% probability level. Hydrogen atoms are omitted for clarity. Pertinent metrical parameters can be found in the text.

Table 13. Crystal data, data collections, and structure refinement for **15**-N_3.

Crystal data	**15**-N_3
formula	$C_{37}H_{39}BN_3P$
M_r	567.49
crystal size (mm^3)	0.55 x 0.15 x 0.09
crystal system	Monoclinic
space group	*P*2(1)/*n*
a (Å)	17.702(2)
b (Å)	8.9863(12)
c (Å)	19.979(3)
α (°)	90
β (°)	95.172(9)
γ (°)	90
V ($Å^3$)	3165.3(7)
Z	4
ρ_{calc} (g cm^{-3})	1.191
μ (mm^{-1})	0.117
F(000)	1208
Data collection	
T (K)	213(2)
scan mode	ω
hkl range	-20 → +20, -10 → +10, -22 → +22
measd reflns	27389
unique reflns [R_{int}]	4956 [0.0582]
reflns used for refinement	4956
Refinement	
refined parameters	379
GooF	1.008
R_1,[a] wR_2[b] all data	0.0777, 0.1496
ρ_{fin} (max/min) (e $Å^{-3}$)	0.253, -0.238

[a] $R_1 = \Sigma||Fo| - |Fc||/\Sigma|Fo|$. [b] $wR_2 = [[\Sigma w(Fo^2 - Fc^2)^2]/[\Sigma w(Fo^2)^2]]^{1/2}$.

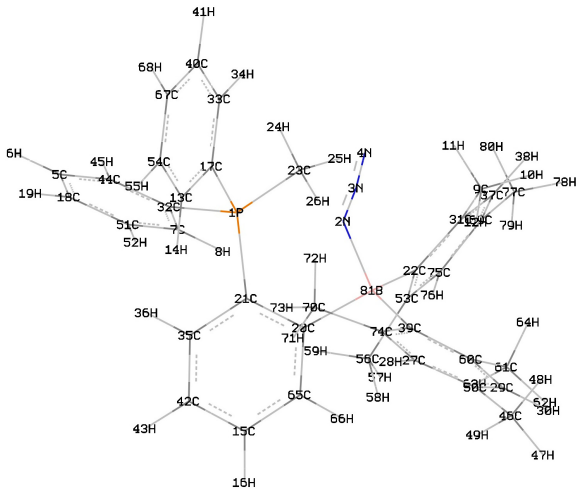

Figure 46. DFT optimized structure of **15**-N_3.

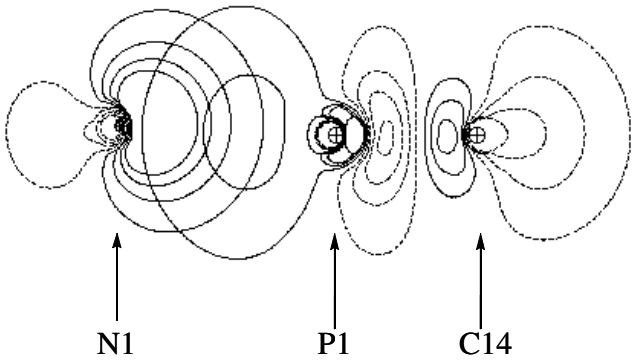

Figure 47. NBO contour plot showing the $lp_{(N)} \rightarrow \sigma^*_{(P\text{-}C)}$ interaction of **15**-N_3.

Table 14. Atom coordinates for the optimized structure of **15**-N_3.

Center Number	Coordinates (Angstroms) X	Y	Z	Center Number	Coordinates (Angstroms) X	Y	Z
P1	2.087396	-0.09284	-0.13657	C42	1.204399	-0.81734	3.761332
N2	-0.51783	-0.59198	-1.02889	H43	1.795228	-1.07379	4.634599
N3	-0.87403	-1.32506	-1.91827	C44	4.860995	-0.58152	0.298452
N4	-1.1146	-2.03057	-2.79724	H45	4.699341	-1.55626	-0.1469
C5	6.145506	-0.22296	0.726817	C46	-6.72005	-2.58813	0.772745
H6	6.964828	-0.92451	0.608859	H47	-7.44614	-1.99066	1.33583
C7	4.024884	1.577374	1.027721	H48	-7.14746	-2.76275	-0.22467
H8	3.210023	2.281549	1.163157	H49	-6.63214	-3.56492	1.262163
C9	-2.39562	1.118725	-2.59471	C50	-5.38053	-1.89141	0.682748
H10	-3.11489	1.642483	-3.23522	C51	5.307832	1.930671	1.452379
H11	-1.67773	0.629553	-3.26434	H52	5.476465	2.904279	1.900557
H12	-2.93651	0.334375	-2.06275	C53	-0.86322	2.865417	0.480185
C13	2.048502	-2.87538	-0.42972	C54	2.238678	-4.07079	-1.12959
H14	1.711607	-2.90046	0.600752	H55	2.058553	-5.01737	-0.63146
C15	-0.18696	-0.6976	3.843193	C56	-0.56582	2.77267	1.971328
H16	-0.69428	-0.86194	4.789391	H57	-0.48939	3.780019	2.395294
C17	2.264843	-1.6412	-1.06994	H58	-1.35611	2.248186	2.515127
C18	6.37134	1.030965	1.302062	H59	0.368922	2.249238	2.199241
H19	7.36732	1.307155	1.632433	C60	-4.051	0.174071	0.56785
C20	-0.34327	-0.15248	1.434172	C61	-4.13988	1.689819	0.669347
C21	1.078807	-0.27522	1.37728	H62	-5.13028	1.976153	1.040593
C22	-1.32641	1.772949	-0.31931	H63	-3.39728	2.107157	1.353718
C23	1.763805	1.307915	-1.26273	H64	-3.99219	2.187585	-0.29367
H24	2.662468	1.477446	-1.86358	C65	-0.92495	-0.37561	2.705209
H25	0.899182	1.106002	-1.88974	H66	-2.00457	-0.30828	2.78061
H26	1.54857	2.206408	-0.67907	C67	2.642401	-4.04635	-2.46975
C27	-4.18784	-2.61021	0.592134	H68	2.780157	-4.97525	-3.01283
H28	-4.22115	-3.69736	0.633901	C69	-1.03199	4.44884	-1.39708
C29	-5.27971	-0.49847	0.696283	C70	-1.75069	-2.93666	0.436483
H30	-6.18434	0.092815	0.822266	H71	-1.97483	-3.81463	1.054033
C31	-1.73006	2.10942	-1.65203	H72	-1.54316	-3.3052	-0.57513
C32	3.7874	0.314906	0.443814	H73	-0.83726	-2.48618	0.821766
C33	2.664157	-1.62131	-2.41963	C74	-2.93791	-1.98068	0.461573
H34	2.8211	-0.68122	-2.93722	C75	-0.71172	4.154302	-0.06982
C35	1.831003	-0.60383	2.535822	H76	-0.35527	4.956234	0.574114
H36	2.909311	-0.69461	2.484885	C77	-0.83519	5.833683	-1.97384
C37	-1.57247	3.409187	-2.15993	H78	-1.69889	6.144995	-2.57361
H38	-1.90072	3.61363	-3.17769	H79	-0.68958	6.577913	-1.18333
C39	-2.82762	-0.55206	0.392012	H80	0.04393	5.877151	-2.63203
C40	2.850573	-2.8215	-3.11337	N81	-1.34777	0.167291	0.155773
H41	3.146824	-2.79665	-4.15654				

4.4. Conclusion

In summary, the results reported here show that cationic boranes can be used for the capture of aqueous N_3^- anions under biphasic conditions. The ability of [**15**]$^+$ to transport this anion in organic phases originates from favourable Coulombic effects which stabilize the B-N_3 linkage against dissociation. Last but not least, the high selectivity observed in these phase-transfer reactions most likely results from the lipophilic character of the azide anion as well as from its ability to interact with both the boron and phosphorus Lewis acidic sites of the receptor.

4.5. Experimental Section

General Considerations. [**15**]I was synthesized as described in *J. Am. Chem. Soc.*, 2008, **130**, 10890. Sodium fluoride was purchased from MCB manufacturing chemists Inc., sodium azide and sodium hydroxide from Fisher scientific company. Solvents were dried by passing through an alumina column (Hexanes, dichloromethane), refluxing under N_2 over Na/K (diethyl ether). Methanol and chloroform (ACS reagent grade) were used as provided. UV-vis and emission spectra were recorded on an Ocean Optics USB4000 spectrometer with a Ocean Optics ISS light source. pH Measurements were carried out with a Radiometer PHM290 pH meter equipped with a VWR SympHony electrode. IR spectra were obtained using a ATI Mattson Genesis Series FT infrared spectrophotometer. Elemental analyses were performed by Atlantic Microlab (Norcross, GA). NMR spectra were recorded on Varian Unity Inova 400 FT NMR (399.59 MHz for ^{1}H, 128.19 MHz for ^{11}B, 100.45 MHz for ^{13}C, 161.75 MHz for ^{31}P) and

Varian Inova 500 FT NMR (499.88 MHz for ^{1}H) spectrometers at ambient temperature. Chemical shifts are given in ppm, and are referenced against external $BF_3 \cdot Et_2O$ (^{11}B) and H_3PO_4 (^{31}P).

Crystallography. The crystallographic measurements were performed using a Bruker APEX-II CCD area detector diffractometer (Mo-K_α radiation, λ= 0.71073 Å) for **15**-N_3. A specimen of suitable size and quality was selected and mounted onto a nylon loop. The structures were solved by direct methods, which successfully located most of the non-hydrogen atoms. Subsequent refinement on F^2 using the SHELXTL/PC package (version 5.1) allowed location of the remaining non-hydrogen atoms.

Synthesis of 15-N_3. [**15**]I (0.030 g, 0.046 mmol) was dissolved in MeOH (10 mL) and treated with NaN_3 (6 mg, 0.092 mmol) in MeOH. After 30 min, the solid was isolated by filtration, washed with MeOH (15.1 mg, 53% yield). ^{1}H NMR (499.88 MHz, $CDCl_3$): 1.76 (bs, 12H, Mes-CH_3), 2.11 (d, $J_{H\text{-}P}$=13 Hz, 3H, P-CH_3), 2.19 (s, 6H, Mes-CH_3), 6.57-6.79 (bm, 4H, Mes-C*H*), 6.92 (m, 1H, Ar-C*H*), 7.05 (bm, 1H, Ar-C*H*), 7.27 (bm, 5H, Ar-C*H*), 7.45 (bm, 1H, Ar-C*H*), 7.59 (bm, 3H, Ar-C*H*), 7.59-7.62 (bm, 2H, Ar-C*H*), 7.69 (bt, 1H, ArC*H*). ^{13}C NMR (100.5 MHz, $CDCl_3$): δ 14.60 (d, $J_{C\text{-}P}$=65.3 Hz, P-*C*H_3), 20.78 (Mes-*C*H_3), 24.41 (br, Mes-*C*H_3), 120.02 (d, $J_{C\text{-}P}$=91.9 Hz, P-C^{Ph}_{ipso}), 124.21 (d, $J_{C\text{-}P}$=14.4 Hz), 129.20 (br, Mes-*C*H), 129.46 (d, $J_{C\text{-}P}$=12.2 Hz, P-C^{Ph}_{meta}), 131.165 (br, P-C^{Ph}_{ortho}), 131.70 (d, $J_{C\text{-}P}$=3.8 Hz), 132.51 (d, $J_{C\text{-}P}$=3.1 Hz, P-C^{Ph}_{para}), 133.60 (Mes-*C*Me), 136.34 (d, $J_{C\text{-}P}$=18.2 Hz), 140.06 (d, $J_{C\text{-}P}$=16.7 Hz), 141.841 (br),

172.497. ^{11}B NMR (128.2 MHz, $CDCl_3$): δ −14.8. ^{31}P NMR (161.75 MHz, $CDCl_3$): 25.5. Anal. Calcd for $C_{37}H_{39}BN_3P$: C, 78.31; H, 6.93. Found: C, 79.18; H, 7.07. IR ν_{N3} = 2109 cm^{-1}.

Synthesis of 15-OH. [**15**]I (0.1 g, 0.15 mmol) was dissolved in $CHCl_3$ (3 mL) and treated with a solution of NaOH (3 mL, 0.9 mmol, 0.3 M in H_2O). The resulting solution was stirred for 3h at rt. The mixture was extracted with dichloromethane (2 x 5 mL), and the organic layers were combined, dried over $MgSO_4$ and the solvent was removed under reduced pressure. The white solid was washed with Et_2O followed by Hexanes and dried under a vacuum (50 mg, 61% yield). ^{1}H NMR (399.572 MHz, $CDCl_3$): δ 1.03 (s, 1H, B-O*H*), 1.85 (bs, 12H, Mes-CH_3), 2.21 (s, 6H, Mes-CH_3), 2.28 (d, 3H, $J_{H\text{-}P}$=14 Hz, P-CH_3), 6.61 (s, 4H, Mes-C*H*), 6.93-7.02 (m, 2H), 7.26-7.48 (m, 9H), 7.56-7.58 (m, 2H), 7.63-7.67 (m, 1H). ^{13}C NMR (100.5 MHz, $CDCl_3$): δ 16.95 (d, $J_{C\text{-}P}$=73.7 Hz, P-*C*H_3), 20.76 (Mes-*C*H_3), 24.94 (br, Mes-*C*H_3), 121.59 (d, $J_{C\text{-}P}$=101 Hz, P-C^{Ph}_{ipso}), 123.48 (d, $J_{C\text{-}P}$=16 Hz). 128.87 (br, Mes-*C*H), 128.93 (d, $J_{C\text{-}P}$=11.3 Hz, P-C^{Ph}_{meta}), 131.14 (br, P-C^{Ph}_{ortho}), 131.52 (d, $J_{C\text{-}P}$=3 Hz), 132.50 (Mes-*C*Me), 135.76 (d, $J_{C\text{-}P}$=19 Hz), 137.65 (d, $J_{C\text{-}P}$=18.2 Hz), 140.90, 155.56, 178.04. ^{11}B NMR (128.2 MHz, $CDCl_3$): δ 0.2. ^{31}P NMR (161.75 MHz, $CDCl_3$): δ 20.8. Anal. Calcd for $C_{37}H_{39}BN_3P$: C, 81.92; H, 7.43. Found: C, 81.07; H, 7.47.

Formation of 15-OH Under Biphasic Conditions. This experiment was carried out by sonicating a biphasic mixture consisting of [**15**]I in $CDCl_3$ (0.0087 M, 0.6 mL)

and NaOH in water (0.1 mL, 0.063 M). Conversion into **15**-OH was complete after 1h 30 min as shown by the detection of a single ^{31}P-NMR resonance at δ 20.8 ppm.

Anion Complexation Under Biphasic Conditions. These experiments were carried out by shaking a biphasic mixture consisting of [**15**]I in $CDCl_3$ (0.0125 M, 0.6 mL) and the sodium salt of the anion in D_2O (0.15 M, 0.1 mL) in a 5 mm NMR tube. The reactions were monitored by ^{31}P and ^{1}H NMR spectroscopy.

Biphasic Hydroxide Binding Test. Mixing a biphasic mixture consisting of [**15**]I in $CDCl_3$ (0.0087 M, 0.6 mL) and NaOH aqueous solution (0.1 mL, 0.063 M) using a sonicator. The conversion to **15**-OH was complete after 1h 30 min showing one peak at δ 20.8 ppm in ^{31}P-NMR.

Computational Details. DFT calculations (full geometry optimization) were carried out with the Gaussian 03 program using the gradient-corrected Becke exchange functional (B3LYP) and the Lee-Yang-Parr correlation functional. Geometry optimization of **15**-N_3 was carried out with the following mixed basis set: 6-31+g(d') for the boron, nitrogen, 6-31+g(d) for the phosphorus atom, 6-31g basis set was used for all carbon and hydrogen atoms. Frequency calculations, which were carried out on the optimized structures of the compounds, confirmed the absence of any imaginary frequencies. The Natural Bond Orbital (NBO) analysis was carried out using the stand along PC version of GENNBO 5.0 program.

CHAPTER V

A SULFONIUM BORANE FOR THE SELECTIVE COMPLEXATION OF CYANIDE IONS IN WATER*

5.1. Introduction

Owing to the presence of low lying σ*-orbitals, sulfonium ions are inherently Lewis acidic and can interact with electron-rich substrates to form donor-acceptor complexes. Although this phenomenon has been documented,[184-189] efforts to use sulfonium ions as binding site in Lewis acidic hosts have not been reported. As part of our fundamental interest in the chemistry of polydentate Lewis acidic boranes,[190-192] we have therefore become interested in probing the synthesis and properties of anion receptors containing accessible sulfonium ions. As an added motivation for these studies, we anticipated that the anion binding properties of sulfonium boranes would also benefit from attractive Coulombic effects similar to those occurring in other cationic boron-based anion receptors.[14, 16, 18-22, 107, 114, 129, 139-141, 150, 174]

5.2. Synthesis and characterization of a sulfonium borane

To test the validity of the aforementioned concepts, we synthesized the cationic borane [**77**]$^+$ which features adjacent sulfonium and boryl moieties connected by a *o*-phenylene linker (Figure 48). To obtain a borane that could easily be converted into a

---

* This is the pre-peer reviewed version of the following article: "Sulfonium Boranes for the Selective Capture of Cyanide Ions in Water"; Kim, Y.; Zhao, H.; Gabbaï, F. P.; *Angew. Chem. Int. Ed.*, **2009**, *48*, 4957-4960, Copyright 2009 by Wiley InterScience.

cationic derivative, we allowed *o*-lithiothioanisole[193] to react with dimesitylboron fluoride in Et_2O at 0 °C. The borane **76** was converted into [**77**]OTf by reaction with MeOTf.

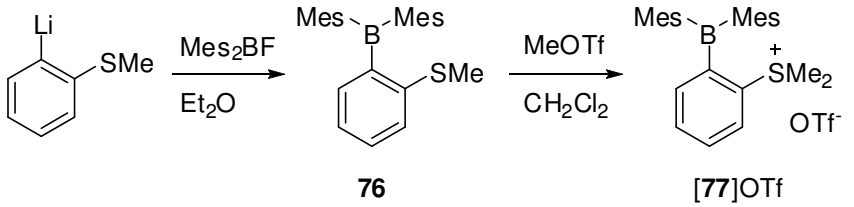

Figure 48. Synthesis of [**77**]OTf.

The salt [**77**]OTf has been isolated and characterized by multinuclear NMR spectroscopy and single crystal X-ray diffraction (Figure 49, Table 15). The detection of a ^{11}B NMR resonance at 77 ppm and the presence of a low energy UV-vis absorption band at 340 nm in MeOH for $[\mathbf{77}]^+$ indicates the presence of a coordinatively unsaturated boron center which mediates π-conjugation of the aromatic ligands.[194-197] The resulting boron-centered chromophores are fluorescent and give rise to a broad emission band at 464 nm for $[\mathbf{77}]^+$ ($\phi = 0.12$) when excited at 340 nm in MeOH. As reported for other sulfonium salts,[198] $[\mathbf{77}]^+$ are sensitive to UV light and should therefore not be irradiated for extended periods of time. The crystal structure of $[\mathbf{77}]^+$ clearly show that: 1) the boron center adopts a trigonal planar coordination geometry ($\sum_{(C\text{-}B\text{-}C)} = 360.0°$); 2) the boron-sulfur separation of 3.12 Å. A Natural Bond Orbital (NBO) analysis carried out at the DFT optimized geometry of $[\mathbf{77}]^+$ indicates the presence of a lp(S)→p(B) donor-

acceptor interaction (Figures 49 and 50, Table 16) whose deletion leads to an increase of the total energy of the molecule by E_{del} = 2.3 Kcal/mol.

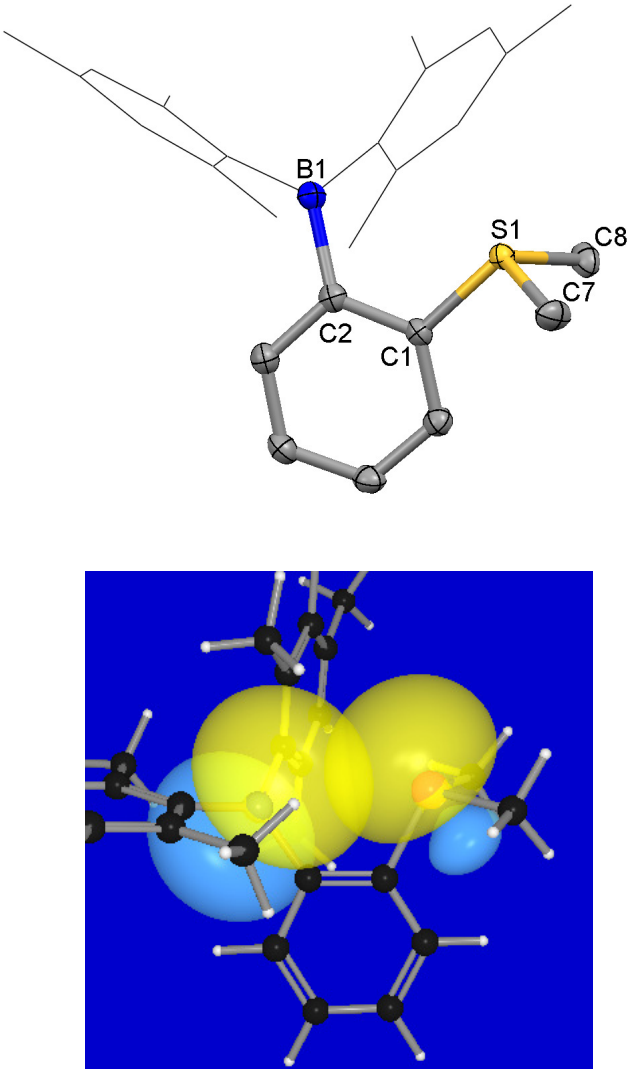

Figure 49. Top: Crystal structure of [**77**]OTf with thermal ellipsoids set at 50% probability level. The triflate anions and H-atoms are omitted for clarity. Bottom: partial view of the molecule of [**77**]$^+$ showing the contour of the NBOs involved in the lp(S)→p(B) donor-acceptor interaction.

Table 15. Crystal data, data collections, and structure refinement for [**77**]OTf.

Crystal data	[**77**]OTf
Formula	$C_{27}H_{32}BF_3O_3S_2$
M_r	536.46
crystal size (mm^3)	0.35 x 0.13 x 0.13
crystal system	Monoclinic
space group	$P2_1/c$
a (Å)	8.5100(17)
b (Å)	23.287(5)
c (Å)	13.710(3)
α (°)	
β (°)	99.22(3)
γ (°)	
V ($Å^3$)	2681.8(9)
Z	4
ρ_{calc} (g cm^{-3})	1.329
μ (mm^{-1})	0.247
F(000)	1128
Data collection	
T (K)	110(2)
scan mode	ω
hkl range	-11 → +11 -31 → +30 -17 → +18
measd reflns	61457
unique reflns [R_{int}]	6455 [0.0322]
reflns used for refinement	6455
Refinement	
refined parameters	325
GooF	1.005
R_1,[a] wR_2[b] all data	0.0532, 0.1258
ρ_{fin} (max/min) (e $Å^{-3}$)	0.501, -0.360

[a] $R_1 = \Sigma||Fo| - |Fc||/\Sigma|Fo|$. [b] $wR_2 = [[\Sigma w(Fo^2 - Fc^2)^2]/[\Sigma w(Fo^2)^2]]^{1/2}$.

Table 16. Atom coordinates for DFT optimized structure of [**77**]$^{+}$.

Center Number	Coordinates (Angstroms) X	Y	Z	Center Number	Coordinates (Angstroms) X	Y	Z
S1	-2.16276	-1.247116	-1.25418	H31	-1.894618	-0.468013	2.457813
C2	-1.697295	2.977028	-0.991032	C32	-3.562452	4.366673	0.022985
H3	-1.752598	3.604609	-1.876623	H33	-3.934784	4.531988	-0.993294
C4	-0.648666	1.10843	0.204195	H34	-3.091635	5.303249	0.350173
C5	4.035123	1.33114	0.542094	H35	-4.420603	4.189609	0.678846
H6	4.550554	2.129485	1.068721	C36	-3.79498	-0.76307	-0.590934
C7	-1.322712	-2.107429	0.096882	H37	-3.622559	0.064607	0.099815
C8	2.649613	1.198716	0.706204	H38	-4.26752	-1.60512	-0.082405
C9	0.068604	-3.488059	2.060583	H39	-4.407905	-0.422072	-1.428757
H10	0.621631	-4.026531	2.822577	C40	0.557433	-2.272977	1.573355
C11	2.708452	-0.736372	-0.798744	H41	1.491573	-1.877858	1.957851
C12	-1.82436	-3.331197	0.563259	B42	0.413112	-0.059581	0.250425
H13	-2.737026	-3.761898	0.165213	C43	-2.63134	-2.590877	-2.405063
C14	-2.479657	2.400111	1.206743	H44	-1.712297	-3.074992	-2.740723
H15	-3.131671	2.591882	2.055162	H45	-3.129929	-2.125217	-3.258628
C16	1.949705	0.137001	0.046943	H46	-3.293548	-3.319614	-1.936102
C17	-0.131896	-1.522438	0.590994	C47	-1.128567	-4.017212	1.562111
C18	-1.548904	1.352315	1.288802	H48	-1.512652	-4.959757	1.93557
C19	1.960386	2.203217	1.612684	C49	2.069208	-1.856257	-1.604661
H20	2.702763	2.803043	2.146758	H50	2.7718	-2.233191	-2.353694
H21	1.325135	1.726425	2.365983	H51	1.174611	-1.520391	-2.144247
H22	1.325023	2.892596	1.045776	H52	1.778011	-2.70493	-0.975478
C23	0.189104	1.796295	-2.135791	C53	-2.575605	3.223964	0.075328
H24	-0.095941	2.481476	-2.939254	C54	4.084338	-0.54221	-0.959022
H25	0.160761	0.778846	-2.546918	H55	4.634412	-1.198034	-1.628668
H26	1.231791	2.002707	-1.873741	C56	4.774581	0.475947	-0.284721
C27	-0.730785	1.962708	-0.940306	C57	6.268538	0.634322	-0.43549
C28	-1.506902	0.550788	2.580091	H58	6.588694	1.655965	-0.209743
H29	-2.111388	1.03785	3.350618	H59	6.598086	0.389237	-1.450495
H30	-0.490375	0.458143	2.977711	H60	6.805014	-0.035667	0.250017

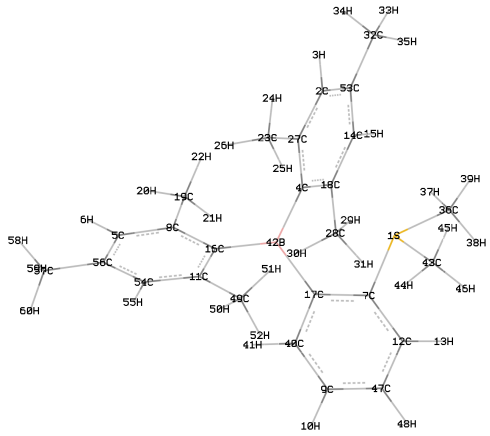

Figure 50. DFT optimized structure of [**77**]$^+$.

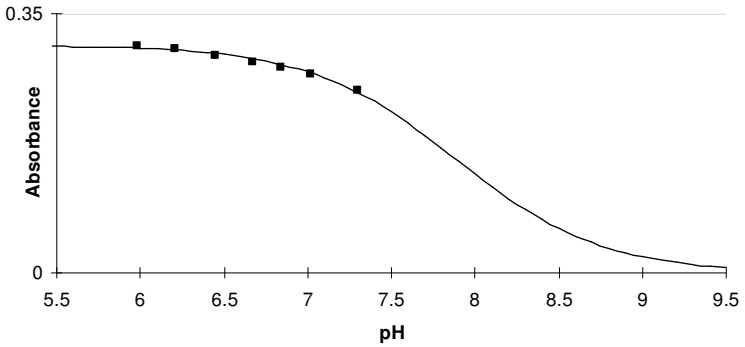

Figure 51. Spectrophotometric titration curve of [**77**]$^+$ in H_2O/MeOH (95/5, v/v). The absorbance was measured at 330 nm. The experimental data was fitted to eq. 1 using ε([**77**]$^+$) = 9300 M^{-1} cm^{-1}, ε(**77**-OH) = 0 M^{-1} cm^{-1}, and pK_{R+} = 7.89 (±0.08). Above pH 7.5 there were precipitations.

5.3 Reaction with hydroxide and pH stability range

Next, we decided to investigate the Lewis acidity of [**77**]$^+$ by studying its behavior in aqueous solution as a function of pH. Since hydroxide binding to the boron center is expected to interrupt the π-conjugation mediated by the boron vacant p-orbital,[9] we monitored the absorbance of the boron centered chromophore as a function of pH in MeOH/H_2O (5/95, v/v) and observed that [**77**]$^+$ is stable up to pH 7.0 (Figure 51). Hydroxide binding to [**77**]$^+$ is reversible as confirmed by the observed revival of the absorbance of the boron-centered chromophore upon acidification of the solution (Figure 52).

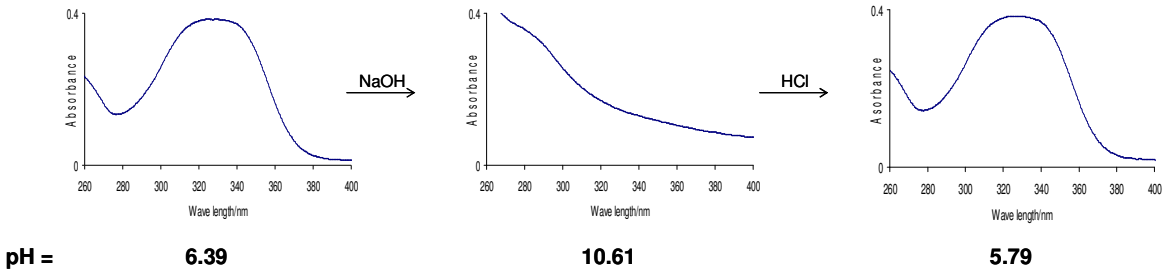

Figure 52. The reversibility test between [**77**]$^+$ and **77**-OH in H_2O/MeOH 95/5 vol. (3 mL; 4.13×10^{-5} M; HEPES buffer).

5.4. Cyanide ion complexation

Having established the pH stability range of this novel cationic borane, we decided to compare its anion affinity in aqueous solutions. Bearing in mind that anion binding to the boron center should results in a quenching of the low energy band observed in the spectra of the boranes, these studies were monitored by UV-vis

spectroscopy. Addition of 15 eq. of Cl^-, Br^-, I^-, NO_3^-, HSO_4^-, $H_2PO_4^-$, and $CH_3CO_2^-$ to a 32 μM solution of [**77**]$^+$ in H_2O/MeOH (95/5, v/v) at pH 7 did not result in any changes of the absorption spectrum indicating the absence of any significant interactions. [**77**]$^+$ gave a small but noticeable response in the presence of fluoride as indicated by the 4% absorption quenching measured upon addition of 15 eq. of F^-. A much more drastic response was observed in the presence of CN^-. Indeed, addition of only 0.2 eq. of CN^- to a [**77**]$^+$ (32 μM) resulted in the formation of a precipitate which was identified as **77**-CN. Increasing the amount of cyanide led to higher yields of **77**-CN. The precipitation of **77**-CN precluded the determination of the cyanide binding constant of [**77**]$^+$ under these conditions. Nevertheless, a titration carried out in H_2O/MeOH (6/4, v/v) at pH 7, conditions under which **77**-CN does not precipitate, showed that the binding constant under these conditions exceeds 10^8 M^{-1} (Figure 53, Table 17).

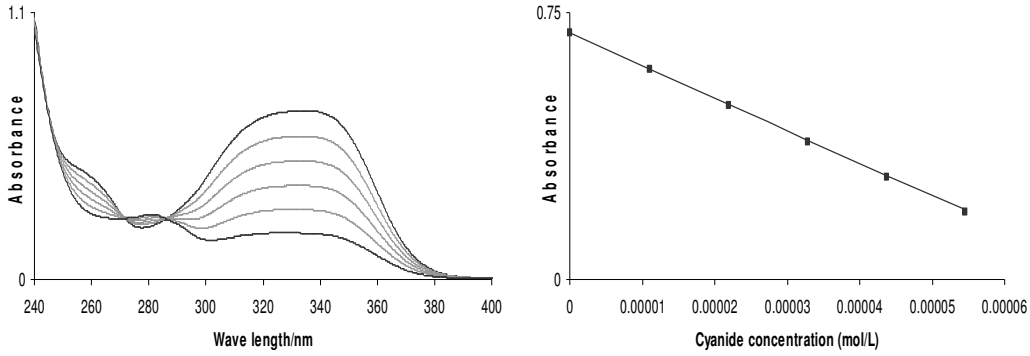

Figure 53. Left: Absorbance change of a solution of [**77**]$^+$ after successive additions of cyanide anions; right: The absorbance was measured at 335 nm. Experimental data and calculated 1:1 binding isotherm with $K > 6 \times 10^8$ M^{-1} using ε([**77**]$^+$) = 9300 $M^{-1}cm^{-1}$ and ε(**77**-CN) = 0 $M^{-1}cm^{-1}$.

Table 17. Absorbance of a solution of [**77**]$^+$ after successive additions of cyanide anions in H_2O/MeOH (6/4, v/v).

$C_{cyanide}$	Abs_{exp}	Abs_{calc}	$C_{cyanide}$	Abs_{exp}	Abs_{calc}
0	0.695	0.6944	3.28E-05	0.387	0.391447
1.10E-05	0.59	0.592803	4.37E-05	0.287	0.292244
2.19E-05	0.488	0.491763	5.45E-05	0.191	0.19529

The identity of **77**-CN has been firmly established using conventional characterization techniques. Some of its salient spectroscopic features include: 1) a ^{11}B NMR resonance at –14.7 ppm indicating the presence of a four coordinate boron center; 2) an intense IR band at 2162 cm^{-1} confirming the presence of the boron-bound cyano group.[20 17, 121] **77**-CN has also been analyzed by single crystal X-ray diffraction (Table 18). The B(1)-C(27) bond connecting the carbon atom of the cyanide anion to the boron center (1.636(5) Å) is comparable to those typically found in triarylcyanoborate anions[199] such as $[Ph_3BCN]^-$ (1.65 Å).[200] The sum of the C_{aryl}-B-C_{aryl} angles ($\sum_{(C\text{-}B\text{-}C)}$ = 337.7°) indicates substantial pyramidalization of the boron atom. The B(1)-C(2)-C(1) angle of 122.4(3)° is close to the ideal value of 120° indicating that the structure is sterically unhindered. Finally, the centroid of the C(27)-N(1) (Ct_{CN}) bond is separated from the sulfur atom by only 3.03 Å and form a Ct_{CN}-S(1)-C(8) angle of 164.2°. In order to investigate the presence of a possible interaction between the sulfur and cyanide atom, we carried out an NBO analysis at the DFT optimized structure (Figures 54 and 55, Table 19). This analysis reveals the presence of a $\pi(C\equiv N)\rightarrow\sigma^*(S\text{-}C)$ donor-acceptor interaction unexpectedly complemented by a back-bonding $lp(S)\rightarrow\pi^*(C\equiv N)$ component.

The concomitant deletion of these two interactions leads to an increase of the total energy of the molecule by 4.1 Kcal/mol, an energy comparable to that of a strong hydrogen bond.[183] In addition to providing some energetic stabilization to the complex via formation of the aforementioned interactions, the sulfonium moiety flanks one side of the boron-bound cyanide anion thus providing steric protection against water molecules.

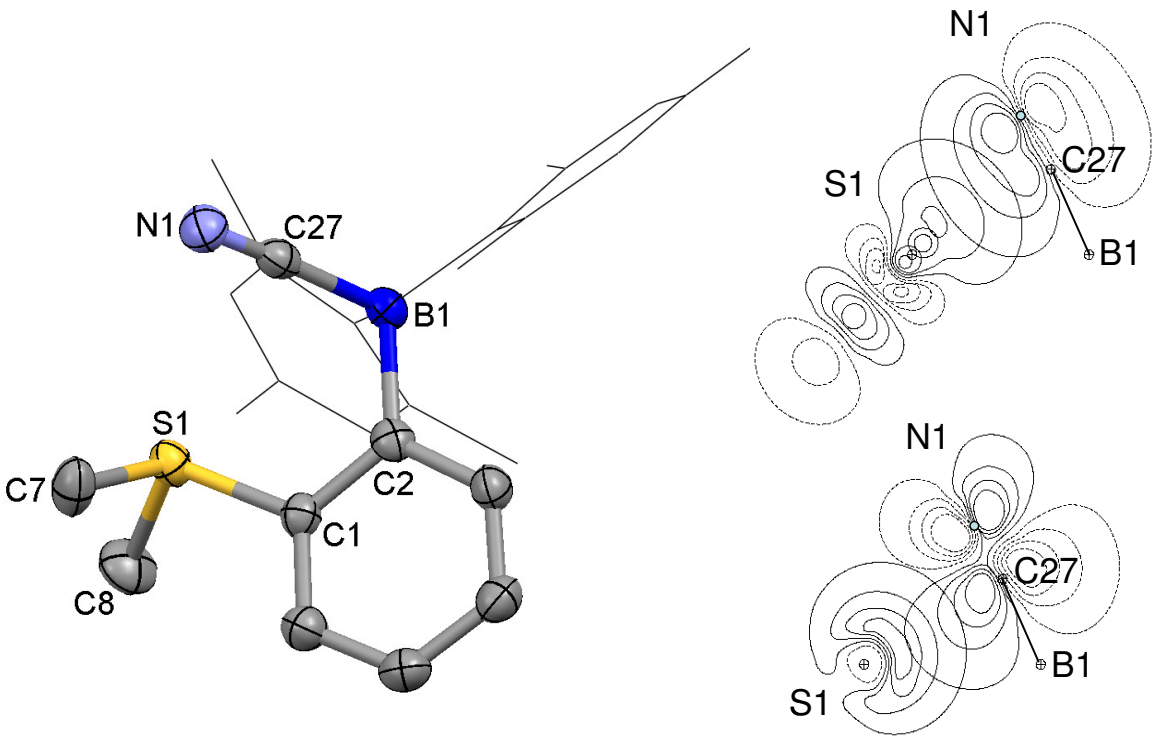

Figure 54. Left: Crystal structure of **77**-CN with thermal ellipsoids set at 50% probability level. Hydrogen atoms are omitted for clarity. Pertinent metrical parameters can be found in the text. Right: NBO contour plots showing π(C≡N)→σ*(S-C) (top) and lp(S)→π*(C≡N) (bottom) interactions.

Table 18. Crystal data, data collections, and structure refinement for **77**-CN.

Crystal data	**77**-CN
Formula	$C_{27}H_{32}BNS$
M_r	413.41
crystal size (mm^3)	0.31 x 0.08 x 0.05
crystal system	Monoclinic
space group	$P2_1/c$
a (Å)	8.6248(17)
b (Å)	14.589(3)
c (Å)	18.030(4)
α (°)	
β (°)	96.42(3)
γ (°)	
V ($Å^3$)	2254.5(8)
Z	4
ρ_{calc} (g cm^{-3})	1.218
μ (mm^{-1})	0.158
F(000)	888
Data collection	
T (K)	110(2)
scan mode	ω
hkl range	-11 → +11 -18 → +19 -23 → +23
measd reflns	21259
unique reflns [R_{int}]	5433 [0.0898]
reflns used for refinement	5433
Refinement	
refined parameters	271
GooF	1.003
R_1,[a] wR_2[b] all data	0.1361, 0.1696
ρ_{fin} (max/min) (e $Å^{-3}$)	1.124 and -0.471

[a] $R_1 = \Sigma||Fo| - |Fc||/\Sigma|Fo|$. [b] $wR_2 = [[\Sigma w(Fo^2 - Fc^2)^2]/[\Sigma w(Fo^2)^2]]^{1/2}$.

Table 19. Atom coordinates for the DFT optimized structure of **77**-CN.

Center Number	Coordinates (Angstroms) X	Y	Z	Center Number	Coordinates (Angstroms) X	Y	Z
S1	-2.54259	-1.21869	0.820103	B32	0.402488	-0.0794	0.302541
N2	-0.25021	-0.85689	2.906286	C33	2.576501	-1.96449	1.532071
C3	2.608232	1.255747	-0.61628	H34	3.416608	-2.66632	1.581155
C4	2.038083	0.168843	0.122948	H35	1.723286	-2.50028	1.111027
C5	4.003493	1.411822	-0.71263	H36	2.306119	-1.69943	2.560071
H6	4.39197	2.25076	-1.28607	C37	-2.97683	-2.48792	2.059496
C7	-0.1044	-1.47585	-0.47167	H38	-2.10142	-2.57814	2.705679
C8	-1.43945	1.275634	-1.21136	H39	-3.2236	-3.4407	1.589008
C9	0.082611	-0.48335	1.850491	H40	-3.82097	-2.10969	2.64145
C10	4.904281	0.533514	-0.10759	C41	6.399147	0.747165	-0.19871
C11	-0.63947	1.183854	-0.0294	H42	6.943599	-0.20235	-0.14396
C12	-1.37206	-2.07129	-0.27557	H43	6.764402	1.378314	0.623629
C13	-0.90776	-3.91858	-1.76114	H44	6.677112	1.243635	-1.13538
H14	-1.20815	-4.84297	-2.24281	C45	-1.82054	3.197501	0.774188
C15	2.975562	-0.7399	0.720724	H46	-1.91982	3.973467	1.530995
C16	1.799832	2.314847	-1.35016	C47	-4.07511	-1.14827	-0.172
H17	2.472865	2.960037	-1.92528	H48	-3.90401	-0.40401	-0.95132
H18	1.233886	2.954492	-0.66656	H49	-4.87483	-0.80066	0.486867
H19	1.079018	1.887289	-2.05026	H50	-4.3325	-2.11421	-0.60828
C20	0.740497	-2.1795	-1.36387	C51	-1.21779	0.424286	-2.45808
H21	1.728566	-1.7719	-1.54653	H52	-0.16834	0.15523	-2.5904
C22	4.361897	-0.54422	0.593929	H53	-1.52846	0.988696	-3.34483
H23	5.033072	-1.26188	1.061362	H54	-1.78436	-0.51574	-2.46095
C24	0.357474	-3.36263	-1.99698	C55	-3.76961	4.25055	-0.46926
H25	1.047577	-3.85942	-2.6722	H56	-3.40168	5.255684	-0.23031
C26	-1.78069	-3.26686	-0.89159	H57	-4.60592	4.04628	0.213691
H27	-2.76019	-3.69653	-0.70316	H58	-4.17392	4.27477	-1.48697
C28	-0.81753	2.22885	0.933972	C59	0.093796	2.395957	2.13964
C29	-2.67505	3.214201	-0.33523	H60	1.108453	2.042461	1.937308
C30	-2.43943	2.262623	-1.33126	H61	-0.26834	1.845727	3.014954
H31	-3.018	2.310814	-2.25271	H62	0.154207	3.45542	2.414412

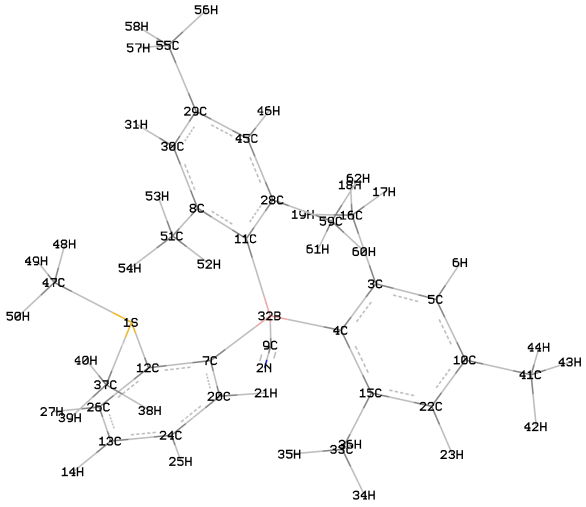

Figure 55. DFT optimized structure of **77**-CN.

Encouraged by the results of our initial anion binding studies, we decided to investigate the use of $[\mathbf{77}]^+$ for the detection of cyanide near the maximum allowable concentration of 50 ppb (1.9 μM) recommended by the European Union for drinking water.[201] To this end, we monitored the fluorescence at 460 nm (λ_{ex} = 300 nm) of a 4.0 μM of $[\mathbf{77}]^+$ in pure water upon addition of CN^-. Remarkably, addition of 50 ppb of CN^- resulted in a 33% quenching of the fluorescence after one hour (Figure 56). Next, we decided to test the behavior of $[\mathbf{77}]^+$ in the presence of 0.2 ppm (7.7 μM) of cyanide which corresponds to the maximum contaminant level set by the US Environmental Protection Agency.[85] Under these conditions, an almost complete quenching of the fluorescence was observed after one hour (Figure 56). The naked-eye observation of this fluorescence quenching can be readily observed when 0.1 ppm of cyanide is added to a 4 μM solution of $[\mathbf{77}]^+$ as shown in Figure 57. Thus, $[\mathbf{77}]^+$ is one of the rare

molecular system competent for cyanide sensing at the sub-ppm level in water.[26, 46, 61, 68, 76, 80, 82-84]

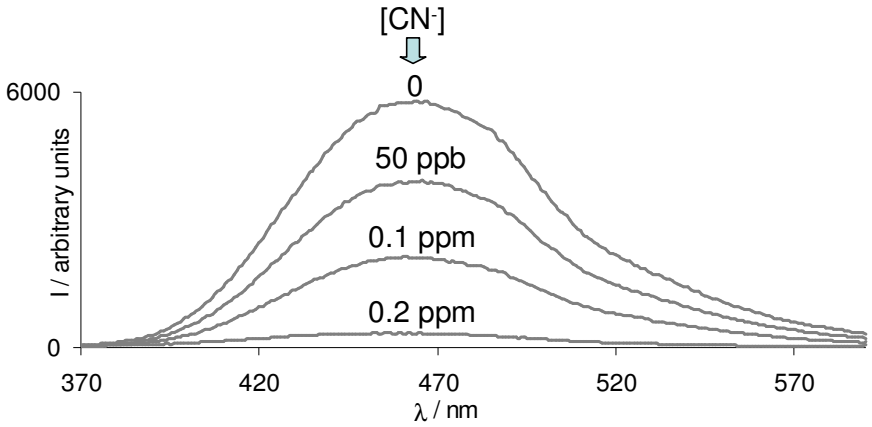

Figure 56. Fluorescence spectrum of [**77**]$^+$ (4.0 μM) in pure water at pH 7 (HEPES 10 mM) before and after addition of cyanide.

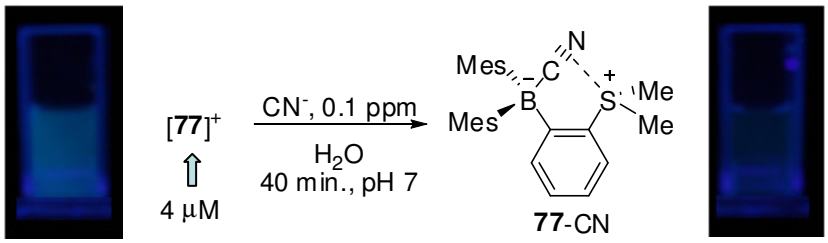

Figure 57. Visible fluorescence changes (under a hand-held UV-lamp) accompanying the formation of **77**-CN. The reaction conditions are provided in the figure.

5.5. Fluoride and azide ion complexation

We find that in addition to cyanide, $[\mathbf{77}]^+$ forms adducts with fluoride and azide in methanol (Figure 58). Compound **77**-F and **77**-N_3 have been isolated and characterized by NMR as well as X-ray crystallography (Figures 59 and 60, Table 20).

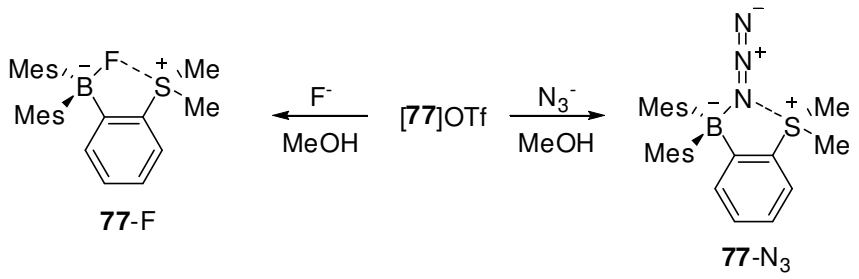

Figure 58. Synthesis of **77**-F and **77**-N_3.

The ^{11}B NMR resonance was observed at +6.02 ppm for **77**-F and +4.41 ppm for **77**-N_3. The crystal structures of these adducts show that: 1) the boron center adopts a trigonalplanar coordination geometry ($\sum(C_{aryl}\text{-}B\text{-}C_{aryl})$ = 340.3° for **77**-F and 334.65° for **77**-N_3); 2) the F-S separation (2.665 Å) in **77**-F and N-S separation (2.900 Å) in **77**-N_3 are well within the sum of van der Waals radii of two atoms.

The fluoride titration was carried out in methanol by monitoring the absorbance of $[\mathbf{77}]^+$ at 340 nm upon fluoride addition (Figure 61, Table 21). Fitting of the resulting isotherms to a 1:1 binding model affords a fluoride binding constant $K = 4\ (\pm 0.5) \times 10^4\ M^{-1}$.

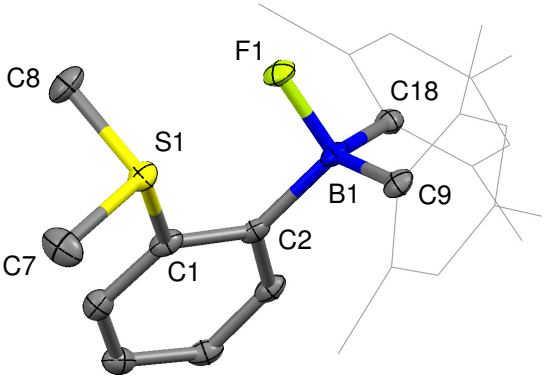

Figure 59. Crystal structure of **77**-F with thermal ellipsoids set at 50% probability level. Hydrogen atoms are omitted for clarity. Pertinent metrical parameters can be found in the text.

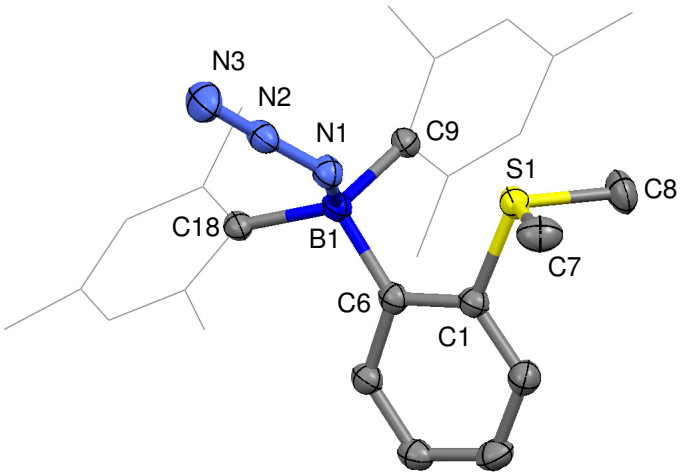

Figure 60. Crystal structure of **77**-N_3 with thermal ellipsoids set at 50% probability level. Hydrogen atoms are omitted for clarity. Pertinent metrical parameters can be found in the text.

Table 20. Crystal data, data collections, and structure refinement for **77**-F and **77**-N_3.

Crystal data	**77**-F·(CH_2Cl_2)	**77**-N_3
Formula	$C_{27}H_{34}BCl_2FS$	$C_{26}H_{32}BN_3S$
M_r	491.31	429.42
crystal size (mm^3)	0.31 x 0.26 x 0.16	0.21 x 0.14 x 0.10
crystal system	Monoclinic	Monoclinic
space group	$P2_1/n$	$C2/c$
a (Å)	11.003(7)	29.424(5)
b (Å)	14.023(9)	8.4596(15)
c (Å)	17.510(11)	19.142(3)
α (°)	90	90
β (°)	106.621(11)	91.055(2)
γ (°)	90	90
V ($Å^3$)	2589(3)	4763.9(14)
Z	4	8
ρ_{calc} (g cm^{-3})	1.261	1.197
μ (mm^{-1})	0.352	0.154
F(000)	1040	1840
Data collection		
T (K)	110(2)	123(2)
scan mode	ω	ω
hkl range	-14 → +14 -18 → +18 -23 → +17	-38 → +39 -11 → +11 -25 → +25
measd reflns	15762	28428
unique reflns [R_{int}]	6116 [0.0899]	5901 [0.0570]
reflns used for	6116	5901
Refinement		
refined parameters	289	280
GooF	1.008	1.006
R_1,[a] wR_2[b] all data	0.0775, 0.1280	0.0815, 0.1221
ρ_{fin} (max/min) (e $Å^{-3}$)	0.578, -0.448	0.630, -0.510

[a] $R_1 = \Sigma||Fo| - |Fc||/\Sigma|Fo|$. [b] $wR_2 = [[\Sigma w(Fo^2 - Fc^2)^2]/[\Sigma w(Fo^2)^2]]^{1/2}$.

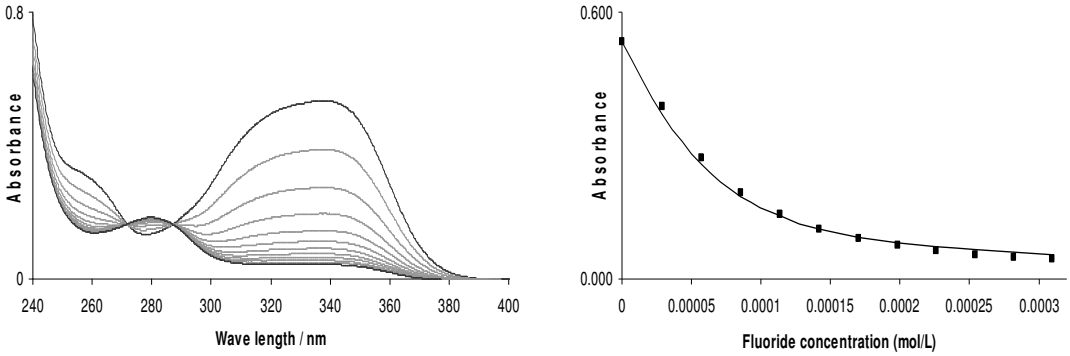

Figure 61. Left: Absorbance change of a solution of [**77**]$^+$ after successive additions of fluoride anions; right: The absorbance was measured at 340 nm. Experimental data and calculated 1:1 binding isotherm with $K = 4 \times 10^4$ M^{-1} using ε([**77**]$^+$) = 9200 M^{-1}cm^{-1} and ε(**77**-F) = 0 M^{-1}cm^{-1}.

Table 21. Absorbance of a solution of [**77**]$^+$ after successive additions of fluoride anions in methanol.

$C_{fluoride}$	Abs_{exp}	Abs_{calc}	$C_{fluoride}$	Abs_{exp}	Abs_{calc}
0	0.534	0.534	0.00017	0.091	0.095
2.86E-05	0.387	0.371	0.000198	0.075	0.082
5.71E-05	0.274	0.257	0.000226	0.065	0.072
8.56E-05	0.195	0.185	0.000254	0.055	0.065
0.000114	0.145	0.141	0.000282	0.05	0.060
0.000142	0.113	0.113	0.00031	0.044	0.056

5.6. Conclusion

In conclusion, we report the synthesis of a sulfonium borane ([**77**]$^+$) which can be used in pure water for the fluorescence detection of cyanide near the EU maximum allowable concentration. The high affinity of this borane arises from favourable Coulombic effects which serve to stabilize the cyanoborate complex against dissociation.

Last, but not least, the sulfonium moiety interacts with the cyanide guest via both bonding and back-bonding interactions thus further enhancing the unusual affinity of [**77**]$^+$ toward cyanide.

5.7. Experimental Section

General Considerations. Dimesitylboron fluoride, methyl triflate and potassium cyanide were purchased from Aldrich, 2-bromothioanisole from TCI. Solvents were dried by passing through an alumina column (n-Hexane, dichloromethane) or refluxing under N_2 over Na/K (Et_2O). UV-vis and emission spectra were recorded on an Ocean Optics USB4000 spectrometer with a Ocean Optics ISS light source and an Aminco-Bowman 2 Luminescence spectrophotometer. IR spectra were obtained using a Bruker Tensor 37 infrared spectrophotometer. Elemental analyses were performed by Atlantic Microlab (Norcross, GA). pH Measurements were carried out with a Radiometer PHM290 pH meter equipped with a VWR SympHony electrode. NMR spectra were recorded on Varian Unity Inova 400 FT NMR (399.59 MHz for ^{1}H, 128.19 MHz for ^{11}B, 100.45 MHz for ^{13}C) spectrometers at ambient temperature. Chemical shifts are given in ppm, and are referenced against external $BF_3{\cdot}Et_2O$ (^{11}B).

Crystallography. The crystallographic measurements were performed using a Bruker APEX-II CCD area detector diffractometer (Mo-K_α radiation, λ= 0.71069 Å) for **[77]**OTf, **77**-CN, **77**-F and **77**-N_3. In each case, a specimen of suitable size and quality was selected and mounted onto a nylon loop. The structures were solved by direct

methods, which successfully located most of the non-hydrogen atoms. Subsequent refinement on F^2 using the SHELXTL/PC package (version 5.1) allowed location of the remaining non-hydrogen atoms.

Synthesis of 76. To 2-bromothioansile (0.83 g, 4.1 mmol) in diethyl ether (20 mL) was added *n*-BuLi (1.95 mL, 4.3 mmol, 2.2M in *n*-hexane) at 0 °C. After stirring the mixture for 1h at 0 °C, dimesitylboron fluoride (1.2 g, 4.5 mmol) was added to the lithiated compound at the same temperature. The mixture was allowed to warm to room temperature (rt) and stirred over night. The mixture was quenched with water (10 mL) and the organic layer was separated, dried over $MgSO_4$, filtered and concentrated in *vacuo* to get yellow solid. . The residue was washed with *n*-Hexane (7 mL) to afford the desired product as a pale-yellow solid (66 % yield). ^{1}H-NMR (400 MHz, $CDCl_3$) δ 2.01 (s, 12H), 2.27 (s, 3H), 2.29 (s, 6H), 6.77 (s, 4H), 7.05 (t, 1H, *J*=7.2 Hz), 7.12-7.18 (m, 2H), 7.33 (t, 1H, *J*=7.2Hz). ^{13}C-NMR (100 MHz, $CDCl_3$) δ 16.61, 21.45, 23.10, 124.50, 124.72, 128.30, 130.95, 134.41, 139.23, 140.94, 142.78, 143.98, 148.00. ^{11}B-NMR (128 MHz, $CDCl_3$) δ + 74.94 (bs).

Synthesis of [77]OTf. Methyl triflate (0.92 mL, 8.1 mmol) was added to a solution of (2-(Dimesityl)phenyl)methylsulfide (0.3 g, 0.81 mmol) in dichloromethane (10 mL) at room temperature. The mixture was refluxed overnight and cooled to rt. The solvent was removed in *vacuo* to yield a foamy solid as a crude product. Purification was achieved by adding n-Hexane into a concentrated diethyl ether solution of the crude

compound and keeping the solution in a refrigerator. The precipitation was filtered and washed with *n*-Hexane (5 mL) to afford the desired product (88% yield). ^{1}H-NMR (400 MHz, $CDCl_3$) δ 2.04 (bs, 12H), 2.30 (s, 6H), 3.00 (bs, 6H), 6.85 (s, 4H), 7.46 (d, 1H, *J*=6.4 Hz), 7.67 (t, 1H, *J*=7.2 Hz) 7.85 (t, 1H, *J*=7.2 Hz), 8.39 (d, 1H, *J*=8.4 Hz). ^{13}C-NMR (100 MHz, $CDCl_3$) δ 21.40, 23.02, 28.82, 118.91, 122.09, 129.32, 129.96, 133.97, 134.26, 134.88, 141.28, 141.80, 153.95. ^{11}B-NMR (128 MHz, $CDCl_3$) δ +77 (bs). Anal. Calcd for $C_{27}H_{32}BF_3O_3S_2$ ([**77**]OTf): C, 60.45; H, 6.01. Found: C, 60.15; H, 6.00.

Synthesis of 77-CN. [**77**]OTf (0.1 g, 0.186 mmol) was dissolved in MeOH (10 mL) and treated with KCN (0.12 g, 1.85 mmo) which resulted in the formation of a white solid. After 30 min, the solid was isolated by filtration, washed with MeOH, and dried in *vacuo* to afford **77**-CN as a white solid (61% yield). ^{1}H-NMR (400 MHz, $CDCl_3$) δ 1.97 (bs, 12H), 2.24 (s, 6H), 2.75 (s, 6H), 6.73 (s, 4H), 7.29-7.46 (m, 4H). ^{13}C-NMR (100 MHz, $CDCl_3$) δ 20.93, 25.52, 28.87, 125.50, 127.86, 129.49, 131.96, 134.19, 138.64, 143.30, 146.77, 166.00. ^{11}B-NMR (128 MHz, $CDCl_3$) δ −14.72 (s). IRν_{CN} = 2162.4 cm^{-1}.

Synthesis of 77-F. [**77**]OTf (0.08 g, 0.15 mmol) was dissolved in MeOH (5 mL) and treated with excess amount of KF which resulted in the formation of a white solid. After 30 min, the solid was isolated by filtration, washed with MeOH, and dried in *vacuo* to afford **77**-F as a white solid (65% yield). ^{1}H-NMR (400 MHz, $CDCl_3$) δ 1.90 (s, 12H), 2.23 (s, 6H), 2.75 (s, 6H), 6.66 (s, 4H), 7.30-7.36 (m, 3H), 7.39-7.41 (m, 1H). ^{13}C-

NMR (100 MHz, $CDCl_3$) δ 21.03, 24.90, 29.24, 123.31, 127.14, 128.85, 128.94, 131.97, 133.41, 137.39 (d, $J_{C\text{-}F}$=6.1 Hz), 141.87, 151.24 (bs), 168.85 (bs). ^{11}B-NMR (128 MHz, $CDCl_3$) δ +6.02 (bs). ^{19}F-NMR (376 MHz, $CDCl_3$) δ −153.32 (s). Anal. Calcd for $C_{26}H_{32}BFS$ (**2**-F): C, 76.84; H, 7.94. Found: C, 75.47; H, 7.75.

Synthesis of 77-N_3. [**77**]OTf (0.08 g, 0.15 mmol) was dissolved in MeOH (5 mL) and treated with excess amount of NaN_3 which resulted in the formation of a white solid. After 30 min, the solid was isolated by filtration, washed with MeOH, and dried in *vacuo* to afford **77**-N_3 as a white solid. ^{1}H-NMR (400 MHz, $CDCl_3$) δ 1.93 (s, 12H), 2.24 (s, 6H), 2.78 (s, 6H), 6.76 (s, 4H), 7.45-7.50 (m, 2H), 7.60 (t, 1H, *J*=6.4 Hz), 8.00 (d, 1H, *J*=8.0 Hz). ^{11}B-NMR (128 MHz, $CDCl_3$) δ 4.41.

Acid-base Titration of $[77]^+$ in H_2O/MeOH (95/5, v/v). A solution of [**77**]OTf (3.0 mL, 3.3×10^{-5} M; HEPES 9.5mM) was titrated by incremental addition of a solution of NaOH in water. The resulting data was fitted to the equilibrium shown in eq 1 and K_{R+} values were converted to pK_{R+} values.

$$[R_3B]^+ + H_2O \xrightarrow{K_{R+}} R_3B{-}OH + H^+ \qquad \text{(eq 1)}$$

Cyanide Titration. A solution of [**77**]OTf (3.0 mL, 7.47×10^{-5} M; H_2O/MeOH 6/4 vol.; HEPES buffer 6mM, pH 7) was titrated by incremental addition of a solution of KCN in water (6.6×10^{-3} M).

Fluoride Titration. A methanol solution of [**77**]OTf (3.0 mL, 5.80×10^{-5} M) was titrated by incremental addition of a solution of KCN in water (1.72×10^{-2} M).

Selectivity Test. To a solution of $[\mathbf{77}]^+$ in 95:5 H_2O/MeOH (3 mL, 3.2×10^{-5} M; pH 7; 9.5 mM HEPES buffer was added 5 μL of a 0.3 M solution of X^- (X = F, Cl, Br, I, NO_3, HSO_4, CH_3CO_2 and H_2PO_4). Only F^- showed absorbance at λ=330 nm changed (4 % decreased). The absorbance remained unchanged for other anions.

Fluorescence Measurements. Measurement was carried out SLM/AMINCO, Model 8100 spectrofluorometer equipped with a xenon lamp. Because of the known light sensitivity of sulfonium salts (see for example W. Zhou, S. M. Kuebler, D. Carrig, J. W. Perry, and S. R. Marder *J. Am. Chem. Soc.* **2002**, 124, 1897-1901), irradiation time was minimized by opening the excitation shutter only during the time necessary to record each spectrum. The same precautions were taken when irradiating the cells with the hand-held UV lamp used to take the pictures. The quantum yields were measured using anthracene as a standard.

Computational Details. DFT calculations (full geometry optimization) were carried out with the Gaussian 03 program using the gradient-corrected Becke exchange functional (B3LYP) and the Lee-Yang-Parr correlation functional. Geometry optimization of [**77**]$^+$ was carried out with the following mixed basis set: 6-31+g(d') for the boron, 6-31+g(d) for the sulfur atom, 6-31g basis set was used for all carbon and hydrogen atoms. Geometry optimization of **77**-CN was carried out with the following mixed basis set: 6-31+g(d') for the boron, nitrogen and C(9) atom, 6-31+g(d) for the sulfur atom, 6-31g basis set was used for other remained carbon and hydrogen atoms. Frequency calculations, which were carried out on the optimized structures of the compounds, confirmed the absence of any imaginary frequencies. The Natural Bond Orbital (NBO) analyses of [**77**]$^+$ and **77**-CN was carried out using the stand along PC version of GENNBO 5.0 program.

CHAPTER VI

SYNTHESIS AND ANION AFFINITY OF A BIDENDATE SULFONIUM FLUOROSILANE LEWIS ACID*

6.1. Introduction

One of the main themes in the chemistry of polydentate Lewis acids is the discovery of new molecular structures that can support anion chelation. Modulating the structures and varying the elements involved in anion binding provides an effective way to control the affinity of such systems. To date, a great deal of effort has been devoted to the chemistry of boron-based polydentate Lewis acids[190-192, 202-204] and their use as sensors for the potentially toxic fluoride anion.[142] By contrast, and despite the widespread use of tetracoordinate halosilanes as Lewis acids in organic synthesis,[205-207] much less is known about silicon based polydentate Lewis acids.[31-35, 41, 43, 44, 208] Some of the most notable examples of such compounds include **28**[41] which displays a high affinity for fluoride anions and **32**[44] in which the silicon atom assists fluoride binding at the boron atom.

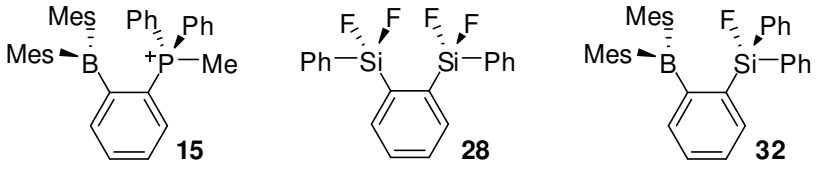

* Reprinted in part with permission from, "Synthesis and Anion Affinity of a Bidendate Sulfonium Fluorosilane Lewis Acid"; Kim, Y.; Kim, M.; Gabbaï, F. P.; *Org. Lett.*, **2010**, *12*, 600-602, Copyright 2010 by the American Chemical Society.

In some of our recent exploratory studies, we have demonstrated that the fluoride ion affinity of boranes could be greatly increased by incorporation of proximal 3rd row onium functionality as in **15**.[19, 209] In addition to facilitating anion binding via inductive and Coulombic effects, the phosphonium ion of **15** becomes hypervalent and engages the anion in a donor-acceptor interaction (Figure 47). Similar effects have been observed in the chemistry of sulfonium boranes as cyanide receptors.[210] As part of our ongoing endeavour in the chemistry of polydentate Lewis acids, we have now decided to determine if this "onium-based strategy" (Figure 62) could be extended to silicon Lewis acids.

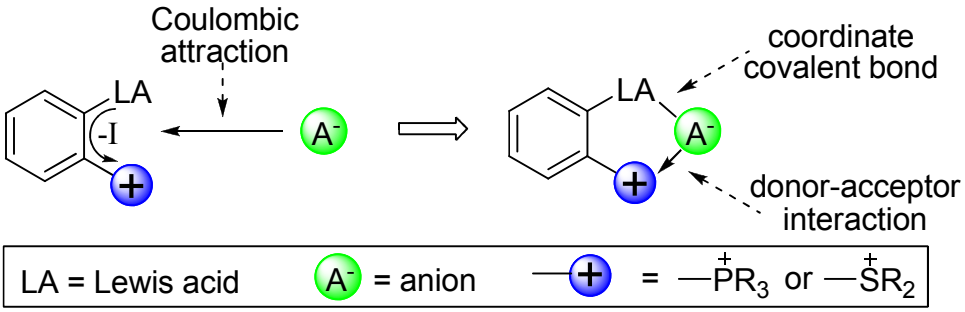

Figure 62. "Onium-based strategy": Illustration of the forces and bonding interactions involved in anion binding by a bidentate 3rd row onium/Lewis acid.

6.2. Synthesis and characterization of a sulfonium fluorosilane

Triarylfluorosilanes bind fluoride anions to form the corresponding triaryldifluorosilicates.[38, 40, 211-214] Careful studies by Tamao and Yamaguchi,[40] who

showed that Ant_3SiF (Ant = 9-anthryl) can be used as a fluoride ion sensor in organic solvents, led us to consider such fluorosilanes as a starting point for our studies. To obtain a fluorosilane that could easily be converted into a cationic derivative, we allowed *o*-lithiothioanisole to react with di(9-anthryl)difluorosilane[39] in THF at −78 °C (Figure 63). The fluorosilane **78** was converted into [**79**]OTf by reaction with MeOTf. Both **78** and [**79**]OTf have been characterized by conventional spectroscopic methods. The ^{29}Si NMR resonances of these new compounds were detected at −2.4 ppm ($^1J_{Si\text{-}F}$ = 284.2 Hz) for **78** and −0.5 ppm ($^1J_{Si\text{-}F}$ = 282.0 Hz) for $[\mathbf{79}]^+$. In the ^{19}F NMR spectra, the slilicon bound fluorine nucleus gives rise to a resonance at −141.0 ppm for **78** and −138.0 ppm for $[\mathbf{79}]^+$ whose chemical shift is close to that of Ant_2PhSiF (δ −143.7).[40] Salt [**79**]OTf is stable in organic solvents but decomposes in the presence of water.

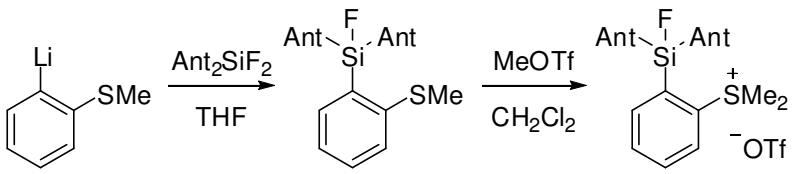

78 [**79**]OTf

Figure 63. Synthesis of neutral and sulfonium fluorosilanes.

6.3. Fluoride ion complexation

With this new cationic silane in hand, we decided to study the responses of [**79**]$^+$ to different anions using ^{19}F NMR spectroscopy. Addition of 5.0 equivalents of Cl^-, Br^- or I^- as tetrabutylammonium salts to a $CDCl_3$ solution of [**79**]$^+$ resulted in the formation of the neutral silane **78** (δ(^{19}F) −141.0 ppm) indicating demethylation of the aryldimethylsulfonium moiety of [**79**]$^+$. By contrast, addition of TBAF to [**79**]$^+$ resulted in the formation of **79**-F (Figure 64). **79**-F could be easily isolated from the reaction of [**79**]OTf with tetrabutylammonium triphenylsilyldifluoride in CH_2Cl_2. Some of its salient NMR spectroscopic features in DMSO-d_6 include: 1) two separate sulfur-bound methyl signals detected at 2.40 and 2.90 ppm in the ^{1}H-NMR spectrum; 2) two doublets at −49.5 and −65.1 with $^2J_{F\text{-}F}$ = 62.4 Hz in the ^{19}F NMR spectrum corresponding to the silyl-bound fluorine atoms (Figure 64); 3) a ^{29}Si NMR resonance at –92.7 ppm (dd, $^1J_{Si\text{-}F}$ = 266.7 Hz, $^1J_{Si\text{-}F}$ = 256.5 Hz) whose chemical shift is comparable to that observed for $[Ant_2PhSiF_2]^-$ (δ = –97.2, $J_{Si\text{-}F}$ = 262.9 Hz).[40] Altogether, these spectroscopic features indicate the presence of two non-equivalent fluorine atoms bound to the silicon center. As indicated by ^{19}F NMR, the chemical shift of one of these two fluorine nuclei is significantly deshielded and exhibits a smaller $^1J_{Si\text{-}F}$, possibly suggesting the presence of an interaction with the neighboring sulfonium center.[187] The detection of two distinct sulfur-bound methyl group resonances corroborates this possibility. To firmly understand the coordination environment of the silicon and sulfur atoms, the crystal structure of in **79**-F was determined (Figure 65, Table 22).

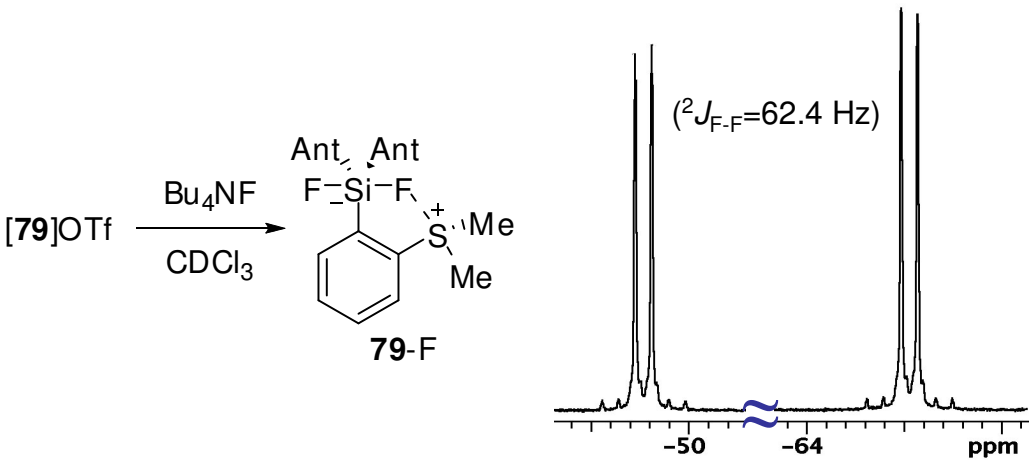

Figure 64. Formation of **79**-F and ^{19}F NMR spectrum.

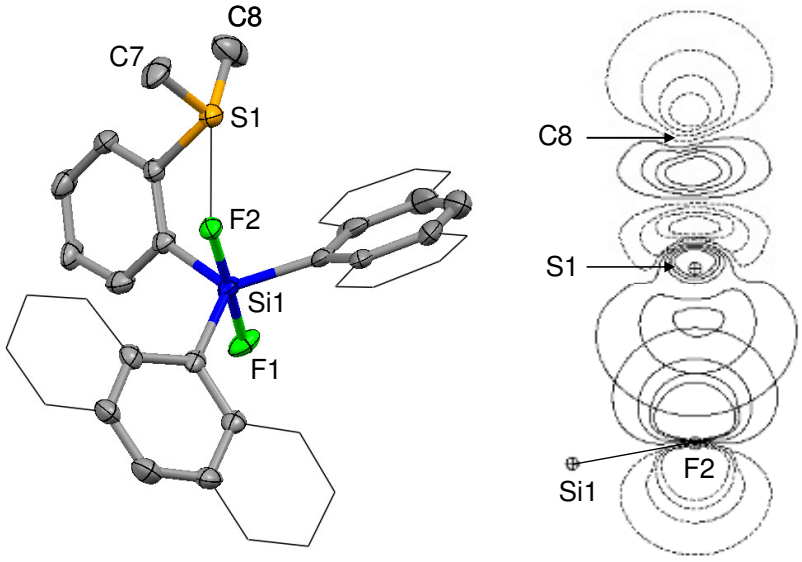

Figure 65. Left: Crystal structure of **79**-F with thermal ellipsoids set at 50% probability level. Hydrogen atoms are omitted for clarity. Pertinent metrical parameters can be found in the text. Right: NBO countour plot showing the lp(F)→σ*(S-C) interaction of **79**-F.

Table 22. Crystal data, data collections, and structure refinement for **79**-F.

Crystal data	**79**-F·$(CH_2Cl_2)_{1.25}$
formula	$C_{37.25}H_{30.50}Cl_{2.50}F_2SSi$
M_r	664.89
crystal size (mm^3)	0.25 x 0.16 x 0.12
crystal system	Tetragonal
space group	*P*4/*n*
a (Å)	24.029(3)
b (Å)	24.029(3)
c (Å)	11.095(2)
α (°)	90
β (°)	90
γ (°)	90
V ($Å^3$)	6406.4(18)
Z	8
ρ_{calc} ($g\ cm^{-3}$)	1.379
μ (mm^{-1})	0.386
F(000)	2756
Data collection	
T (K)	163(2)
scan mode	ω
hkl range	-27 → +15 -27 → +27 -11 → +12
measd reflns	29982
unique reflns [R_{int}]	5022 [0.0769]
reflns used for refinement	5022
Refinement	
refined parameters	401
GooF	1.001
R_1,[a] wR_2[b] all data	0.1032, 0.1703
ρ_{fin} (max/min) (e $Å^{-3}$)	0.969, -0.812

[a] $R_1 = \Sigma||Fo| - |Fc||/\Sigma|Fo|$. [b] $wR_2 = [[\Sigma w(Fo^2 - Fc^2)^2]/[\Sigma w(Fo^2)^2]]^{1/2}$.

Examination of the crystal structure of **79**-F confirmed that the silicon atom adopts a trigonal-bipyramidal geometry (F(1)-Si(1)-F(2) = 177.32(15)°, Σ(C-Si-C) = 360°) (Figure 65). Although close to those observed in the $[Ant_3SiF_2]^-$ anion (1.710-1.716 Å),[40] the silicon-fluorine bond distances in **79**-F (Si(1)-F(1) = 1.706(3) Å; Si(1)-F(2) = 1.732(3) Å) differ by almost 0.03 Å. Further inspection of the structure indicates that the F(2) atom is separated from S(1) by only 2.741(3) Å which is well within the sum of van der Waals radii of two elements (*ca*. 3.27 Å). The resulting F(2)-S(1)-C(8) angle of 166.5(2)° is also close to linearity. Collectively, these metrical parameters suggest the presence of a bonding interaction between the F(2) and S(1) atoms. This view is confirmed by an NBO analysis carried out at the DFT optimized geometry (Figures 65 and 66, Table 23). This analysis reveals a donor-acceptor interaction involving a fluorine lone pair (lp(F)) as a donor and a carbon-sulfur σ*-orbital (σ*(S-C)) as the acceptor (Figure 65). A deletion calculation suggests that this interaction stabilizes the molecule by 5.60 Kcal/mol. Presumably, existence of this interaction is responsible for the lengthening of the Si(1)-F(2) bond as well as for the somewhat deshielded ^{19}F NMR chemical shift measured for the F(2) nucleus.

Table 23. Atom coordinates for the DFT optimized structure of **79**-F.

Center Number	Coordinates (Angstroms) X	Y	Z	Center Number	Coordinates (Angstroms) X	Y	Z
S1	2.281252	1.6768	1.3842	H35	4.015273	-3.7094	0.793816
Si2	-0.15841	0.2619	-0.457	C36	2.010751	-3.05688	1.220642
F3	-0.18519	0.0361	-2.176	C37	1.793849	-4.0366	2.244678
C4	1.535514	2.6793	0.0664	H38	2.592982	-4.74275	2.454751
F5	-0.0749	0.6894	1.3068	C39	0.611358	-4.08731	2.93773
C6	0.567882	2.0518	-0.747	H40	0.454188	-4.83571	3.708377
C7	0.063014	2.8398	-1.808	C41	-0.41955	-3.14948	2.639766
H8	-0.65756	2.3885	-2.48	H42	-1.35487	-3.1921	3.188959
C9	0.463321	4.1629	-2.01	C43	-0.24663	-2.19574	1.664642
H10	0.038971	4.7357	-2.828	H44	-1.04736	-1.49737	1.470856
C11	1.410178	4.7527	-1.163	C45	0.967605	-2.09843	0.89891
H12	1.72398	5.7802	-1.314	C46	-2.0726	-0.00149	-0.34394
C13	1.961058	4.0044	-0.122	C47	-2.94345	0.975959	0.233389
H14	2.707768	4.4615	0.5183	C48	-2.48746	2.232662	0.767508
C15	1.644668	2.4046	2.9318	H49	-1.43032	2.445702	0.76414
H16	2.191449	1.954	3.7641	C50	-3.34976	3.165785	1.2931
H17	0.594069	2.1176	2.9769	H51	-2.95884	4.10199	1.681266
H18	1.762982	3.4899	2.9285	C52	-4.75287	2.921867	1.339246
C19	4.014186	2.2578	1.4191	H53	-5.41947	3.668767	1.759217
H20	4.529229	1.6705	2.1836	C54	-5.24567	1.740007	0.849068
H21	4.106472	3.3213	1.6431	H55	-6.31204	1.531016	0.871573
H22	4.449858	2.0345	0.4431	C56	-4.37823	0.74619	0.28684
C23	1.159695	-1.128	-0.135	C57	-4.90429	-0.44834	-0.21259
C24	2.402506	-1.136	-0.846	H58	-5.97697	-0.61956	-0.15789
C25	2.706127	-0.228	-1.925	C59	-4.08591	-1.42558	-0.78663
H26	1.929801	0.4305	-2.284	C60	-4.65184	-2.64252	-1.29023
C27	3.932734	-0.218	-2.55	H61	-5.72689	-2.77874	-1.20644
H28	4.111136	0.4724	-3.369	C62	-3.86383	-3.60807	-1.8622
C29	4.961476	-1.126	-2.162	H63	-4.30141	-4.52663	-2.24084
H30	5.9198	-1.108	-2.672	C64	-2.45805	-3.3982	-1.96216
C31	4.718248	-2.032	-1.162	H65	-1.83629	-4.15958	-2.42266
H32	5.480246	-2.748	-0.863	C66	-1.87997	-2.2439	-1.48957
C33	3.455715	-2.072	-0.482	H67	-0.81372	-2.114	-1.60303
C34	3.228354	-3.005	0.5341	C68	-2.65381	-1.19857	-0.87307

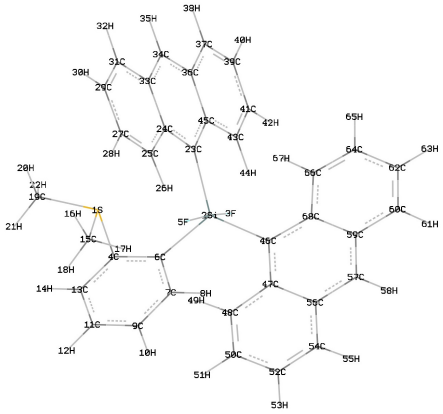

Figure 66. DFT optimized structure of **79-F**.

Formation of **79**-F can be followed by monitoring the UV-vis absorption spectrum of [**79**]$^+$ in chloroform upon incremental addition of TBAF (Figure 67, Table 24). Analysis of the spectral changes indicate that formation of **79**-F induces a blue shift of the anthryl-based absorption bands. As previously explained for other anthrylfluorosilane species,[40] this response can be assigned to a decrease in intramolecular anthryl-anthryl π-stacking interactions induced by the change in coordination geometry at the silicon center. Fitting of this data to a 1:1 binding isotherm affords a fluoride binding constant K of 7 (±1) × 10^6 M^{-1} (Figure 67). Under these conditions, neutral silane **78** captures fluoride with an association constant K of 8(±1) M^{-1} (Figure 68, Table 25). These experiments demonstrate that the fluoride affinity of [**79**]$^+$ exceeds that of neutral silane by at least five orders of magnitude. The drastic enhancement observed in the fluoride ion affinity of [**79**]$^+$ is assigned to the presence of the sulfonium moiety which: 1) provides a Coulombic and inductive drive for the

formation of the difluorosilicate compound; 2) engages the fluoride anion in a stabilizing lp(F)→σ*(S-C) interaction. Although triarylfluorosilanes typically display a lower fluoride affinity than triarylboranes,[215] we note that the fluoride binding constant of [**79**]$^+$ in chloroform is almost equal to the value of 6.5 (±0.5) × 10^6 M^{-1} measured for the boron-based receptor [*p*-$Mes_2B(C_6H_4)PMePh_2]^+$.[18, 174]

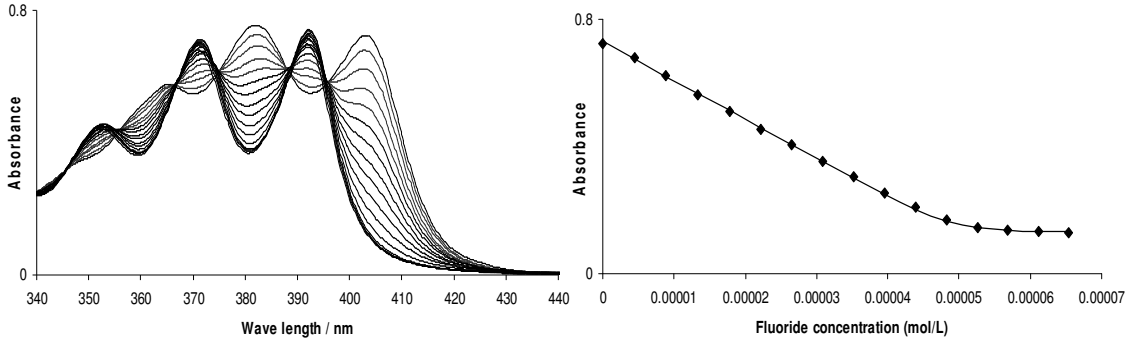

Figure 67. Left: Absorbance change of a solution of [**79**]$^+$ (5.00 × 10^{-5} M) upon successive additions of fluoride in chloroform. Right: Binding isotherm measured at 403 nm and fitted with K = 7 × 10^6 M^{-1}, ε([**79**]$^+$) = 14,600 M^{-1} cm^{-1} and ε(**79**-F) = 2600 M^{-1} cm^{-1}.

Table 24. Absorbance of a solution of [**79**]OTf after successive additions of fluoride anions in chloroform.

$C_{fluoride}$	Abs_{exp}	Abs_{calc}	$C_{fluoride}$	Abs_{exp}	Abs_{calc}
0	0.724	0.73	3.53E-05	0.306	0.301387
4.46E-06	0.679	0.675442	3.96E-05	0.254	0.250504
8.90E-06	0.623	0.621102	4.39E-05	0.21	0.202637
1.33E-05	0.563	0.566992	4.82E-05	0.169	0.163973
1.77E-05	0.51	0.513132	5.25E-05	0.144	0.144068
2.21E-05	0.456	0.459553	5.68E-05	0.136	0.136744
2.65E-05	0.405	0.406311	6.11E-05	0.132	0.133514
3.09E-05	0.353	0.353513	6.54E-05	0.128	0.13171

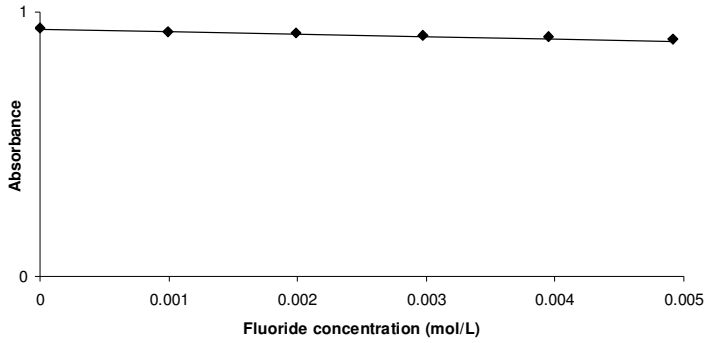

Figure 68. Absorbance change of a solution of **78** at 401 nm after successive additions of fluoride anions. Experimental data and calculated 1:1 binding isotherm with K = 8(±1) M^{-1}. The same binding constant could be derived from a ^{1}H NMR experiment.

Table 25. Absorbance of a solution of **78** after successive additions of fluoride anions in chloroform.

$C_{fluoride}$	Abs_{exp}	Abs_{calc}	$C_{fluoride}$	Abs_{exp}	Abs_{calc}
0	0.938	0.93518	0.00297	0.913	0.905309
0.000997	0.927	0.925002	0.003947	0.906	0.895779
0.001987	0.922	0.915047	0.004918	0.9	0.886453

6.4. Conclusion

The results reported in this communication indicate that proximal 3rd row onium ions can serve to enhance the fluoride affinity of fluorosilanes via cooperative effects. These results also demonstrate the viability of sulfonium ions as Lewis acidic binding sites for fluoride binding.

6. 5. Experimental Section

General Considerations. Di(9-anthryl)difluorosiane was prepared by following the known method (S. Yamaguchi, S. Akiyama, and K. Tamao, *Organometallics* **1998,** *17,* 4347). Methyl triflate and tetrabutylammonium triphenyldifluorosilicate were purchased from Aldrich, 2-bromothioanisole from TCI. Solvents were dried by passing through an alumina column (*n*-pentane, dichloromethane, toluene) or refluxing under N_2 over Na/K (Et_2O, THF). UV-vis was recorded on an Ocean Optics USB4000 spectrometer with a Ocean Optics ISS light source. Elemental analyses were performed by Atlantic Microlab (Norcross, GA). NMR spectra were recorded on Varian Unity Inova 400 FT NMR (399.59 MHz for ^{1}H, 128.19 MHz for ^{11}B, 100.45 MHz for ^{13}C, 79.374 MHz for ^{29}Si) spectrometers at ambient temperature. Chemical shifts are given in ppm, and are referenced against external $BF_3{\cdot}Et_2O$ for ^{19}F and TMS for ^{29}Si.

Crystallography. The crystallographic measurements were performed using a Siemens SMART-CCD area detector diffractometer (Mo-K_α radiation, λ= 0.71069 Å) for **79**-F. A specimen of suitable size and quality was selected and mounted onto a nylon loop. The structure was solved by direct methods, which successfully located most of the non-hydrogen atoms. Subsequent refinement on F^2 using the SHELXTL/PC package (version 5.1) allowed location of the remaining non-hydrogen atoms.

Synthesis of 78. *o*-lithiothioanisole (1.13 mmol) in Et_2O (6 mL) was added to di(9-anthryl)difluorosiane (0.5g, 1.19 mmol) in THF (6 mL) at −78 °C. The reaction

mixture was warmed to room temperature and stirred for 2h. All volatile compounds were removed in vacuo. Addition of benzene (30 mL) to the residue followed by filtration and evaporation of the solvent afforded a yellow solid which was washed with pentane (5 mL) twice to afford **78**. Compound **78** could be recrystallized from dichloromethane and *n*-pentane solution (60% yield). mp 133-135 ºC. ^{1}H-NMR (400 MHz, $CDCl_3$) δ 1.98 (s, 3H), 7.10 (m, 5H), 7.35 (t, J=7.6 Hz, 4H), 7.43-7.49 (m, 3H), 8.02 (d, J=8.4 Hz, 4H), 8.38 (d, J=8.4 Hz, 4H), 8.26 (s, 2H); ^{13}C-NMR (100 MHz, $CDCl_3$) δ 18.27, 124.93, 126.04, 126.21, 128.50 (d, *J*=4.6 Hz), 129.52, 129.60, 130.72 (d, $^{2}J_{C\text{-}F}$=13.7 Hz), 131.47, 131.91, 132.19, 137.10, 137.39, 138.49 (d, $^{2}J_{C\text{-}F}$=15.2 Hz), 146.33; ^{19}F-NMR (128 MHz, $CDCl_3$) δ −141.00; ^{29}Si-NMR (79.37 MHz, $CDCl_3$) δ −2.34 ($^{1}J_{Si\text{-}F}$=284.2 Hz); Anal. Calcd for (**78**-0.3C_5H_{12}-0.1CH_2Cl_2) $C_{36.6}H_{28.8}FSSiCl_{0.2}$: C, 79.13; H, 5.21. Found: C, 79.28; H, 5.20.

Synthesis of [79]OTf. 78 (0.5 g, 1.0 mmol) was allowed to react with methyl triflate (0.92 mL, 8.1 mmol) in dichloromethane (15 mL). The resulting mixture was stirred at room temperature for 2h. The solvent was removed in vacuo to yield a solid. The solid was washed with diethyl ether (5 mL) twice to remove excess methyl triflate. Chloroform (20 m) was added to the solid. The organic layer was washed with water (20 mL) twice, dried over $MgSO_4$ and concentrated in vacuo to afford a yellow solid which was washed with diethyl ether. Further purification, the solid was recrystallized from chloroform and *n*-pentane to afford [**79**]OTf (52% yield). ^{1}H-NMR (400 MHz, $CDCl_3$) δ 2.67 (s, 6H), 7.21 (t, *J*=8.2 Hz, 4H), 7.44-7.50 (m, 5H), 7.60 (t, *J*=7.5 Hz, 1H), 7.93 (t,

J=7.5 Hz, 1H), 8.15 (d, *J*=8.2 Hz, 8H), 8.52 (d, *J*=7.5 Hz, 1H), 8.80 (s, 2H); ^{13}C-NMR (100 MHz, $CDCl_3$) δ 28.37, 125.64, 126.63 (d, $^2J_{C\text{-}F}$=12.1 Hz), 127.48, 130.26, 131.15, 131.50, 131.61, 134.09, 134.86, 135.35, 137.27, 137.86, 137.89, 142.10 (d, $^2J_{C\text{-}F}$=18.2 Hz); ^{19}F-NMR (128 MHz, $CDCl_3$) δ −78.82 (triflate), −138.00 (Si-F); ^{29}Si-NMR (79.37 MHz, $CDCl_3$) δ −0.46 ($^1J_{Si\text{-}F}$=282.0 Hz); MS (ESI) *m/e* 539 (M-OTf). This compound is hygroscopic (Anal. Calcd for ([**79**]OTf-$(H_2O)_{3.8}$) $C_{37}H_{35.6}F_4O_{6.8}S_2Si\ Cl_{0.3}$: C, 58.68; H, 4.74. Found: C, 58.59; H, 4.71.)

Synthesis of 79-F. [**79**]OTF (0.25 g, 0.36 mmol) was dissolved in dichloromethane (5 mL) and treated with a dichloromethane solution (5 mL) of tetrabutylammonium triphenylsilyldifluoride (0.2 g, 0.36 mmol). The resulting solution was stirred for 10 min. The solvent was removed in vacuo to yield a sticky solid. The solid was washed with methanol followed by *n*-pentane and dried under vacuum to afford the desired product **79**-F as a yellow powder (42% yield). mp 120 ºC. ^{1}H-NMR (400 MHz, DMSO-d_6) δ 2.40 (s, 3H), 2.90 (s, 3H), 6.66-6.73 (m, 2H), 6.897 (t, *J*=7.6 Hz, 1H), 7.12 (t, *J*=7.2 Hz, 1H), 7.21 (m, 2H), 7.29 (t, *J*=7.2 Hz, 1H), 7.388 (t, *J*=7.2 Hz, 1H), 7.53 (t, *J*=7.2 Hz, 1H), 7.68 (t, *J*=7.2 Hz, 1H), 7.77 (d, *J*=7.6 Hz, 1H), 7.95 (d, *J*=8.4 Hz, 2H), 8.01 (d, *J*=8.4 Hz, 1H), 8.08-8.14 (m, 2H), 8.20 (d, *J*=8.0 Hz, 1H), 8.46-8.61(m, 5H); ^{13}C-NMR (100 MHz, DMSO) δ 24.86, 29.98, 122.75, 122.87, 123.50, 124.04 (t, *J*=18.6 Hz), 127.27, 127.36, 127.49, 128.15 (d, *J*=6.1 Hz), 128.64, 129.14, 129.80, 129.88, 130.41, 131.01 (d, *J*=6.1 Hz), 131.26, 131.48 (d, *J*=8.4 Hz), 131.71, 131.91 (d, *J*=8.4 Hz), 132.95, 133.61, 134.53, 134.78, 135.65 (d, *J*=5.3Hz), 136.50 (d, *J*=6.1 Hz), 137.64, 147.37 (t, $^2J_{C\text{-}F}$=39.5 Hz), 148.50 (t, $^2J_{C\text{-}F}$=38 Hz), 157.87 (t, $^2J_{C\text{-}}$

$_F$=39.5 Hz); ^{29}Si-NMR (79.37 MHz, DMSO) δ −92.69 (dd, $^1J_{Si-F}$=266.7 Hz, $^1J_{Si-F}$=256.5 Hz); ^{19}F-NMR (376 MHz, DMSO) δ −49.54 (d, $^2J_{F-F}$=62.4 Hz), −65.06 (d, $^2J_{F-F}$=62.4 Hz); MS (ESI) *m/e* 539 (M-F). The elemental analysis showed partial loss of the interstitial CH_2Cl_2 solvent. Anal. Calcd. for (**79**-F-$(CH_2Cl_2)_{0.15}$) $C_{36.15}H_{28.3}F_2SSi\ Cl_{0.3}$: C, 75.97; H, 4.99. Found: C, 76.08; H, 4.90.

Titration of 78 and [79]$^+$ with Fluoride in Chloroform. A solution of the fluorosilanes (**78**: 3.0 mL, 3.80×10^{-5} M), [**79**]OTf: 3.0 mL, 5.00×10^{-5} M) was titrated by incremental addition of a solution of TBAF in chloroform (0.3 M for **78** and 0.00268 M for [**79**]$^+$).

Computational Details. DFT calculations (full geometry optimization) were carried out with the Gaussian 03 program using the gradient-corrected Becke exchange functional (B3LYP) and the Lee-Yang-Parr correlation functional. Geometry optimization of **79**-F was carried out with the following mixed basis set: 6-31+g(d') for the fluorine, 6-31+g(d) for the silicon and sulfur atoms, 6-31g basis set was used for all carbon and hydrogen atoms. Frequency calculations, which were carried out on the optimized structures of the compound, confirmed the absence of any imaginary frequencies. The Natural Bond Orbital (NBO) analyses of **79**-F was carried out using the stand along PC version of GENNBO 5.0 program.

CHAPTER VII

SYNTHESIS, CHARACTERIZATION AND ELECTROCHEMICAL PROPERTIES OF A GOLD COMPLEX FEATURING AN UNUSUAL Au→C^+ INTERACTION

7.1. Introduction

Organometallic compounds can be described according to the $ML_lX_xZ_z$ formalism where the ligating atoms are classified as L, X and Z ligands.[216, 217] L type ligands provide two electrons for a L→M bond. X type ligands are one electron donors that form the classical covalent bond of M–X. Z type ligands accept a pair of electrons from the metal to form a M→Z bond. (Figure 69).

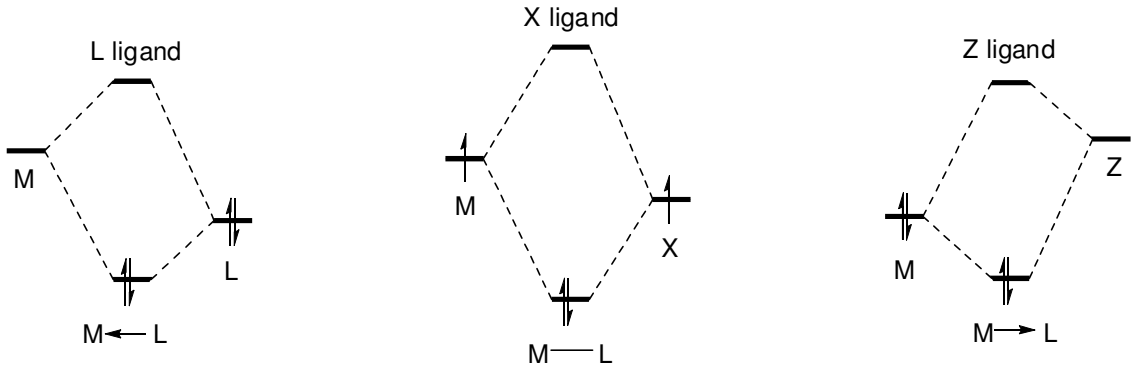

Figure 69. Three types of interactions between a metal and a ligand.

Recently, complexes such as **80** featuring M→B interactions have been attracted a great deal of attention.[218-222] However, because the degree of electron transfer is hard to measure, the oxidation state of the metal in such complexes is difficult to assign. This difficulty has sparked an active debate. Hill proposed that the metal center binds to

boron center maintaining its d^n configuration. Parkin, however, suggested a model in which a reduced $[BR_3]^{2-}$ species binds to the oxidized metal center (Figure 70).[217, 223, 224]

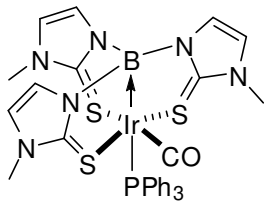

80

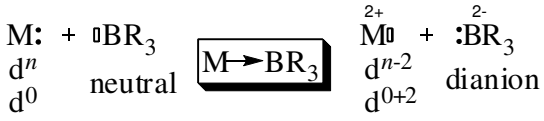

Figure 70. The new bonding paradigms for the M→B bonds.

In order to understand such an unusual bond of M→B, complex **81** featuring a gold center as a donor and a borane as an acceptor has been investigated.[224] Because the gold center adopts a square-planar geometry with a short Au-B distance of 2.31 Å, **81** can be considered a d^8 gold (III) complex. However, a moderate change in NBO charge, accompanied by a Au→B interaction leads to **81** being described as a gold (I) rather than a gold (III) complexe. This result is further confirmed by Mössbauer spectroscopic measurements.

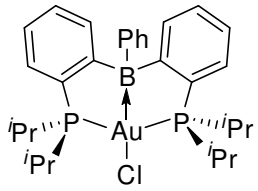

81

Utilizing an electron-deficient borafluorene moiety, the gold complex **82** displays an unusual bonding motif involving gold (I) as an electron donor and boron as an electron acceptor.[225] The Au-B distance of 2.66 Å is well within the sum of van der Waals radii of Au and B, thus confirming the presence of a Au→B bond. Computational results reveal that the shortening of the Au-B distance is accompanied by an increase of electron transfer from the gold(I) center to the borane moiety.

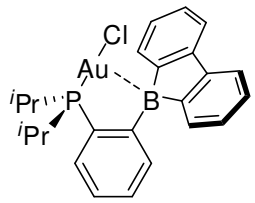

82

The synthesis and study of ambiphilic ligands containing a Lewis basic functionality and a Lewis acidic carbocationic center is of interest. This work is inspired by the aforementioned series of efforts concerning boron containing ambiphilic ligands and their complexes. In these complexes, the metal is bound to the boron center *via* a

very unusual donor-acceptor interaction in which the metal acts as a donor. Interestingly, efforts to prepare related ambiphilic ligands containing a carbocationic center rather than a boron center have not been reported. In order to determine how the structure and bonding in such complexes is affected by substitution of the boron center by a carbocationic center, we have investigated the synthesis of cationic ligands such as **I** which are related to the phosphinoborane **II** present in complex **82** (Figure 71). These new ambiphilic ligands were incorporated in gold complexes whose structures and bonding characteristics were studied using a both experiment and theory.

Figure 71. Ambiphilic ligands.

7.2. Synthesis and characterization of a gold complex

The type of cationic ambiphilic ligand considered in these studies contains a phosphine as a donor and a xanthenium unit as an acceptor. In order to prepare such species, *o*-lithio-diphenylphosphino-benzene (obtained by reaction of **83** with *n*-BuLi) was allowed to react with xanthone at −78 °C in THF to afford the corresponding alcohol **84** (Figure 72). Attempts to generate the corresponding xanthylium phosphine $[\mathbf{85}]^+$ by treatment with various acids failed. Interestingly, treatment of **84** with thionyl

chloride afforded the xanthylium phosphine oxide species [**86**]$^+$ as a chloride salt indicating oxidation of the phosphorus.

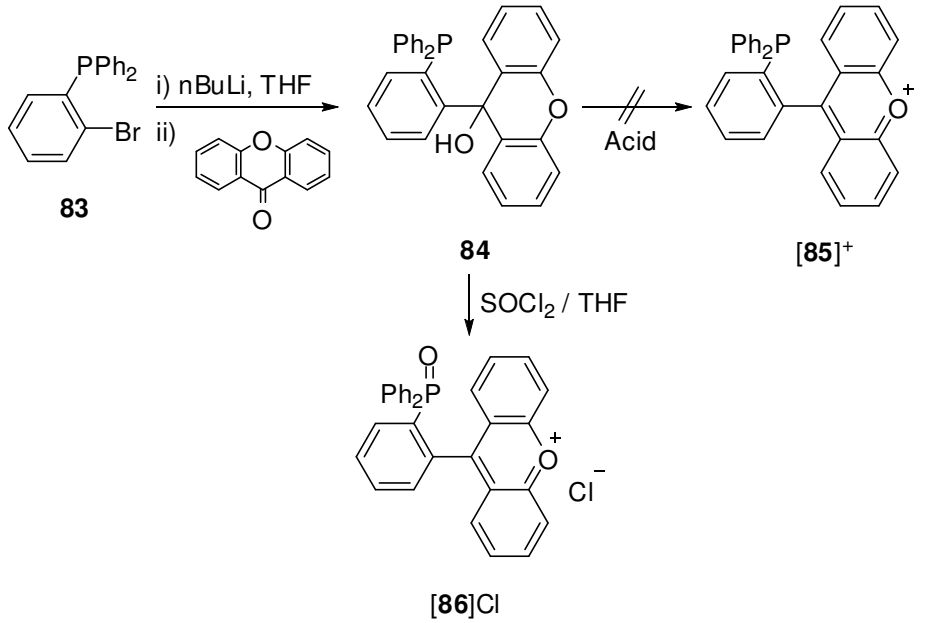

Figure 72. Synthesis of [**86**]Cl.

The $[PF_6]^-$ salt of this cation has been obtained after treatment with $NaPF_6$ and has been characterized by X-ray analysis (Figure 73, Table 26). The oxygen atom of the P=O unit is localized only 2.817 Å away from the methylium carbon atom C(19) suggesting the presence of a weak interaction.

Table 26. Crystal data, data collections, and structure refinement for [**86**]PF_6.

Crystal data	[**86**]PF_6
formula	$C_{31}H_{22}F_6O_2P_2$
M_r	602.43
Crystal size (mm^3)	0.11 x 0.09 x 0.05
crystal system	Monoclinic
space group	$P2_1/c$
a (Å)	11.3030(16)
b (Å)	16.708(2)
c (Å)	14.014(2)
α (°)	90
β (°)	95.597(3)
γ (°)	90
V ($Å^3$)	2634.0(7)
Z	4
ρ_{calc} (g cm^{-3})	1.519
μ (mm^{-1})	0.238
F(000)	1232
Data collection	
T (K)	146(2)
scan mode	ω
hkl range	-12 → +12, -19 → +19, -16 → +16
measd reflns	22719
Unique reflns [R_{int}]	4127 [0.0582]
reflns used for refinement	4127
Refinement	
refined parameters	370
GooF	1.003
R_1,[a] wR_2[b] all data	0.0874, 0.1713
ρ_{fin} (max/min) (e $Å^{-3}$)	0.941, -0.296

[a] $R_1 = \Sigma||Fo| - |Fc||/\Sigma|Fo|$. [b] $wR_2 = [[\Sigma w(Fo^2 - Fc^2)^2]/[\Sigma w(Fo^2)^2]]^{1/2}$.

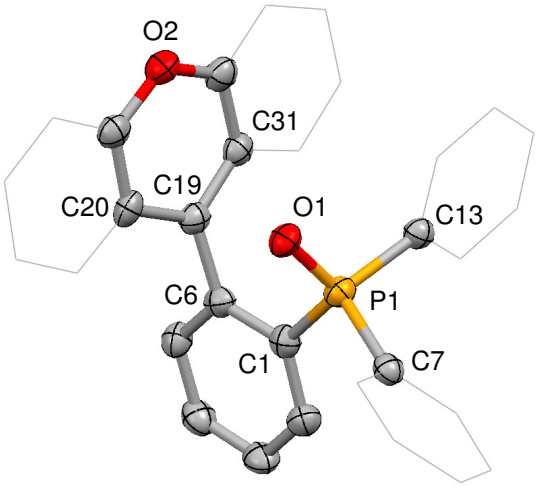

Figure 73. Crystal structure of [**86**]$^+$ with thermal ellipsoids set at 50% probability level. The PF_6^- anion and hydrogen atoms are omitted for clarity. Pertinent metrical parameters can be found in the text.

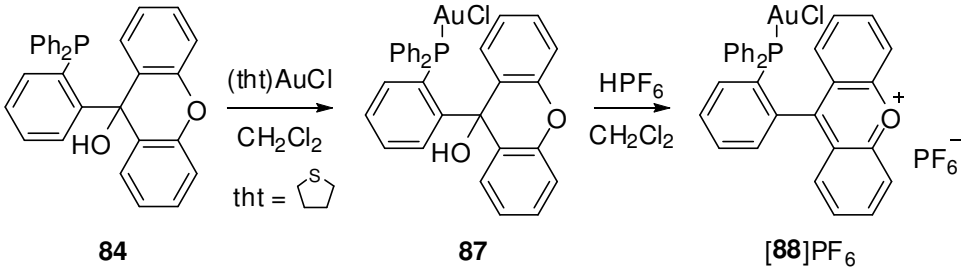

Figure 74. Synthesis of [**88**]PF_6.

Because the targeted the xanthenium phosphine ligand [**85**]$^+$ could not be obtained directly from the alcohol, we decided to determine if metal complexes containing this ligand could be prepared by first incorporating the metal and then dehydrating the xanthenol. With this in mind, **84** was treated with (tht)AuCl (tht =

tetrahydrothienyl) to produce **87** as a white solid (Figure 74). Reaction of **87** with HPF_6 afforded the target gold compound $[\mathbf{88}]^+$ as a $[PF_6]^-$ salt. This salt is air-stable and yellow in color.

It has been characterized by X-ray analysis which shows that the gold atom Au(1) is separated by 3.13 Å from the methylium carbon atom C(19) suggesting a weak interaction (Figure 75, Table 27). Presumably, the methylium atom of the xanthenium unit is too electron rich because of the aromaticity of the central six-member ring. We carried out AIM analysis at ADF optimized geometry of $[\mathbf{88}]^+$ (Figures 76 and 77, Table 28). The electron density maps show the presence of bond paths between Au and carbocation with localized bond critical points whose electron density $\rho(r)$ is 1.7×10^{-2} ebohr^{-3}.

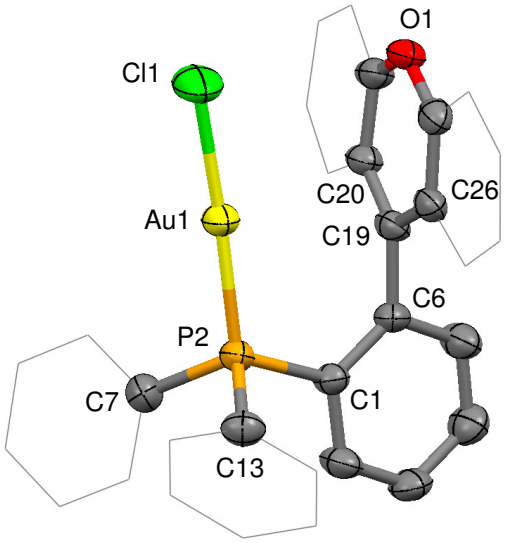

Figure 75. Crystal structure of $[\mathbf{88}]^+$ with thermal ellipsoids set at 50% probability level. The PF_6^- anion and hydrogen atoms are omitted for clarity. Pertinent metrical parameters can be found in the text.

Table 27. Crystal data, data collections, and structure refinement for [**88**]PF_6.

Crystal data	[**88**]PF_6
formula	$C_{31}H_{22}AuClF_6OP_2$
M_r	818.84
Crystal size (mm^3)	0.29 x 0.10 x 0.07
crystal system	Triclinic
space group	*P*-1
a (Å)	8.5451(17)
b (Å)	10.210(2)
c (Å)	17.440(4)
α (°)	75.05(3)
β (°)	77.74(3)
γ (°)	83.77(3)
V ($Å^3$)	1434.2(5)
Z	2
ρ_{calc} (g cm^{-3})	1.896
μ (mm^{-1})	5.398
F(000)	792
Data collection	
T (K)	110(2)
scan mode	ω
hkl range	-10 → +8, -10 → +12, -21 → +21
measd reflns	8130
Unique reflns [R_{int}]	5622 [0.0311]
reflns used for refinement	5622
Refinement	
refined parameters	379
GooF	1.006
R_1,[a] wR_2[b] all data	0.0517, 0.1152
ρ_{fin} (max/min) (e $Å^{-3}$)	1.055, -1.312

[a] $R_1 = \Sigma||Fo| - |Fc||/\Sigma|Fo|$. [b] $wR_2 = [[\Sigma w(Fo^2 - Fc^2)^2]/[\Sigma w(Fo^2)^2]]^{1/2}$.

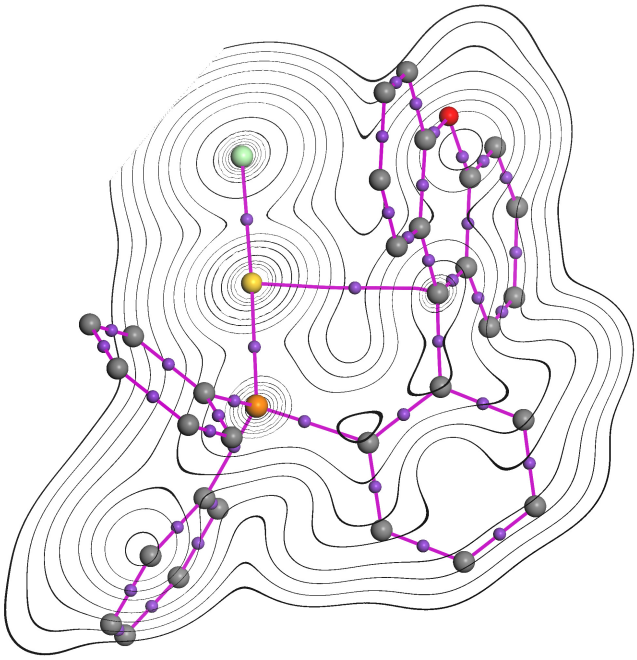

Figure 76. Calculated electron density maps for complexes [**88**]$^{+}$ with relevant bond paths and bond critical points.

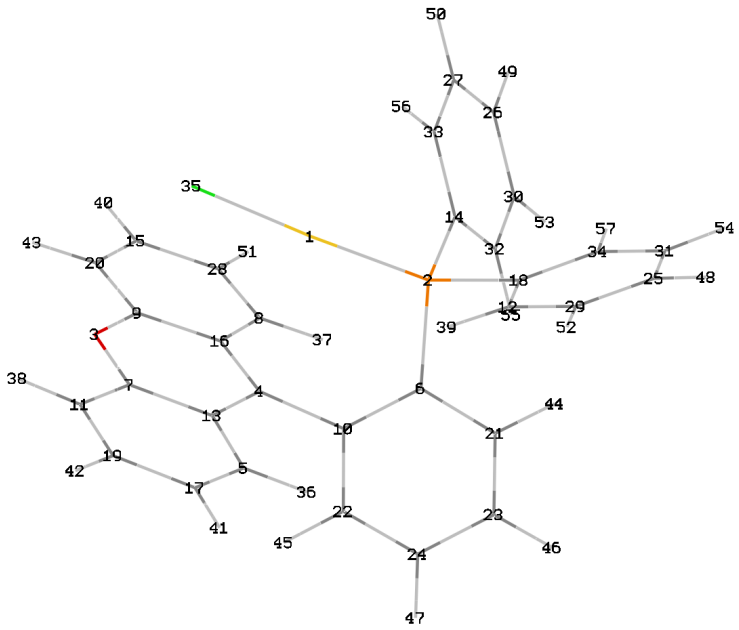

Figure 77. DFT optimized structure of [**88**]$^{+}$

Table 28. Atom coordinates for the DFT optimized structure of [**88**]$^{+}$.

Center Number	Coordinates (Angstroms) X	Y	Z	Center Number	Coordinates (Angstroms) X	Y	Z
Au1	0.292	-0.473	-1.360	C30	-3.398	3.512	0.520
P2	-1.464	-0.118	0.010	C31	-5.123	-1.991	-0.370
O3	3.905	0.664	-0.050	C32	-2.824	2.265	0.790
C4	1.519	0.211	1.380	C33	-2.206	2.055	-1.540
C5	2.219	-2.190	1.570	C34	-4.149	-1.004	-0.190
C6	-1.003	-0.184	1.800	Cl35	2.041	-0.784	-2.830
C7	3.624	-0.581	0.400	H36	1.314	-2.421	2.130
C8	1.073	2.671	1.210	H37	0.154	2.555	1.780
C9	3.074	1.702	0.210	H38	5.435	-1.328	-0.480
C10	0.327	-0.018	2.250	H39	-1.360	-2.979	-0.370
C11	4.552	-1.581	0.100	H40	2.960	5.035	-0.340
C12	-2.416	-2.705	-0.350	H41	2.962	-4.198	1.610
C13	2.435	-0.849	1.140	H42	5.015	-3.660	0.300
C14	-2.225	1.528	-0.240	H43	4.394	3.045	-0.820
C15	2.663	4.051	0.010	H44	-3.030	-0.619	2.400
C16	1.865	1.518	0.940	H45	1.621	0.043	3.980
C17	3.136	-3.175	1.280	H46	-2.541	-0.677	4.820
C18	-2.791	-1.359	-0.170	H47	-0.193	-0.340	5.620
C19	4.303	-2.869	0.540	H48	-5.511	-4.094	-0.680
C20	3.468	2.957	-0.260	H49	-3.825	5.003	-0.980
C21	-2.013	-0.435	2.750	H50	-2.763	3.698	-2.820
C22	0.595	-0.081	3.630	H51	0.857	4.786	0.960
C23	-1.737	-0.483	4.110	H52	-3.099	-4.724	-0.660
C24	-0.428	-0.298	4.560	H53	-3.860	4.078	1.330
C25	-4.749	-3.328	-0.530	H54	-6.176	-1.709	-0.400
C26	-3.379	4.029	-0.770	H55	-2.843	1.877	1.810
C27	-2.785	3.298	-1.800	H56	-1.728	1.495	-2.350
C28	1.467	3.910	0.750	H57	-4.447	0.040	-0.090
C29	-3.394	-3.684	-0.520				

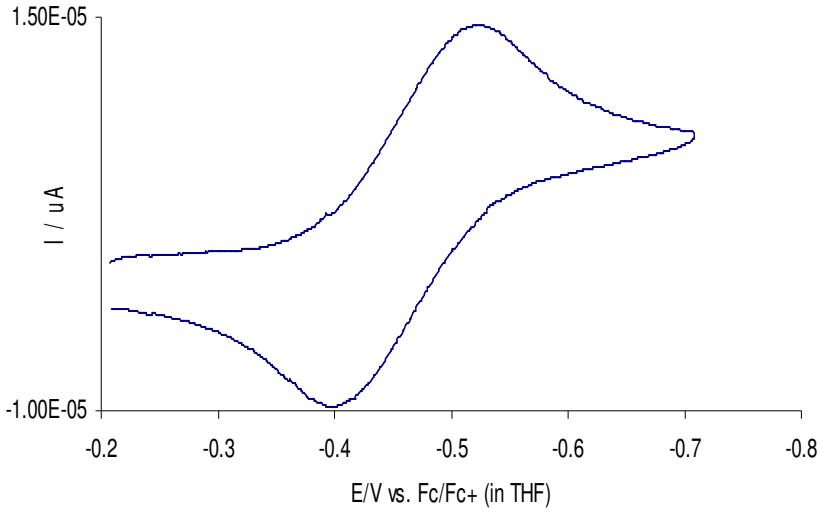

Figure 78. Cyclic voltammogram of [**88**]PF_6 measured at a scan rate of 0.1 V/s in THF with a carbon working electrode: 0.1 M NBu_4PF_6.

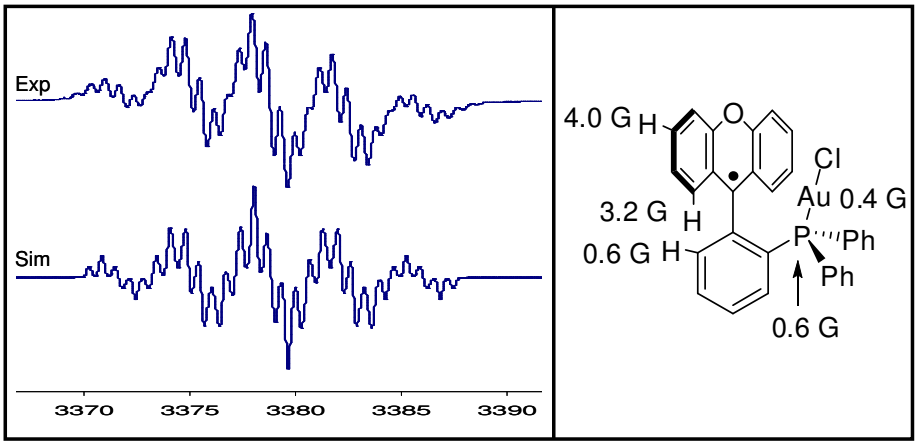

Figure 79. Left: the EPR spectrum of **88•** in THF at room temperature and the simulated EPR spectrum. Right: Observed hyperfine coupling constants for **88•**.

7.3. Electrochemistry of [**88**]$^+$

The cyclic voltammogram of [**88**]$^+$ in THF displays a single reversible reduction wave at $E_{1/2}$=–0.46 V vs Fc/Fc^+ which is close to that of 9-phenylxanthen-9-ylium cation (Figure 78).[226] Encouraged by the reversibility of the reduction of [**88**]$^+$, we have investigated the chemical generation of the corresponding radical. To this end, [**88**]PF_6 was treated with powdered magnesium metal in THF to produce a yellow solution containing the radical **88•**. The EPR simulation shows that the radical is mostly based on the 9-phenylxanthen-9-ylium moiety in an agreement with the reduction potential of [**88**]$^+$ (Figure 79).

7.4. Conclusion

The gold complex [**88**]$^+$ featuring the cationic ambiphilic ligand was successfully prepared. Because the carbocation of the xanthenium moiety is stabilized by the aromaticity of the central six-member ring, the Au→C^+ interaction presenting [**88**]$^+$ is weak.

7.5. Experimental section

General Considerations. 2-Bromophenyldiphenylphosphine was prepared by following the known method (D. Brauer, M. Hingst, M., K. Kottsieper, C. Liek, T. Nickel, M. Tepper, O. Stelzer and W. Sheldrick, *J.Organomet. Chem.*, **2002**, *645*, 14.). 1-bromo-2-iodobenzene and xanthone were purchased from Alfa Aesar. Solvents were dried by passing through an alumina column (dichloromethane, toluene) or refluxing

under N_2 over Na/K (THF). NMR spectra were recorded on Varian Unity Inova 400 FT NMR (399.59 MHz for ^{1}H, 128.19 MHz for ^{11}B, 100.45 MHz for ^{13}C, 79.374 MHz for ^{29}Si) spectrometers at ambient temperature. Chemical shifts are given in ppm, and are referenced against external $BF_3{\cdot}Et_2O$ for ^{19}F and H_3PO_4 for ^{31}P.

Crystallography. The crystallographic measurements were performed using a Siemens SMART-CCD area detector diffractometer (Mo-K_α radiation, λ= 0.71069 Å) for [**86**]PF_6 and [**88**]PF_6. In each case, a specimen of suitable size and quality was selected and mounted onto a nylon loop. The structure was solved by direct methods, which successfully located most of the non-hydrogen atoms. Subsequent refinement on F^2 using the SHELXTL/PC package (version 5.1) allowed location of the remaining non-hydrogen atoms.

Synthesis of 84. To *o*-diphenylphosphinobenzenbromide (0.3 g, 0.88 mmol) in THF (5 mL) was added *n*-BuLi (0.35 mL, 0.88 mmol, 2.5 M in *n*-Hexane) at −78 °C. After stirring the mixture for 1h at −78 °C, a solutiono of xanthone (0.19 g, 0.97 mmol) in THF (5 mL) was added to the lithiated compound at the same temperature. The solution was warmed to room temp (rt) and stirred overnight. The solvent was removed in *vacou*. The residue was treated with diethyl ether and saturated aqueous NH_4Cl solution. The organic layer was separated, dried over $MgSO_4$, filtered through silca-gel, and concentrated in *vacuo* to yield a solid. The solid was washed with acetonitrile to afford the desired product **84** as a white solid (Yield : 55%). ^{1}H-NMR (300 MHz ,

actone-d_6) : δ 6.59-6.64 (m, 4H), 6.70-6.75 (m, 2H), 6.87-6.90 (m, 2H), 7.05-7.15 (m, 11H), 7.32 (t, *J*=7.5 Hz, 1H), 7.56 (t, *J*=7.5 Hz, 1H), 8.60 (m, 1H). ^{13}C-NMR (400 MHz, actone-d_6) : δ 70.65 (d, *J*=9.1 Hz), 116.46, 123.17, 126.99 (d, *J*=6.8 Hz), 128.41, 128.58 (d, *J*=6.1 Hz), 129.21, 129.40, 130.76, 133.53 (d, *J*=19.7 Hz), 136.18 (d, *J*=19.8 Hz), 138.50 (d, *J*=14.4 Hz), 138.79, 138.82, 151.08, 151.11 , 154.68 (d, *J*=23.5 Hz). ^{31}P-NMR (121 MHz, acetone-d_6) : δ −18.70

Synthesis of 87. 84 (0.1 g, 0.22 mmol) was added to a solution of (tht)AuCl (0.067 g, 0.22 mmol) in dichloromethane (4 mL) at rt. The white precipitation was formed after overnight. The solid was isolated by filtration, washed with dichloromethane, and dried in *vacuo* to afford **87** as a white solid (Yield : 53%). ^{1}H-NMR (400 MHz , $CDCl_3$) : δ 2.77 (s, 1H), 6.94-6.98 (m, 1H), 7.02 (t, *J*=7.8 Hz, 2H), 7.12 (t, *J*=7.6 Hz, 1H), 7.17 (d, *J*=7.6 Hz, 2H), 7.26-7.31 (m, 4H), 7.36 (m, 2H), 7.47-7.53 (m, 6H), 7.79 (m, 4H). ^{13}C-NMR (100 MHz, $CDCl_3$) : δ 116.88, 123.89, 127.15, 127.25, 129.16 (d, *J*=12.2 Hz), 129.86, 130.21, 131.41, 131.43, 132.51 (d, *J*=63.8 Hz), 133.45, 134.55 (d, *J*=14.4 Hz), 134.91, 149.29, 152.80. ^{31}P-NMR (161 MHz, $CDCl_3$) : δ 39.85 (bs). Anal. Calcd for $C_{31}H_{23}AuClO_2P$: C, 53.89; H, 3.36. Found: C, 53.65; H, 3.25

Synthesis of [88]PF_6. 87 (0.05 g, 0.072 mmol) was dissolved in dichloromethane (2 mL) and treated with excess HPF_6. After 10 min, the solvent was removed in *vacuo*. The residue was washed with diethyl ether and dried in *vacuo* to afford [**88**]PF_6 as a yellow solid (Yield : 85%). ^{1}H-NMR (400 MHz, CD_3CN) : δ 7.39-7.50 (m, 8H), 7.57-

7.63 (m, 3H), 7.64-7.72 (m, 5H), 7.91-7.99 (m, 2H), 8.39-8.41 (m, 2H), 8.53-8.57 (m, 2H). ^{13}C-NMR (400 MHz, CD_3CN) : δ 121.07, 126.36, 127.95 (d, *J*=63.6 Hz), 130.65 (d, *J*=12.4 Hz), 131.59, 131.67, 131.74, 132.99 (d, *J*=8.5 Hz), 133.41 (d, *J*=2.0 Hz), 133.74 (d, *J*=3.0 Hz), 135.26 (d, *J*=14.1 Hz), 136.73 (d, *J*=4.6 Hz), 146.49, 158.96, 174.17. ^{31}P-NMR (161 MHz, CD_3CN) : δ 25.91, −143.18 (septet, *J*=706 Hz, *P*F_6). ^{19}F-NMR (376 MHz, CD_3CN) : δ −76.18 (d, *J*=706 Hz, P*F*$_6$). MS (ESI) *m*/*e* 673.0355 (M-PF_6).

Synthesis of [86]Cl. 84 (0.05 g, 0.11 mmol) was dissolved in THF (2 mL) and treated with excess $SOCl_2$ at 0 °C which resulted in the formation of a yellow solid. After 10 min, the solid was isolated by filtration, washed with THF, and dried in *vacuo* to afford [**86**]Cl as a yellow solid (Yield : 88%). ([**86**]Cl was air and moisture sensitive). ^{1}H-NMR (300 MHz, $CDCl_3$) : δ 7.33-7.37 (m, 8H), 7.49-7.69 (m, 8H), 7.84 (t, *J*=7.2 Hz, 1H), 7.92 (t, *J*=7.2 Hz, 1H), 8.25-8.27 (m, 2H), 8.39 (m, 2H). ^{13}C-NMR (100 MHz, $CDCl_3$) : δ 119.61, 124.34, 128.62, 129.03 (d, *J*=12.9 Hz), 129.17, 130.13 (d, *J*=9.1 Hz), 130.22, 130.83, 131.38 (d, *J*=12.1 HZ), 131.63 (d, *J*=10.6 Hz), 132.32, 133.09(d, *J*=2.2 Hz), 133.64 (d, *J*=10.6 Hz), 135.75 (d, *J*=6.0 Hz), 143.72, 157.03, 172.94. ^{31}P-NMR (121 MHz, CD_3CN) : δ 31.70.

To obtain the single crystal of [**86**]$^+$, the ion exchange reaction was performed. To [**86**]Cl in acetonitrile 2 eq. of $NaPF_6$ was added in a dry box. The crystal of [**86**]PF_6

was grown by slow diethyl ether diffusion to the acetonitrile solution of [**86**]PF_6 in the dry box.

Computational Results. For [**88**]$^+$, density functional theory (DFT) calculations were carried out using ADF 2008.01. All calculations were carried out using the BP86 functional with a TZP basis set for all atoms as implemented in ADF. All calculations were performed using the Zero Order Regular Approximation (ZORA). The topology of the electron density of the ADF optimized structures was subjected to an Atoms-In Molecules analysis using the Dgrid program (version 4.4). Visualization of the geometry (including bond paths and bond critical points) as well as of the electron density map in the plane containing the Au, Cl and C atoms was carried with Material Studio (version 4.4).

CHAPTER VIII

SUMMARY

8.1. Fluoride and cyanide sensing using phosphonium borane in water

In order to understand how simple variations in the structure and composition of boranes impacts their anion binding properties, we have investigated phosphonium boranes of the general formula [*p*-Mes_2B-C_6H_4-PPh_2R]$^+$ with R = Me ([**14**]$^+$) Et ([**70**]$^+$), *n*-Pr ([**71**]$^+$), and Ph ([**72**]$^+$). These boranes are water stable but undergo conversion to the corresponding zwitterionic hydroxide species upon elevation of the pH. The pK_{R+} values of these boranes, which were derived from spectrophotmetric acid-base titrations, indicate that the Lewis acidity of the boranes increases with their hydrophobicity. A similar trend is observed in the fluoride affinity of these compounds as shown by the fluoride binding constant *K* of [**72**]$^+$ which exceeds that of [**14**]$^+$ by more than one order of magnitude. Presumably, the increased hydrophobicity and decreased solvation of [**72**]$^+$ facilitates the covalent ion pairing process that occurs upon reaction with fluoride (or hydroxide). None of these phosphonium boranes interact with other commonly encountered anions, such as Cl^-, Br^-, I^-, OAc^-, NO_3^-, $H_2PO_4^-$, and HSO_4^-. From an applied perspective, these hydrophobic effects are significant as shown by the ability of [**72**]$^+$ to detect fluoride ions in water below the maximum contaminant level of 4 ppm set by the EPA.

We have demonstrated that cyanide binding to the boron center of phosphonium boranes [**73**]$^+$ and [**74**]$^+$ results in a turn-on response of the fluorescence of the anthracenyl and dansyl chromophores, respectively. This increase can be explained by

assuming 1) that the chromophore of [**73**]$^+$ and [**74**]$^+$ is quenched via intramolecular charge transfer from the excited chromophore to the electron deficient boron center; 2) that addition of cyanide to the boron center annuls its electron accepting properties leading to a revival of the fluorescence of the chromophore. While [**73**]$^+$ decomposes in water, [**74**]$^+$ allows for sensitive and selective detection of cyanide with a detection limit of 26 ppb in H_2O/MeOH (6/4, v/v). The high affinity of this borane arises from favourable Coulombic effects which serve to stabilize the cyanoborate complex against dissociation.

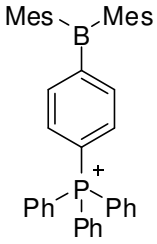

[**72**]$^+$

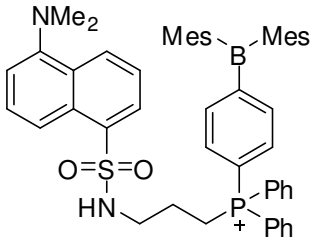

[**74**]$^+$

8.2. Anion affinity of bidentate cationic boranes

Due to the presence of low lying σ* orbitals, phosphonium and sulfonium ions are inherently Lewis acidic and can interact with electron-rich substrates to form donor/acceptor complexes. To test the validity of these concepts, the anion binding properties of phosphonium borane [**15**]$^+$ and sulfonium borane [**77**]$^+$ were investigated. We find that the phosphonium borane [**15**]$^+$ is selective for N_3^- over F^- in $CHCl_3/H_2O$ biphasic mixtures. The high selectivity observed in these phase-transfer reactions most

likely results from the lipophilic character of the azide anion as well as from its ability to interact with both the boron and phosphorus Lewis acidic sites of the receptor via chelation ($lp_{(N)} \rightarrow \sigma^*_{(P\text{-}C)}$) in **15**-$N_3$.

Sulfonium borane [**77**]$^+$ behaves as a selective cyanide sensor that can be used in pure water for the fluorescence detection of cyanide at the EU maximum allowed concentration of 50 ppb. A structural analysis of **77**-CN shows that the sulfonium moiety interacts with the cyanide guest via both a bonding $\pi(C\equiv N) \rightarrow \sigma^*(S\text{-}C)$ and back-bonding $lp(S) \rightarrow \pi^*(C\equiv N)$ interaction. The results obtained in the chemistry of the phosphonium borane [**15**]$^+$ and sulfonium borane [**77**]$^+$ demonstrate that Coulombic and chelate effects are additive and can be combined to boost the anion affinity of the Lewis acidic hosts.

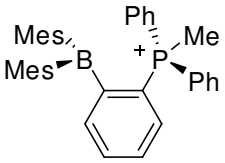

[**15**]$^+$

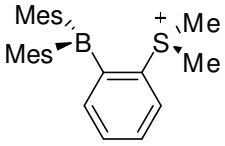

[**77**]$^+$

8.3. Anion affinity of a bidentate sulfonium fluorosilane

This "onium-based strategy" used to enhance the anion affinity of Lewis acids has been extended to silicon Lewis acids. The fluoride affinity of sulfonium fluorosilane [**79**]$^+$ is higher than that of the neutral silane **78** by several orders of magnitude. This dramatic enhancement observed in the fluoride ion affinity of [**79**]$^+$ is assigned to the presence of the sulfonium moiety which: 1) provides a Coulombic and inductive drive

for the formation of the difluorosilicate compound; and 2) engages the fluoride anion in a stabilizing $lp_{(F)} \rightarrow \sigma^*_{(S\text{-}C)}$ interaction in **79**-F.

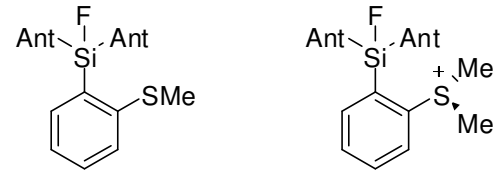

Ant = 9-anthryl

78

[**79**]$^+$

8.4. Conclusion

This dissertation illustrates how the introduction of cationic groups impacts the anion binding properties of Lewis acids. Because of favorable Coulombic effects, cationic Lewis acids show an increase Lewis acidity when compared to their neutral counterparts. Cationic boranes can be used to detect ppm levels of fluoride and ppb levels of cyanide in water due to a combination of Coulombic, cooperative and hydrophobic effects.

REFERENCES

1. Carton, R. J.; *Fluoride* **2006,** *39*, 163-172.

2. Holland, M. A.; Kozlowski, L. M.; *Clinical Pharmacy* **1986,** *5*, 737-41.

3. Baud, F. J.; *Hum Exp Toxicol* **2007,** *26*, 191-201.

4. Timoshkin, A. Y.; Frenking, G.; *Organometallics* **2008,** *27*, 371-380.

5. Melaïmi, M.; Sole, S.; Chiu, C.-W.; Wang, H.; Gabbaï, F. P.; *Inorg. Chem.* **2006,** *45*, 8136-8143.

6. Huh, J. O.; Kim, H.; Lee, K. M.; Lee, Y. S.; Do, Y.; Lee, M. H.; *Chem. Commun.* **2010**, 1138-1140.

7. Broomsgrove, A. E. J.; Addy, D. A.; Di Paolo, A.; Morgan, I. R.; Bresner, C.; Chislett, V.; Fallis, I. A.; Thompson, A. L.; Vidovic, D.; Aldridge, S.; *Inorg. Chem.* **2010,** *49*, 157-173.

8. Hudson, Z. M.; Wang, S.; *Acc. Chem. Res.* **2009,** *42*, 1584-1596.

9. Yamaguchi, S.; Akiyama, S.; Tamao, K.; *J. Am. Chem. Soc.* **2001,** *123*, 11372-11375.

10. Hoefelmeyer, J. D.; Gabbaï, F. P.; *Organometallics* **2002,** *21*, 982-985.

11. Hoefelmeyer, J. D.; Solé, S.; Gabbaï, F. P.; *Dalton Trans.* **2004**, 1254-1258.

12. Solé, S.; Gabbaï, F. P.; *Chem. Commun.* **2004**, 1284-1285.

13. Melaïmi, M.; Gabbaï, F. P.; *J. Am. Chem. Soc.* **2005,** *127*, 9680-9681.

14. Lee, M. H.; Gabbaï, F. P.; *Inorg. Chem.* **2007,** *46*, 8132-8138.

15. Hudnall, T. W.; Melaïmi, M.; Gabbaï, F. P.; *Org. Lett.* **2006,** *8*, 2747-2749.

16. Chiu, C.-W.; Gabbaï, F. P.; *J. Am. Chem. Soc.* **2006,** *128*, 14248-14249.

17. Hudnall, T. W.; Gabbaï, F. P.; *J. Am. Chem. Soc.* **2007,** *129*, 11978-11986.

18. Lee, M. H.; Agou, T.; Kobayashi, J.; Kawashima, T.; Gabbaï, F. P.; *Chem. Commun.* **2007**, 1133-1135.

19. Hudnall, T. W.; Kim, Y.-M.; Bebbington, M. W. P.; Bourissou, D.; Gabbaï, F. P.; *J. Am. Chem. Soc.* **2008,** *130*, 10890-10891.

20. Chiu, C.-W.; Kim, Y.; Gabbaï, F. P.; *J. Am. Chem. Soc.* **2009,** *131*, 60-61.

21. Agou, T.; Kobayashi, J.; Kim, Y.; Gabbaï, F. P.; Kawashima, T.; *Chem. Lett.* **2007,** *36*, 976-977.

22. Agou, T.; Sekine, M.; Kobayashi, J.; Kawashima, T.; *Chem. Eur. J.* **2009,** *15*, 5056-5062.

23. Badugu, R.; Lakowicz, J. R.; Geddes, C. D.; *Anal. Biochem.* **2004,** *327*, 82-90.

24. Badugu, R.; Lakowicz, J. R.; Geddes, C. D.; *Anal. Chim. Acta* **2004,** *522*, 9-17.

25. Badugu, R.; Lakowicz, J. R.; Geddes, C. D.; *Dyes and Pigments* **2005,** *64*, 49-55.

26. Badugu, R.; Lakowicz, J. R.; Geddes, C. D.; *J. Am. Chem. Soc.* **2005,** *127*, 3635-3641.

27. Jamkratoke, M.; Ruangpornvisuti, V.; Tumcharern, G.; Tuntulani, T.; Tomapatanaget, B.; *J. Org. Chem.* **2009,** *74*, 3919-3922.

28. Liu, X. Y.; Bai, D. R.; Wang, S.; *Angew. Chem. Int. Ed.* **2006,** *45*, 5475-5478.

29. Bai, D.-R.; Liu, X.-Y.; Wang, S.; *Chem. Eur. J.* **2007,** *13*, 5713-5723.

30. Huh, J. O.; Do, Y.; Lee, M. H.; *Organometallics* **2008,** *27*, 1022-1025.

31. Brondani, D.; Carre, F. H.; Corriu, R. J. P.; Moreau, J. J. E.; Man, M. W. C.; *Angew. Chem., Int. Ed. Engl.* **1996,** *35*, 324-26.

32. Hoshi, T.; Takahashi, M.; Kira, M.; *Chem. Lett.* **1996**, 683-684.

33. Asao, N.; Shibato, A.; Itagaki, Y.; Jourdan, F.; Maruoka, K.; *Tetrahedron Lett.* **1998,** *39*, 3177-3180.

34. Jung, M. E.; Xia, H.; *Tetrahedron Lett.* **1988,** *29*, 297-300.

35. Kira, M.; Kwon, E.; Kabuto, C.; Sakamoto, K.; *Chem. Lett.* **1999**, 1183-1184.

36. Kano, N.; Komatsu, F.; Kawashima, T.; *J. Am. Chem. Soc.* **2001,** *123*, 10778-10779.

37. Setaka, W.; Nirengi, T.; Kabuto, C.; Kira, M.; *J. Am. Chem. Soc.* **2008,** *130*, 15762-15763.

38. Yamaguchi, S.; Akiyama, S.; Tamao, K.; *Organometallics* **1999,** *18*, 2851-2854.

39. Yamaguchi, S.; Akiyama, S.; Tamao, K.; *Organometallics* **1998,** *17*, 4347-4352.

40. Yamaguchi, S.; Akiyama, S.; Tamao, K.; *J. Am. Chem. Soc.* **2000,** *122*, 6793-6794.

41. Tamao, K.; Hayashi, T.; Ito, Y.; *J. Organomet. Chem.* **1996,** *506*, 85-91.

42. Tamao, K.; Hayashi, T.; Ito, Y.; Shiro, M.; *J. Am. Chem. Soc.* **1990,** *112*, 2422-4.

43. Katz, H. E.; *J. Am. Chem. Soc.* **1986,** *108*, 7640-7645.

44. Kawachi, A.; Tani, A.; Shimada, J.; Yamamoto, Y.; *J. Am. Chem. Soc.* **2008,** *130*, 4222-4223.

45. Xu, Z.; Chen, X.; Kim Ha, N.; Yoon, J.; *Chem. Soc. Rev.* **2010,** *39*, 127-37.

46. Niu, H.-T.; Su, D.; Jiang, X.; Yang, W.; Yin, Z.; He, J.; Cheng, J.-P.; *Org. Biomol. Chem.* **2008,** *6*, 3038-3040.

47. Niu, H.-T.; Jiang, X.; He, J.; Cheng, J.-P.; *Tetrahedron Lett.* **2008,** *49*, 6521-6524.

48. Peng, L.; Wang, M.; Zhang, G.; Zhang, D.; Zhu, D.; *Org. Lett.* **2009,** *11*, 1943-1946.

49. Chen, C.-L.; Chen, Y.-H.; Chen, C.-Y.; Sun, S.-S.; *Org. Lett.* **2006,** *8*, 5053-5056.

50. Chen, C.-L.; Lin, T.-P.; Chen, Y.-S.; Sun, S.-S.; *Eur. J. Org. Chem.* **2007**, 3999-4010.

51. El-Sayed, M. A.; *Acc. Chem. Res.* **1968,** *1*, 8-16.

52. de Silva, A. P.; Gunaratne, H. Q. N.; Gunnlaugsson, T.; Huxley, A. J. M.; McCoy, C. P.; Rademacher, J. T.; Rice, T. E.; *Chem. Rev.* **1997,** *97*, 1515-1566.

53. Jo, J.; Lee, D.; *J. Am. Chem. Soc.* **2009,** *131*, 16283-16291.

54. Lee, K.-S.; Kim, H.-J.; Kim, G.-H.; Shin, I.; Hong, J.-I.; *Org. Lett.* **2008,** *10*, 49-51.

55. Kwon, S. K.; Kou, S.; Kim, H. N.; Chen, X.; Hwang, H.; Nam, S.-W.; Kim, S. H.; Swamy, K. M. K.; Park, S.; Yoon, J.; *Tetrahedron Lett.* **2008,** *49*, 4102-4105.

56. Sun, Y.; Liu, Y.; Guo, W.; *Sens. Actuators, B* **2009,** *B143*, 171-176.

57. Lou, B.; Chen, Z.-Q.; Bian, Z.-Q.; Huang, C.-H.; *New J. Chem.* **2010,** *34*, 132-136.

58. Kwart, H.; Baevsky, M. M.; *J. Am. Chem. Soc.* **1958,** *80*, 580-8.

59. Schowen, R. L.; Kuebrich, J. P.; *J. Am. Chem. Soc.* **1971,** *93*, 1220-3.

60. Clerici, A.; Porta, O.; *J. Org. Chem.* **1994,** *59*, 1591-2.

61. Cho, D.-G.; Kim, J. H.; Sessler, J. L.; *J. Am. Chem. Soc.* **2008,** *130*, 12163-12167.

62. Chung, Y.; Lee, H.; Ahn, K. H.; *J. Org. Chem.* **2006,** *71*, 9470-9474.

63. Cho, D.-G.; Sessler, J. L.; *Chem. Soc. Rev.* **2009,** *38*, 1647-1662.

64. Zelder, F. H.; Mannel-Croise, C.; *Chimia* **2009,** *63*, 58-62.

65. Yang, Y.-K.; Tae, J.; *Org. Lett.* **2006,** *8*, 5721-5723.

66. Garcia, F.; Garcia, J. M.; Garcia-Acosta, B.; Martinez-Manez, R.; Sancenon, F.; Soto, J.; *Chem. Commun.* **2005**, 2790-2792.

67. Abalos, T.; Royo, S.; Martinez-Manez, R.; Sancenon, F.; Soto, J.; Costero, A. M.; Gil, S.; Parra, M.; *New J. Chem.* **2009,** *33*, 1641-1645.

68. Tomasulo, M.; Raymo, F. M.; *Org. Lett.* **2005,** *7*, 4633-4636.

69. Tomasulo, M.; Sortino, S.; White, A. J. P.; Raymo, F. M.; *J. Org. Chem.* **2006,** *71*, 744-753.

70. Shiraishi, Y.; Adachi, K.; Itoh, M.; Hirai, T.; *Org. Lett.* **2009,** *11*, 3482-3485.

71. Ros-Lis, J. V.; Martinez-Manez, R.; Soto, J.; *Chem. Commun.* **2002**, 2248-2249.

72. Zhang, X.; Li, C.; Cheng, X.; Wang, X.; Zhang, B.; *Sens. Actuators, B* **2008,** *B129*, 152-157.

73. Ros-Lis, J. V.; Martinez-Manez, R.; Soto, J.; *Chem. Commun.* **2005**, 5260-5262.

74. Palomares, E.; Martinez-Diaz, M. V.; Torres, T.; Coronado, E.; *Advanced Functional Materials* **2006,** *16*, 1166-1170.

75. Gimeno, N.; Li, X.; Durrant, J. R.; Vilar, R.; *Chem.--Eur. J.* **2008,** *14*, 3006-3012.

76. Männel-Croisé, C.; Zelder, F.; *Inorg. Chem.* **2009,** *48*, 1272-1274.

77. Mannel-Croise, C.; Probst, B.; Zelder, F.; *Anal. Chem.* **2009,** *81*, 9493-9498.

78. Lou, X.; Qiang, L.; Qin, J.; Li, Z.; *ACS Appl. Mater. Interfaces* **2009,** *1*, 2529-2535.

79. Xiang, Y.; Tong, A.; Jin, P.; Yong, J.; *Org. Lett.* **2006,** *8*, 2863-2866.

80. Lou, X.; Zhang, L.; Qin, J.; Li, Z.; *Chem. Commun.* **2008**, 5848-5850.

81. Chung, S.-Y.; Nam, S.-W.; Lim, J.; Park, S.; Yoon, J.; *Chem. Commun.* **2009**, 2866-2868.

82. Touceda-Varela, A.; Stevenson, E. I.; Galve-Gasion, J. A.; Dryden, D. T. F.; Mareque-Rivas, J. C.; *Chem. Commun.* **2008**, 1998-2000.

83. Shang, L.; Zhang, L.; Dong, S.; *Analyst* **2009,** *134*, 107-113.

84. Poland, K.; Topoglidis, E.; Durrant, J. R.; Palomares, E.; *Inorg. Chem. Commun.* **2006,** *9*, 1239-1242.

85. *EPA National Primary Drinking Water Standards* **2003**.

86. Gale, P. A.; Garcia-Garrido, S. E.; Garric, J.; *Chem. Soc. Rev.* **2008,** *37*, 151-190.

87. Sessler, J. L.; Gale, P. A.; Cho, W.-S., *Anion Receptor Chemistry*. Royal Society of Chemistry: Cambridge, 2006; p 414.

88. Martinez-Manez, R.; Sancenon, F.; *Chem. Rev.* **2003,** *103*, 4419-4476.

89. Choi, K.; Hamilton, A. D.; *Coord. Chem. Rev.* **2003,** *240*, 101-110.

90. Bondy, C. R.; Loeb, S. J.; *Coord. Chem. Rev.* **2003,** *240*, 77-99.

91. Gale, P. A.; *Coord. Chem. Rev.* **2003,** *240*, 191-221.

92. Sessler, J. L.; Camiolo, S.; Gale, P. A.; *Coord. Chem. Rev.* **2003,** *240*, 17-55.

93. Sessler, J. L.; Davis, J. M.; *Acc. Chem. Res.* **2001,** *34*, 989-997.

94. Beer, P. D.; Gale, P. A.; *Angew. Chem. Int. Ed.* **2001,** *40*, 486-516.

95. Miyaji, H.; Sato, W.; Sessler, J. L.; *Angew. Chem. Int. Ed.* **2000,** *39*, 1777-1780.

96. Snowden, T. S.; Anslyn, E. V.; *Curr. Opin. Chem. Biol.* **1999,** *3*, 740-746.

97. Schmidtchen, F. P.; Berger, M.; *Chem. Rev.* **1997,** *97*, 1609-1646.

98. Boiocchi, M.; Del Boca, L.; Gomez, D. E.; Fabbrizzi, L.; Licchelli, M.; Monzani, E.; *J. Am. Chem. Soc.* **2004,** *126*, 16507-16514.

99. Lin, Z.-H.; Ou, S.-J.; Duan, C.-Y.; Zhang, B.-G.; Bai, Z.-P.; *Chem. Commun.* **2006**, 624-626.

100. Newcomb, M.; Blanda, M. T.; *Tetrahedron Lett.* **1988,** *29*, 4261-4.

101. Chaniotakis, N.; Jurkschat, K.; Mueller, D.; Perdikaki, K.; Reeske, G.; *Eur. J. Inorg. Chem.* **2004**, 2283-2288.

102. Tagne Kuate, A. C.; Reeske, G.; Schurmann, M.; Costisella, B.; Jurkschat, K.; *Organometallics* **2008,** *27*, 5577-5587.

103. Badr, I. H. A.; Meyerhoff, M. E.; *J. Am. Chem. Soc.* **2005,** *127*, 5318-5319.

104. Bayer, M. J.; Jalisatgi, S. S.; Smart, B.; Herzog, A.; Knobler, C. B.; Hawthorne, M. F.; *Angew. Chem. Int. Ed.* **2004,** *43*, 1854-1857.

105. Bresner, C.; Day, J. K.; Coombs, N. D.; Fallis, I. A.; Aldridge, S.; Coles, S. J.; Hursthouse, M. B.; *Dalton Trans.* **2006**, 3660-3667.

106. Bresner, C.; Aldridge, S.; Fallis, I. A.; Jones, C.; Ooi, L.-L.; *Angew. Chem. Int. Ed.* **2005,** *44*, 3606-3609.

107. Dusemund, C.; Sandanayake, K. R. A. S.; Shinkai, S.; *J. Chem. Soc., Chem. Commun.* **1995**, 333-334.

108. Yamamoto, H.; Ori, A.; Ueda, K.; Dusemund, C.; Shinkai, S.; *Chem. Commun.* **1996**, 407-408.

109. Cooper, C. R.; Spencer, N.; James, T. D.; *Chem. Commun.* **1998**, 1365-1366.

110. Arimori, S.; Davidson, M. G.; Fyles, T. M.; Hibbert, T. G.; James, T. D.; Kociok-Koehn, G. I.; *Chem. Commun.* **2004**, 1640-1641.

111. Badugu, R.; Lakowicz, J. R.; Geddes, C. D.; *Current Analytical Chemistry* **2005,** *1*, 157-170.

112. DiCesare, N.; Lakowicz, J. R.; *Anal. Biochem.* **2002,** *301*, 111-116.

113. Oehlke, A.; Auer, A. A.; Jahre, I.; Walfort, B.; Rueffer, T.; Zoufala, P.; Lang, H.; Spange, S.; *J. Org. Chem.* **2007,** *72*, 4328-4339.

114. Day, J. K.; Bresner, C.; Coombs, N. D.; Fallis, I. A.; Ooi, L.-L.; Aldridge, S.; *Inorg. Chem.* **2008,** *47*, 793-804.

115. Cui, Y.; Li, F.; Lu, Z.-H.; Wang, S.; *Dalton Trans.* **2007**, 2634-2643.

116. Hudnall, T. W.; Gabbaï, F. P.; *Chem. Commun.* **2008**, 4596-4597.

117. Katz, H. E.; *J. Org. Chem.* **1985,** *50*, 5027-5032.

118. Broomsgrove, A. E. J.; Addy, D. A.; Bresner, C.; Fallis, I. A.; Thompson, A. L.; Aldridge, S.; *Chem. Eur. J.* **2008,** *14*, 7525-7529.

119. Katz, H. E.; *J. Am. Chem. Soc.* **1985,** *107*, 1420-1421.

120. Boshra, R.; Venkatasubbaiah, K.; Doshi, A.; Lalancette, R. A.; Kakalis, L.; Jäkle, F.; *Inorg. Chem.* **2007,** *46*, 10174-10186.

121. Parab, K.; Venkatasubbaiah, K.; Jäkle, F.; *J. Am. Chem. Soc.* **2006,** *128*, 12879-12885.

122. Miyata, M.; Chujo, Y.; *Polym. J.* **2002,** *34*, 967-969.

123. Matsumi, N.; Chujo, Y.; *Polym. J.* **2008,** *40*, 77-89.

124. Williams, V. C.; Piers, W. E.; Clegg, W.; Elsegood, M. R. J.; Collins, S.; Marder, T. B.; *J. Am. Chem. Soc.* **1999,** *121*, 3244-3245.

125. Dorsey, C. L.; Jewula, P.; Hudnall, T. W.; Hoefelmeyer, J. D.; Taylor, T. J.; Honesty, N. R.; Chiu, C.-W.; Schulte, M.; Gabbaï, F. P.; *Dalton Trans.* **2008**, 4442-4450.

126. Sun, Y.; Ross, N.; Zhao, S. B.; Huszarik, K.; Jia, W. L.; Wang, R. Y.; Macartney, D.; Wang, S.; *J. Am. Chem. Soc.* **2007,** *129*, 7510-7511.

127. Sakuda, E.; Funahashi, A.; Kitamura, N.; *Inorg. Chem.* **2006,** *45*, 10670-10677.

128. You, Y.; Park, S. Y.; *Adv. Mater.* **2008,** *20*, 3820-3826.

129. Zhao, Q.; Li, F.; Liu, S.; Yu, M.; Liu, Z.; Yi, T.; Huang, C.; *Inorg. Chem.* **2008,** *47*, 9256-9264.

130. Zhao, S.-B.; McCormick, T.; Wang, S.; *Inorg. Chem.* **2007,** *46*, 10965-10967.

131. Yamaguchi, S.; Shirasaka, T.; Akiyama, S.; Tamao, K.; *J. Am. Chem. Soc.* **2002,** *124*, 8816-8817.

132. Kubo, Y.; Yamamoto, M.; Ikeda, M.; Takeuchi, M.; Shinkai, S.; Yamaguchi, S.; Tamao, K.; *Angew. Chem. Int. Ed.* **2003,** *42*, 2036-2040.

133. Liu, Z.-Q.; Shi, M.; Li, F.-Y.; Fang, Q.; Chen, Z.-H.; Yi, T.; Huang, C.-H.; *Org. Lett.* **2005,** *7*, 5481-5484.

134. Agou, T.; Kobayashi, J.; Kawashima, T.; *Org. Lett.* **2005,** *7*, 4373-4376.

135. Yuan, M.-S.; Liu, Z.-Q.; Fang, Q.; *J. Org. Chem.* **2007,** *72*, 7915-7922.

136. Tan, W.; Zhang, D.; Wang, Z.; Liu, C.; Zhu, D.; *J. Mater. Chem.* **2007,** *17*, 1964-1968.

137. Cao, D.; Liu, Z.; Li, G.; *Sens. Actuators, B* **2008,** *B133*, 489-492.

138. Zhou, G.; Baumgarten, M.; Müllen, K.; *J. Am. Chem. Soc.* **2008,** *130*, 12477-12484.

139. Venkatasubbaiah, K.; Nowik, I.; Herber, R. H.; Jäkle, F.; *Chem. Commun.* **2007**, 2154-2156.

140. Welch, G. C.; Cabrera, L.; Chase, P. A.; Hollink, E.; Masuda, J. D.; Wei, P.; Stephan, D. W.; *Dalton Trans.* **2007**, 3407-3414.

141. Agou, T.; Kobayashi, J.; Kawashima, T.; *Inorg. Chem.* **2006,** *45*, 9137-9144.

142. Hudnall, T. W.; Chiu, C.-W.; Gabbaï, F. P.; *Acc. Chem. Res.* **2009,** *42*, 388-397.

143. Cametti, M.; Dalla Cort, A.; Bartik, K.; *ChemPhysChem* **2008,** *9*, 2168-2171.

144. Roesler, R.; Piers, W. E.; Parvez, M.; *J. Organomet. Chem.* **2003,** *680*, 218-222.

145. Deno, N. C.; Jaruzelski, J. J.; Schriesheim, A.; *J. Am. Chem. Soc.* **1955,** *77*, 3044-51.

146. Liu, H.; Shao, X. B.; Jia, M.; Jiang, X. K.; Li, Z. T.; Chen, G. J.; *Tetrahedron* **2005,** *61*, 8095-8100.

147. Kim, Y.-H.; Hong, J.-I.; *Chem. Commun.* **2002**, 512-513.

148. Chow, C.-F.; Lam, M. H. W.; Wong, W.-Y.; *Inorg. Chem.* **2004,** *43*, 8387-8393.

149. Agou, T.; Sekine, M.; Kobayashi, J.; Kawashima, T.; *J. Organomet. Chem.* **2009,** *694*, 3833-3836.

150. Chiu, C.-W.; Gabbaï, F. P.; *Dalton Trans.* **2008**, 814-817.

151. Wade, C. R.; Gabbai, F. P.; *Inorg. Chem. 49*, 714-720.

152. Sun, Y.; Wang, S.; *Inorg. Chem.* **2009,** *48*, 3755-3767.

153. Olmstead, M. M.; Power, P. P.; *J. Am. Chem. Soc.* **1986,** *108*, 4235-6.

154. Krause, E.; Polack, H.; *Ber. Dtsch. Chem. Ges.* **1926,** *59*, 777-785.

155. Chu, T. L.; Weissmann, T. J.; *J. Am. Chem. Soc.* **1956,** *78*, 23-26.

156. Leffler, J. E.; Watts, G. B.; Tanigaki, T.; Dolan, E.; Miller, D. S.; *J. Am. Chem. Soc.* **1970,** *92*, 6825-6830.

157. Eisch, J. J.; Dluzniewski, T.; Behrooz, M.; *Heteroat. Chem* **1993,** *4*, 235-241.

158. Kwaan, R. J.; Harlan, C. J.; Norton, J. R.; *Organometallics* **2001,** *20*, 3818-3820.

159. Cummings, S. A.; Iimura, M.; Harlan, C. J.; Kwaan, R. J.; Trieu, I. V.; Norton, J. R.; Bridgewater, B. M.; Jäkle, F.; Sundararaman, A.; Tilset, M.; *Organometallics* **2006,** *25*, 1565-1568.

160. Elschenbroich, C.; Kuehlkamp, P.; Behrendt, A.; Harms, K.; *Chem. Ber.* **1996,** *129*, 859-869.

161. Brown, H. C.; Dodson, V. H.; *J. Am. Chem. Soc.* **1957,** *79*, 2302-2306.

162. Weissman, S. I.; van Willigen, H.; *J. Am. Chem. Soc.* **1965,** *87*, 2285-2286.

163. Lindner, S. M.; Kaufmann, N.; Thelakkat, M.; *Org. Electron.* **2007,** *8*, 69-75.

164. Paddon, C. A.; Banks, C. E.; Davies, I. G.; Compton, R. G.; *Ultrason. Sonochem.* **2006,** *13*, 126-132.

165. Guy, J.; Caron, K.; Dufresne, S.; Michnick, S. W.; Skene, W. G.; Keillor, J. W.; *J. Am. Chem. Soc.* **2007,** *129*, 11969-11977.

166. Singh, A. K.; Singh, U. P.; Aggarwal, V.; Mehtab, S.; *Anal. bioanal. Chem.* **2008,** *391*, 2299-2308.

167. Prasad, R.; Gupta, V. K.; Kumar, A.; *Anal. Chim. Acta* **2004,** *508*, 61-70.

168. Lehn, J. M.; Sonveaux, E.; Willard, A. K.; *J. Am. Chem. Soc.* **1978,** *100*, 4914-16.

169. Fabbrizzi, L.; Faravelli, I.; *Chem. Commun.* **1998**, 971-972.

170. Harding, C. J.; Mabbs, F. E.; MacInnes, E. J. L.; McKee, V.; Nelson, J.; *Dalton Trans.* **1996**, 3227-3230.

171. Fabbrizzi, L.; Pallavicini, P.; Parodi, L.; Taglietti, A.; *Inorg. Chim. Acta* **1995,** *238*, 5-8.

172. Uhl, W.; Hannemann, F.; *J. Organomet. Chem.* **1999,** *579*, 18-23.

173. Chai, J.; Lewis, S. P.; Collins, S.; Sciarone, T. J. J.; Henderson, L. D.; Chase, P. A.; Irvine, G. J.; Piers, W. E.; Elsegood, M. R. J.; Clegg, W.; *Organometallics* **2007,** *26*, 5667-5679.

174. Kim, Y.; Gabbaï, F. P.; *J. Am. Chem. Soc.* **2009,** *131*, 3363-3369.

175. Bebbington, M. W. P.; Bontemps, S.; Bouhadir, G.; Bourissou, D.; *Angew. Chem. Int. Ed.* **2007,** *46*, 3333-3336.

176. Tachikawa, T.; Ramaraj, R.; Fujitsuka, M.; Majima, T.; *J. Phys. Chem. B* **2005,** *109*, 3381-3386.

177. Fraenk, W.; Klapotke, T. M.; Krumm, B.; Noth, H.; Suter, M.; Vogt, M.; Warchhold, M.; *Can. J. Chem.* **2002,** *80*, 1444-1450.

178. Bondi, A.; *J. Phys. Chem.* **1964,** *68*, 441-51.

179. Canac, Y.; Lepetit, C.; Abdalilah, M.; Duhayon, C.; Chauvin, R.; *J. Am. Chem. Soc.* **2008,** *130*, 8406-8413.

180. Kornath, A.; Neumann, F.; Oberhammer, H.; *Inorg. Chem.* **2003,** *42*, 2894-2901.

181. Terada, M.; Kouchi, M.; *Tetrahedron* **2005,** *62*, 401-409.

182. Mukaiyama, T.; Kashiwagi, K.; Matsui, S.; *Chem. Lett.* **1989**, 1397-400.

183. Vorobyov, I.; Yappert, M. C.; DuPre, D. B.; *J. Phys. Chem. A* **2002,** *106*, 668-679.

184. Picard, C.; Cazaux, L.; Jaud, J.; *Perkin Trans. 2* **1981**, 1554-1557.

185. Akiba, K.; Takee, K.; Ohkata, K.; Iwasaki, F.; *J. Am. Chem. Soc.* **1983,** *105*, 6965-6.

186. Iwasaki, F.; Akiba, K.; *Acta Crystallogr. Sect. B* **1985,** *41*, 445-452.

187. Akiba, K. Y.; Takee, K.; Shimizu, Y.; Ohkata, K.; *J. Am. Chem. Soc.* **1986,** *108*, 6320-6327.

188. Kuti, M.; Rabai, J.; Kapovits, I.; Kucsman, A.; Parkanyi, L.; Argay, G.; Kalman, A.; *J. Mol. Struct.* **1994,** *318*, 161-169.

189. Erhart, M.; Mews, R.; *Z. Anorg. Allg. Chem.* **1992,** *615*, 117-22.

190. Katz, H. E.; *Inclusion Compd.* **1991,** *4*, 391-405.

191. Piers, W. E.; Irvine, G. J.; Williams, V. C.; *Eur. J. Inorg. Chem.* **2000**, 2131-2142.

192. Gabbaï, F. P.; *Angew. Chem. Int. Ed.* **2003,** *42*, 2218-2221.

193. Meek, D. W.; Dyer, G.; Workman, M. O.; *Inorg. Synth.* **1976,** *16*, 168-174.

194. Entwistle, C. D.; Marder, T. B.; *Angew. Chem. Int. Ed.* **2002,** *41*, 2927-2931.

195. Entwistle, C. D.; Marder, T. B.; *Chem. Mater.* **2004,** *16*, 4574-4585.

196. Yamaguchi, S.; Wakamiya, A.; *Pure Appl. Chem.* **2006,** *78*, 1413-1424.

197. Elbing, M.; Bazan, G. C.; *Angew. Chem. Int. Ed.* **2008,** *47*, 834-838.

198. Zhou, W.; Kuebler, S. M.; Carrig, D.; Perry, J. W.; Marder, S. R.; *J. Am. Chem. Soc.* **2002,** *124*, 1897-1901.

199. Hannant, M. H.; Wright, J. A.; Lancaster, S. J.; Hughes, D. L.; Horton, P. N.; Bochmann, M.; *Dalton Trans.* **2006**, 2415-2426.

200. Kuz'mina, L. G.; Struchkov, Y. T.; Lemenovsky, D. A.; Urazowsky, I. F.; *J. Organomet. Chem.* **1984,** *277*, 147-151.

201. *Official Journal of the European Communities* **1998,** *L 300*, 32-54.

202. Piers, W. E.; *Adv. Organomet. Chem.* **2005,** *52*, 1-76.

203. Jäkle, F., *Boron: Organoboranes in Encyclopedia of Inorganic Chemistry*. 2nd ed.; Wiley: Chichester, UK, 2005.

204. Melaïmi, M.; Gabbaï, F. P.; *Adv. Organomet. Chem.* **2005,** *53*, 61-99.

205. Dilman, A. D.; Ioffe, S. L.; *Chem. Rev.* **2003,** *103*, 733-772.

206. Rendler, S.; Oestreich, M.; *Synthesis* **2005**, 1727-1747.

207. Denmark, S. E.; Stavenger, R. A.; *Acc. Chem. Res.* **2000,** *33*, 432-440.

208. Ebata, K.; Inada, T.; Kabuto, C.; Sakurai, H.; *J. Am. Chem. Soc.* **1994,** *116*, 3595-6.

209. Kim, Y.; Hudnall, T. W.; Bouhadir, G.; Bourissou, D.; Gabbaï, F. P.; *Chem. Commun.* **2009**, 3729-3731.

210. Kim, Y.; Zhao, H.; Gabbaï, F. P.; *Angew. Chem. Int. Ed.* **2009,** *48*, 4957-4960.

211. Harland, J. J.; Payne, J. S.; Day, R. O.; Holmes, R. R.; *Inorg. Chem.* **1987,** *26*, 760-5.

212. Chuit, C.; Corriu, R. J. P.; Reye, C.; Young, J. C.; *Chem. Rev.* **1993,** *93*, 1371-1448.

213. Pilcher, A. S.; Ammon, H. L.; Deshong, P.; *J. Am. Chem. Soc.* **1995,** *117*, 5166-5167.

214. Handy, C. J.; Lam, Y. F.; DeShong, P.; *J. Org. Chem.* **2000,** *65*, 3542-3543.

215. Yamaguchi, S.; Akiyama, S.; Tamao, K.; *J. Organomet. Chem.* **2002,** *652*, 3-9.

216. Green, M. L. H.; *J. Organomet. Chem.* **1995,** *500*, 127-48.

217. Parkin, G.; *Organometallics* **2006,** *25*, 4744-4747.

218. Hill, A. F.; Owen, G. R.; White, A. J. P.; Williams, D. J.; *Angew. Chem., Int. Ed.* **1999,** *38*, 2759-2761.

219. Crossley, I. R.; Hill, A. F.; Willis, A. C.; *Organometallics* **2005,** *24*, 1062-1064.

220. Crossley, I. R.; Hill, A. F.; Willis, A. C.; *Organometallics* **2006,** *25*, 289-299.

221. Landry, V. K.; Melnick, J. G.; Buccella, D.; Pang, K.; Ulichny, J. C.; Parkin, G.; *Inorg. Chem.* **2006,** *45*, 2588-2597.

222. Blagg, R. J.; Charmant, J. P. H.; Connelly, N. G.; Haddow, M. F.; Orpen, A. G.; *Chem. Commun.* **2006**, 2350-2352.

223. Hill, A. F.; *Organometallics* **2006,** *25*, 4741-4743.

224. Sircoglou, M.; Bontemps, S.; Mercy, M.; Saffon, N.; Takahashi, M.; Bouhadir, G.; Maron, L.; Bourissou, D.; *Angew. Chem., Int. Ed.* **2007,** *46*, 8583-8586.

225. Bontemps, S.; Bouhadir, G.; Miqueu, K.; Bourissou, D.; *J. Am. Chem. Soc.* **2006,** *128*, 12056-12057.

226. Samanta, A.; Gopidas, K. R.; Das, P. K.; *J. Phys. Chem.* **1993,** *97*, 1583-8.

VITA

Youngmin Kim

Department of Chemistry, Texas A&M University
PO Box 30012, College Station, TX 77842-3012

EDUCATION

2010	Texas A&M University, College Station, TX Chemistry, Ph.D. (Advisor - Prof. François P. Gabbaï)
2005	Sogang University, Seoul, Republic of Korea Chemistry, M.S. (Advisor - Prof. Jahyo Kang)
2003	Sogang University, Seoul, Republic of Korea Chemistry, B.S.

SELECTED PUBLICATIONS

Y. Kim, M. Kim, F. P. Gabbaï, *Org. Lett.* **2010**, *12*, 600-602.

Y. Kim, T. W. Hudnall, G. Bouhadir, D. Bourissou, F. P. Gabbaï, *Chem. Commun.* **2009**, 3729-3731.

Y. Kim, H. Zhao, F. P. Gabbaï, *Angew. Chem. Int. Ed.* **2009**, *48*, 4957-4960.

Y. Kim, F.P. Gabbaï, *J. Am. Chem. Soc.* **2009**, *131*, 3363-3369.

C. Chiu, Y. Kim, F. P. Gabbaï, *J. Am. Chem. Soc.* **2009**, *131*, 60-61.

T.W. Hudnall, Y.-M. Kim, M. Bebbington, D. Bourissou, F. P. Gabbaï, *J. Am. Chem. Soc.* **2008**, *130*, 10890-10891.

AWARDS

DIC Young Investigator Award, American Chemical Society, 2010

Dow Chemical Graduate Student Endowed Scholarship, 2009-2010

Marie M. And Jim H. Galloway Endowed Graduate Scholarship, 2009